STRUCTURE AND ENVIRONMENT

KIELCE UNIVERSITY OF TECHNOLOGY

Quarterly
Vol. 15, No. 2, 2023

ISSN 2081-1500
e-ISSN 2657-6902

• Architecture and urban planning • Civil engineering and transport • Environmental engineering, mining and energy

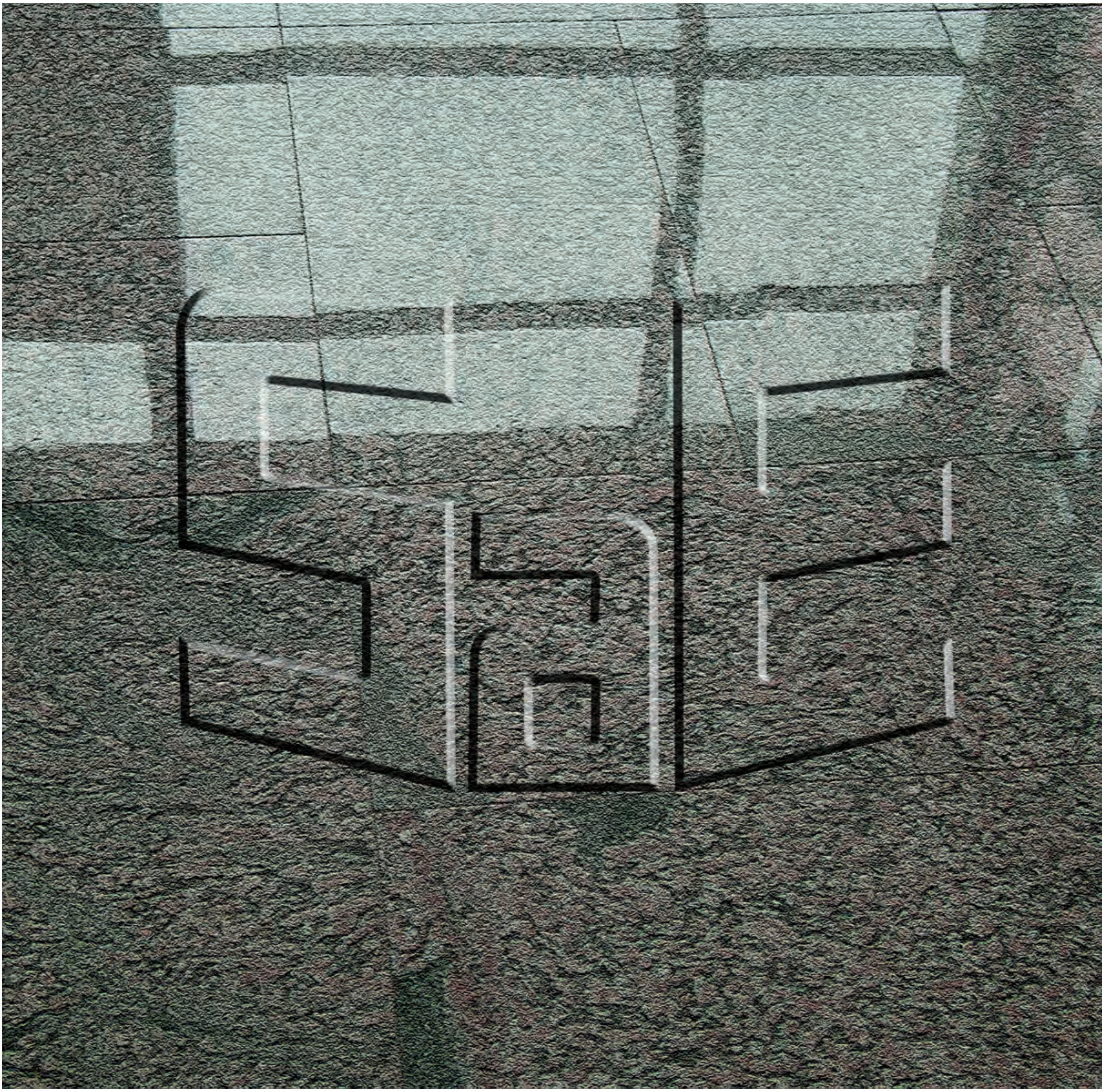

Available online at: https://sae.tu.kielce.pl

Contents

structure

General data:

Format of the journal – electronic form

Frequency of publication – quarterly

The quarterly issues of Structure and Environment are their original versions

e-ISSN 2657-6902

ISSN 2081-1500

DOI: 10.30540/sae/0000

The journal published by:

Kielce University of Technology Tysiąclecia Państwa Polskiego 7 Str. 25-314 Kielce, Poland
T.:+ 48 41 342 45 41

De Gruyter Poland:
Bogumiła Zuga 32A Str. 01 – 811 Warsaw, Poland
T.: +48 22 701 50 15

Journal Metrics:

Index Copernicus Value (IVC) 2020 = 100

The Polish Ministry of Education and Science 2021 = 40 pkt

Kielce University of Technology
2023

INDEX COPERNICUS
INTERNATIONAL

structure

structure

Luong Minh Chinh
Structure and Environment 2023, vol. 15, (2), pp. 63-72, Article number: el 006
https://doi.org/10.30540/sae-2023-006

Structure and Environment
ISSN 2081-1500
e-ISSN 2657-6902
https://content.sciendo.com/sae
https://sae.tu.kielce.pl

sciendo

Kielce University of Technology

DOI: 10.30540/sae-2023-006

USING SATELLITE IMAGES TO RETRIEVE THE RIVER TURBIDITY AND WATER FLOW VELOCITY FOR MONITORING THEIR INFLUENCES ON BRIDGE SUBSTRUCTURES

WYKORZYSTANIE ZDJĘĆ SATELITARNYCH DO OKREŚLENIA MĘTNOŚCI WODY ORAZ PRĘDKOŚCI PRZEPŁYWU WODY RZEKI W CELU MONITOROWANIA ICH WPŁYWU NA PODPORY MOSTÓW

Luong Minh Chinh*
Thuyloi University Hanoi, Vietnam

Abstract

Turbidity is an important indicator of water quality in rivers, lakes, and coastal areas. Research on turbidity issues in these areas is significant not only for the development and utilization of water resources for aquaculture, tourism, and other purposes but also for assessing the level of silt (sand) in the river, allowing sediment alluvial to build up a bank of the river, and monitoring the degree of water corrosion in the bridge substructure. This allows for the building of an effective maintenance and conservation program for the bridge in response to climate change.

Traditional methods have defined the turbidity of water in a local area, on a small scale. Interpolation errors of traditional methods for large areas may exceed over 20%. The use of remote sensing technology as Landsat-8 satellite images with a high geometric resolution of 30-meter multispectral channels allows us to estimate and distribute the water turbidity in a 30 × 30 m grid in detail.

Using multi-temporal Landsat-8 data in 2014 and 2015 for modeling water turbidity of Tien and Hau rivers and coastal areas in South Vietnam, the obtained mean absolute error is approximately 20%, the Root Mean Square Error (RMSE) does not exceed 10 NTU. The models have a high coefficient of efficiency ME, approximately 90% (ME = 0.862), and the correlation coefficient R stronger than 90%. This allows an overall assessment of changes in water flow velocity concerning the amount of sediment in the river.

Keywords: turbidity monitoring, river banks erosion, bridge erosion, bridge maintenance, remote sensing

Streszczenie

Mętność jest ważnym wskaźnikiem jakości wody w rzekach, jeziorach i obszarach przybrzeżnych. Badania nad tą kwestią są istotne nie tylko dla rozwoju i wykorzystania zasobów wodnych na potrzeby akwakultury, turystyki i innych celów, ale także dla oceny poziomu mułu (piasku) w rzece, pozwalającego osadom aluwialnym budowanie brzegu rzeki oraz monitorowanie stopnia korozji w podporach mostu. Umożliwi to opracowanie skutecznego programu konserwacji i utrzymania mostu w odpowiedzi na zmiany klimatyczne.

Tradycyjne metody pozwalają określić mętność wody w obszarze lokalnym, w małej skali. Błędy interpolacji tradycyjnych metod do dużych obszarów mogą przekraczać 20%. Zastosowanie technologii teledetekcji w postaci zdjęć satelitarnych Landsat-8 o wysokiej rozdzielczości geometrycznej 30-metrowych kanałów wielospektralnych pozwala na szczegółowe oszacowanie i rozmieszczenie zmętnienia wody w siatce 30 × 30 m.

*Thuyloi University Hanoi Vietnam, e-mail: chinhlm@tlu.edu.vn

Wykorzystując wieloczasowe dane Landsat-8 z lat 2014 i 2015 do modelowania zmętnienia wody rzek Tien i Hau oraz obszarów przybrzeżnych w południowym Wietnamie, uzyskany średni błąd bezwzględny wynosi około 20%, a średni błąd kwadratowy (RMSE) nie przekracza 10 NTU. Modele mają wysoki współczynnik efektywności ME, około 90% (ME = 0,862), a współczynnik korelacji R jest wyższy niż 90%, co stwarza możliwość dokonania ogólnej oceny zmian prędkości przepływu wody w odniesieniu do ilości osadów w rzece.

Słowa kluczowe: monitoring mętności, erozja brzegów rzek, erozja mostów, konserwacja mostów, teledetekcja

1. INTRODUCTION

Riverbank erosion is one of the natural disasters causing many serious consequences in the floodplain of the Mekong Delta. The Tien River is one of the two main tributaries to the Mekong (along with the Hau River) as it flows into Vietnam. The Tien river across the Mekong Delta approximately 122.9 km [11]. The width of the Tien River changes many times, the thinnest point in An Long (Tam Nong) is about 450 m, the widest point in Long Khanh is 2.200 m, the average depth is about 10-15 m. The Tien River accounts for about 80% of the total water flow to the Mekong, average flow is 11500 m^3/s, maximum is 41504 m^3/s, smallest is about 2000 m^3/s, there are many curved and torsional sections, so very strong erosional activity and sedimentation take place [11, 12].

There are several large bridges across the Tien River: My Thuan Bridge (2000) (Figure 1), Cao Lanh Bridge (2018), Rach Mieu Bridge (2002), My Thuan Bridge 2 (under construction), while across the Hau River there are: Can Tho Bridge (2011), Co Chien Bridge (2018), Vam Cong Bridge (2018). These are cable-stayed bridges with large spans over 270 m, so all the impacts of the surrounding environmental factors on these structures are of significant importance, especially the impact of the flow velocity [13].

Figure 1. The location of the My Thuan Bridge on the Tien River in Vinh Long Province

The study of changes in the Tien and Hau riverbed, especially erosional situation to identify causes as a scientific basis to propose solutions to stabilize river banks, ensure structural diagrams of bridges (My Thuan Bridge), respond to climate change, and minimizing the damaging impact to the bridge is essential.

Figure 2. Riverbank erosion of the Tien River, near to the My Thuan Bridge

Traditional methods have defined the turbidity of water in a local area, on a small scale. Interpolation errors of traditional methods for large areas may exceed over 20%. Remote sensing technology as Landsat-8 satellite images with a high geometric resolution of 30-meter multispectral channels allows us to distribute the water turbidity in a 30 × 30 m grid in detail.

Remote sensing has been used around the world for several decades, started in the 1970s and 1980s when Landsat and Spot images appeared on the market. Since the beginning of the 21st century, many countries have been using remote sensing technology to monitor the quality of surface waters, not just those with their own satellites [2, 4, 5, 9]. High spatial resolution satellite images such as Worldview-2 (less than 0.5 m accuracy for the panchromatic – PAN image and 2.0 m for the multi-spectral image) were used to monitor coastal and continental water quality [4, 10, 15]. In Vietnam, the National Department of Remote Sensing, started using remote sensing technology to monitor surface water quality in 2010.

By utilizing multi-temporal Landsat-8 data from 2014 and 2015, water turbidity modeling was carried out for the Tien and Hau rivers, as well as the coastal areas in South Vietnam, the obtained mean absolute error is approximately 20%, the root means square error (*RMSE*) does not exceed 10 *NTU*. The models have a high coefficient of efficiency *ME*, approximately 90% ($ME = 0.862$), and the correlation coefficient *R* stronger than 90%. This allows for an overall assessment of the trend of changes in water flow velocity concerning the amount of sediment in the river.

2. RESEARCH SIGNIFICANCE

In this paper, the author used Landsat-8 multispectral satellite images with a high geometric resolution of 30-meter to analyze the turbidity of the Tien and Hau rivers. Statistical data was collected from the turbidity model based on sample points at the site to determine the amount of alluvium in the river, determining the relation between the turbidity and the erosion of the river bed and the river banks, as well as the river flow velocity imparted to the bridge substructure.

3. CURRENT STATE OF EROSION AND ASSESSMENT METHOD

3.1. State of Erosion of The Tien River

During the period from 2009 to 2013, erosion of the Tien riverbank in the section passing through Dong Thap Province continued to take place at high intensity and scale (Table 1) [11].

Table 1. The riverbank erosion of the Tien River in the Dong Thap province in 2009-2013 [11]

Years	2009	2010	2011	2012	2013
Places eroded	96	92	95	95	113
The districts had been eroded	34	35	39	36	32
The districts can be eroded	43	43	47	46	42
Affected length (km)	74.0	23.0	95.0	56.4	38.7
Eroded area (ha)	36.6	22.0	49.0	26.6	10.3

In Table 1, we can see that the erosion of the Tien riverbank in Dong Thap Province in 2009-2013 is as follows:

- Table 1 shows that from 2009 to 2013, the erosion of the Tien riverbank in Dong Thap Province exhibited the following characteristics.
- The length of the riverbank eroded or threatened with erosion ranges from 23-95 km along the entire length of the mainstream of approximately 122.9 km.
- Between 2009 and 2013, the riverbank of the Tien River lost a total of 144.42 ha of land due to riverbank erosion.

One of the main reasons for the erosion of the Tien river bank is determined by the hydrological and dynamic characteristics of the flow; geological, soil, topographical characteristics, conductor morphology, and human socio-economic activities – uncontrollable sand exploitation [11, 14].

This leads to a change in the depth of the Tien river bed. According to the statistics of the Southern Sub-Department of Inland Waterways, the depth of the Tien and Hau rivers from 2008 to the present became deeper quite fast, with an average of 3-7 m on the whole route (Figure 3).

Figure 3. Regions of Tien and Hau rivers where the bottom of the river became deeper [12]

In particular, in the area near the My Thuan Bridge, the riverbed depth was around 9-10 m prior to 2008, but after 2016 the depth was more than 14 m, increasing by more than 4 m, increase the effects of the water flow onto the substructure of the bridge, increasing erosion at the piers of the My Thuan bridge (Table 2).

Furthermore, the hydrological characteristics of the Mekong Delta, particularly the Tien River, are influenced by floods, rainfall, and tides, which lead to the formation of two seasons – the flood season and the dry season. Considering both the flood season and the dry season, the flow velocity of the Tien River is faster than the average velocity without erosion of the river bank (Table 2). With high flow velocity, and the ability to maintain for a relatively long time (the flood season lasts 2-3 months), the ability to erode the riverbed of the Tien river province is very high. This also leads to a significant change in the turbidity of the Tien River [12].

Table 2. The average flow velocity and allowable average velocity without erosion of the Tien River

Location	**Flood season**	
	Flow velocity [m/s]	**Allowable velocity [m/s]**
Tan Chau	2.70	0.58
Sa Dec	2.40	0.58
My Thuan	2.45	0.55
Location	Dry season	
	Flow velocity [m/s]	Allowable velocity [m/s]
Sa Dec	1.10	0.58
My Thuan	1.20	0.55

3.2. Documentation of Turbidity Survey Area by Satellite Image

The turbidity of the Tien and Hau rivers, as well as the estuary area, including the Saigon River, is monitored. Tien River has main estuaries flowing into the East sea such as Cung Hau, Co Chien, Ham Luong, Ba Lai, and Cua Dai. The Hau River has two main estuaries, Tranh De and Dinh An. Saigon River‘s main gate is Soi Rap [14].

The satellite images used for turbidity monitoring are multi-time Landsat-8 images for the period January 24, 2015, and January 24, 2014. Figure 1 shows the RGB color composite images of Landsat-8 for the period 2015 and 2014. Image 2014 is influenced by quite a lot of clouds.

Along Tien and Hau rivers, water sampling and turbidity analysis were conducted (unit: *NTU*). Water samples were taken from river cross-sections at three locations, between the river and the left and right sides of the river bank.

For the year 2015, the total number of sampling and measuring points with GPS location is 63 points. After excluding the combined raw error in the image processing, the number of points that can be used is 52 points; 45 of which are used to model turbidity, and 7 points are used as checkpoints.

For the year 2014, due to the large fraction of clouds, the total number of water sampling points at the site was 63, but in fact, only 28 water sampling points were used because clouds were obscured, near 44.44%. Out of 28 water sample points, 3 points found unreasonable points 17-T, 17-P, 18-G. Thus, the number of water sample points used for estimating the water turbidity model is 25, in which 20 points are used to build a model turbidity and 5 points are used as model checkpoints. Locations of the field sampling points are posted on the Landsat-8 image as shown in Figure 4.

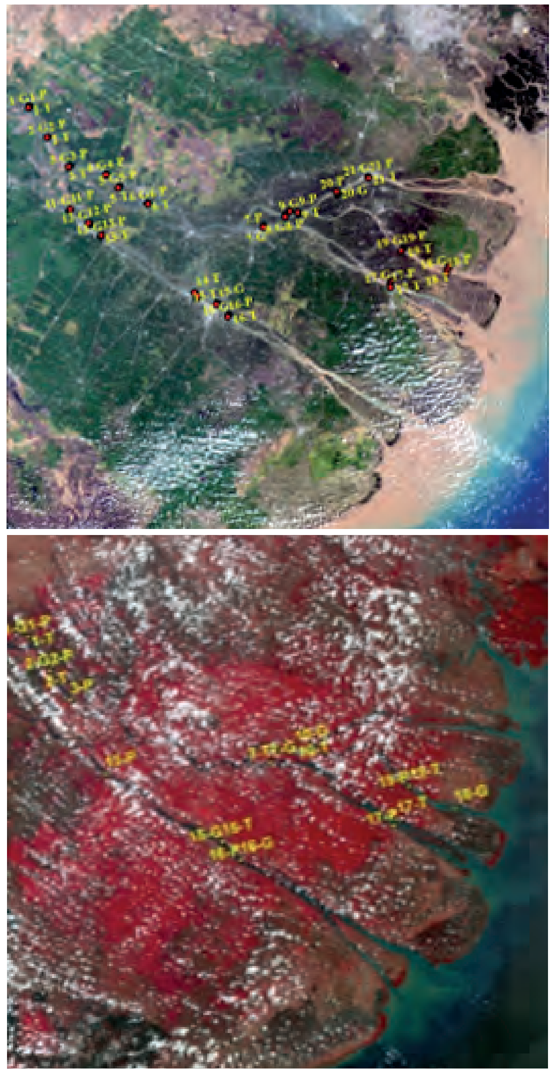

Figure 4. Landsat-8 images from two dates 24/01/2015 (above), 24/01/2014 (down)

3.3. Methodology

Figure 5 introduces L_t synthesized light rays going to the receiver (sensor) from single solar rays carrying energy E_s, including four components: scattered rays in the atmosphere L_p, rays reflecting water surface L_s, reflected rays from the inside the waterbed L_w (or the water-leaving reflection), and the bottom reflection L_b; means [3, 6]:

$$L_t = L_p + L_s + L_w + L_b \tag{1a}$$

Among the four components, only the L_w component– the water-leaving reflection that carries information about water quality, namely turbidity (*NTU*):

$$L_w = L_t - L_s - L_p - L_b \tag{1b}$$

Depending on the depth and turbidity of the water, L_b component can be zero. Equation (1b) shows that:

firstly, we need to correct the spectral radiation of the L_t image due to the influence of the atmospheric environment (L_p). If the remote sensing reflection on the water surface is R_{rs} and the remote sensing reflection below the water surface is ρ_{rs}, the relationship between them showed as [1, 7]:

$$R_{rs} = \frac{c \cdot R_{rs}}{(1 - k \cdot R_{rs})} \tag{2}$$

Where parameter c depends on the radiation transmission coefficient in two directions from the bottom to the top of the water surface and vice versa, and also on the refractive index of the water medium. The parameter k depends on the reflectivity on the water-air interface, and the ratio between the rising radiation from the water body to the radiating completely [6]. R_{rs} is defined as the ratio of the radiation leaving the water surface to the receiver L_w and the downward solar spectrum radiation E_s (Fig. 5) [7, 8]:

$$R_{rs} = \frac{L_w}{E_s} \tag{3}$$

After correcting for the atmospheric effects on the image radiation and treating the surface reflectivity (R_{rs}), the bottom water reflection (R_{rs}) is determined from the following Equation (2).

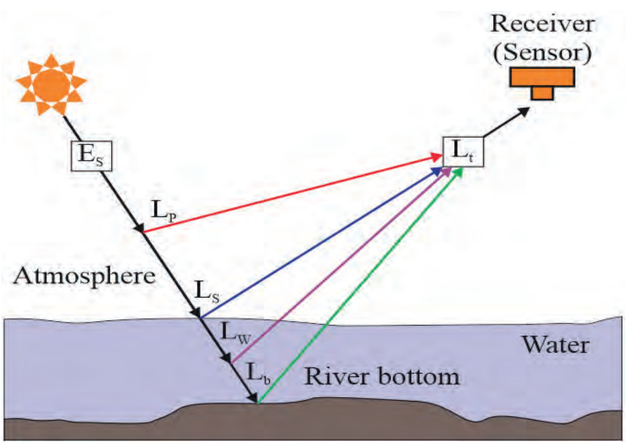

Figure 5. Diagram of reflected ray components going to the receiver

4. RESULTS AND EVALUATION

4.1. Set Up the Turbidity Model

Before establishing the turbidity model, it was crucial to process the satellite image radiation. The steps involved in processing satellite images are summarized below:

- Masking the land and leaves only the water surface of the Tien, and Hau River, and coastal areas.
- Adjusting image geometry and match the field sampling point grid according to the coordination on the image.
- Separating clouds and clouds shadow.
- Processing R-radiation images at the top of the atmosphere from the original DN image (quantization image)
- Processing reflective images of ρ surface.
- Processing remote sensing reflection image ρ_{rs}.
- Creating high layer image channels from remote sensing reflection image ρ_{rs} of channels R, G, B.
- Finding the relationship between the site turbidity sample and the remote sensing reflection ρ_{rs} and remove the unsatisfactory image channels.
- Setting up the turbidity model.
- Calculating errors such as mean squared error, mean absolute error, etc.
- Eliminating raw errors, then reset the turbidity model and recalculate the errors.
- The process of establishing the turbidity model and calculating the error have to satisfy the following conditions:
  - An average absolute error has to be smaller than 30%, or accuracy is over 70%.
  - Correlation coefficient while building model R^2 is not less than 0.7.

After processing satellite image radiation and removing the raw error from site sample data, the turbidity model is built based on the relationship between remote sensing reflection of high layer image and turbidity from site samples. Then a turbidity model is selected to meet upper requirements. Figure 6 shows the turbidity model selected based on 45 field sample points for the period 2015 which is the linear equation: $y = 1.1542x - 3.247$ (4) with strong correlation coefficient $R^2 = 0.8617$ ($R = 92.84\%$). The turbidity model based on 20 points for the period 2014 is an exponential Equation (5), with a strong correlation coefficient $R^2 = 0.9048$ ($R = 95.12\%$) (Figure 6).

- Model of turbidity period 2015 has a form:

$$\begin{gathered} DODUC(NTU) = 1.1542 \cdot x - 3.247 \\ x = 173.16 \cdot b_{ü} + 53.65 \cdot b + 55.65 \cdot b - 211.95 \end{gathered} \tag{4}$$

where: b_1, b_2, b_3 are high-layer images generated from remote sensing reflection ρ_{rs} of RBG channels.

- Model of turbidity period 2014 has a form:

$$\begin{gathered} DODUC(NTU) = 5.648 \cdot e^x \\ x = 5.818 \cdot b_1 + 1.803 \cdot b_2 + 1.870 \cdot b_3 - 7.122 \end{gathered} \tag{5}$$

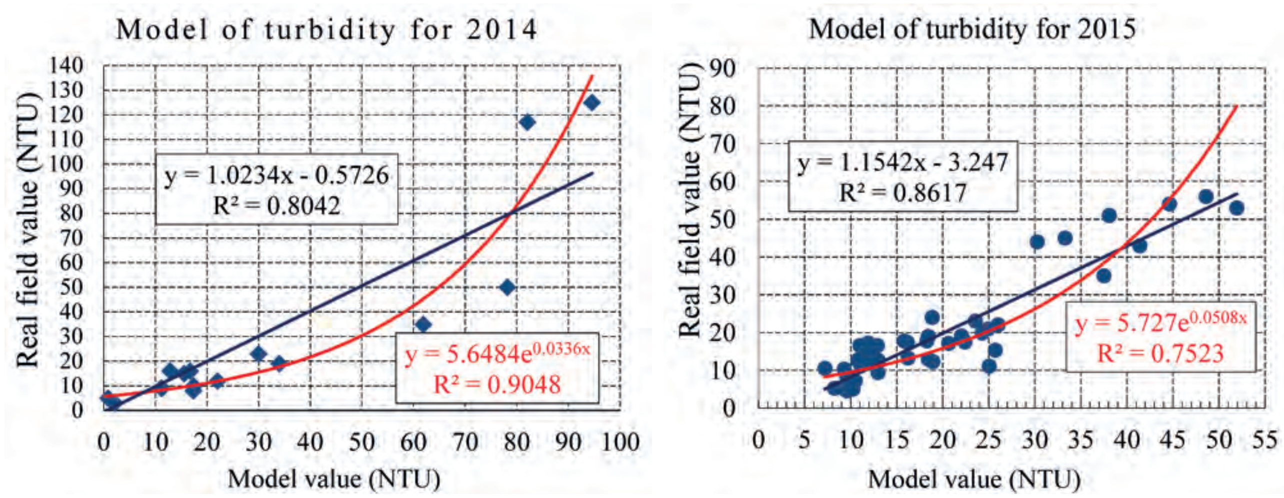

Figure 6. Turbidity model for 2014 and 2015

where: b_1, b_2, b_3 are high-layer images generated from remote sensing reflection ρ_{rs} of RBG channels.

The next important step is to evaluate the reliability and accuracy of the two models Equation (4) and Equation (5) presented in sections 4.2 and 4.3. Therefore, other statistical parameters were used to assess model performance. In this paper (Table 3), useful statistical parameters are as follows:

- Correlation coefficients, R^2:

$$R^2 = \left[\frac{\sum_{i=1}^{n}(x_i - \bar{x}_i)(y_i - \bar{y}_i)}{\sqrt{\sum_{i=1}^{n}(x_i - \bar{x}_i)^2}\sqrt{\sum_{i=1}^{n}(y_i - \bar{y}_i)^2}}\right]^2 \tag{6}$$

- Root mean square error, *RMSE*:

$$RMSE = \sqrt{\frac{1}{n}\sum_{i=1}^{n}(x_i - y_i)^2} \tag{7}$$

- Mean absolute error, *MAE*:

$$MAE = \frac{1}{n}\left[\sum_{i=1}^{n}(x_i - y_i)^2\right]$$
$$MAE \text{ in } \% = \frac{MAE}{\bar{x}_i}\cdot 100 \tag{8}$$

- Coefficient of modeling efficiency, *ME*:

$$ME = 1 - \left[\frac{\sum_{i=1}^{n}(x_i - y_i)^2}{\sum_{i=1}^{n}(x_i - \bar{x}_i)^2}\right] \tag{9}$$

where: x_i are the observed values with the mean of; y_i are the modeled values with the mean of; n is the number of observations; $i = 1, 2, 3, ..., n$.

4.2. Evaluate a Turbidity Model Based on Field Sample Points

The results of the evaluation of the turbidity model on 45 sample points for 2015 and 20 sample points for

Table 3. The parameters to evaluate the turbidity model on the constructed model points for 2 periods

For 2014		For 2015	
Parameters	**Real value**	**Parameters**	**Real value**
Mean square error	9.987(*NTU*)	Mean square error	5.267(*NTU*)
Average absolute error	5.778(*NTU*) ≡ 23.63%	Average absolute error	4.186(*NTU*) ≡ 21.29%
Correlation coefficient *R* (R^2)	0.958 (R^2 = 0.9048)	Correlation coefficient *R* (R^2)	0.928 (R^2 = 0.8617)
Linear regression coefficient *α*	1.0234	Linear regression coefficient *α*	1.154
Linear regression deviation *β*	0.573	Linear regression deviation *β*	3.247
Minimize the field turbidity	3.0(*NTU*), point 2T	Minimize the field turbidity	4.5(*NTU*), point 2G
Number of model points	20	Number of model points	45
Efficiency coefficients model *ME*	0.914	Efficiency coefficients model *ME*	0.862

2014 are summarized in Table 3. Both turbidity models for 2015 and 2014 both have a high ME coefficient, nearly 1, with a difference of only 5%. In 2015 the model uses twice more points than 2014, giving a small mean square error approximately half that of 2014, and an average absolute error of 1.11 times less.

4.3. Evaluate the Model on The Checkpoints

4.3.1. Evaluation by mean square error and average absolute error

After setting up a model with 7 points for 2015 and 5 points for 2014 (Table 4) called checkpoints were used to evaluate the model. The mean square error and average absolute error were calculated based on the difference in *NTU* values from the model and the field sample points as shown in Tables 4 and 5. The average absolute error for 2015 was 20.54%; for 2014 was 22.50%, both less than 30%.

4.3.2. Evaluation by regression function

The turbidity model was evaluated using checkpoints based on the regression function shown in Figure 7. The correlation coefficient of the regression function for 2015 and 2014 is quite strong with R^2 = 0.8829 (R = 93.96%) and R^2 = 0.8920 (R = 94.44%). The coefficient of the regression line angle of both periods compared to the ideal value is about ±17% difference, (α = 0.823 and α = 1.174). Table 6 summarized the results of the turbidity model assessment based on the checkpoints for 2015 and 2014. The statistical parameters in Table 5 for the 2 periods are not significantly different. It should be noted that the mean square error and the mean absolute error of the two periods are both smaller than the field minimum values.

The turbidity of the Tien river and Hau river in Southern Vietnam based on the turbidity model by functions (4) and (5) for 2015, 2014 is shown in Figure 8. Additionally, the distribution of turbidity maps for the Tien River, Hau River, and estuary coast in Southern Vietnam is shown in Figure 9.

Table 4. Evaluate the turbidity model accuracy at the sample points

For 2014					For 2015				
No.	Point	Turbidity from field samples ($NTU_{TĐ}$)	Turbidity from the model (NTU_A)	Absolute error	No.	Point	Turbidity from field samples ($NTU_{TĐ}$)	Turbidity from the model (NTU_A)	Absolute error
1.	1-T	5	5.15864	0.15864	1.	2-T	10.4	6.7946	3.6054
2.	13-P	9	5.75	3.25	2.	5-G	8.5	14.5287	6.0287
3.	15-P	20	11.5061	8.4939	3.	12-T	12.6	13.0733	0.4733
4.	17-T	30	25.1651	4.8349	4.	9-P	35	25.8761	9.1239
5.	16-P	11	10.8576	0.1424	5.	15-P	25	27.8328	2.8328
					6.	18-G	49	61.8167	12.8168
					7.	17-G	43	57.0483	14.0483
Average value		15	11.6874	3.3759	Average value		26.214	29.5672	3.3532
Mean square error				4.6072	Mean square error				8.4723
Average absolute error				22.50%	Average absolute error				20.54%

Table 5. The parameters evaluate the turbidity model at the checkpoints for 2 periods

For 2014		For 2015	
Parameters	**Real value**	**Parameters**	**Real value**
Mean square error	4.607(*NTU*)	Mean square error	8.472(*NTU*)
Average absolute error	3.376(*NTU*) ≡ 22.50%	Average absolute error	6.,990(*NTU*) ≡ 20.54%
Correlation coefficient R (R^2)	0.944 (0.892)	Correlation coefficient R (R^2)	0.940 (0.883)
Linear regression coefficient α	1.174	Linear regression coefficient α	0.823
Linear regression deviation β	1.281	Linear regression deviation β	2.817
Minimize the field turbidity	5.0(*NTU*), point 1T	Minimize the field turbidity	8.5(*NTU*), point 5G
Number of model points	5	Number of model points	7

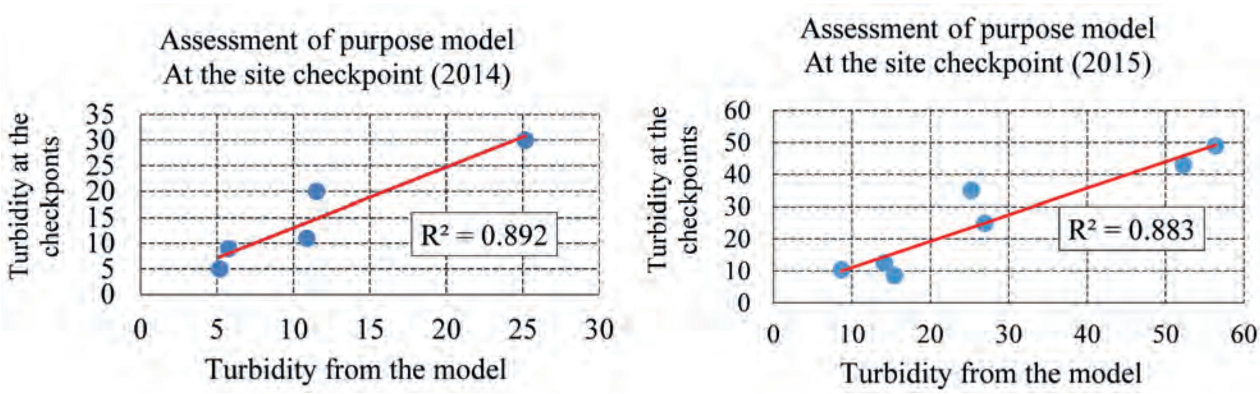

Figure 7. Evaluation of the turbidity model at the checkpoints based on the regression function for 2015 and 2014

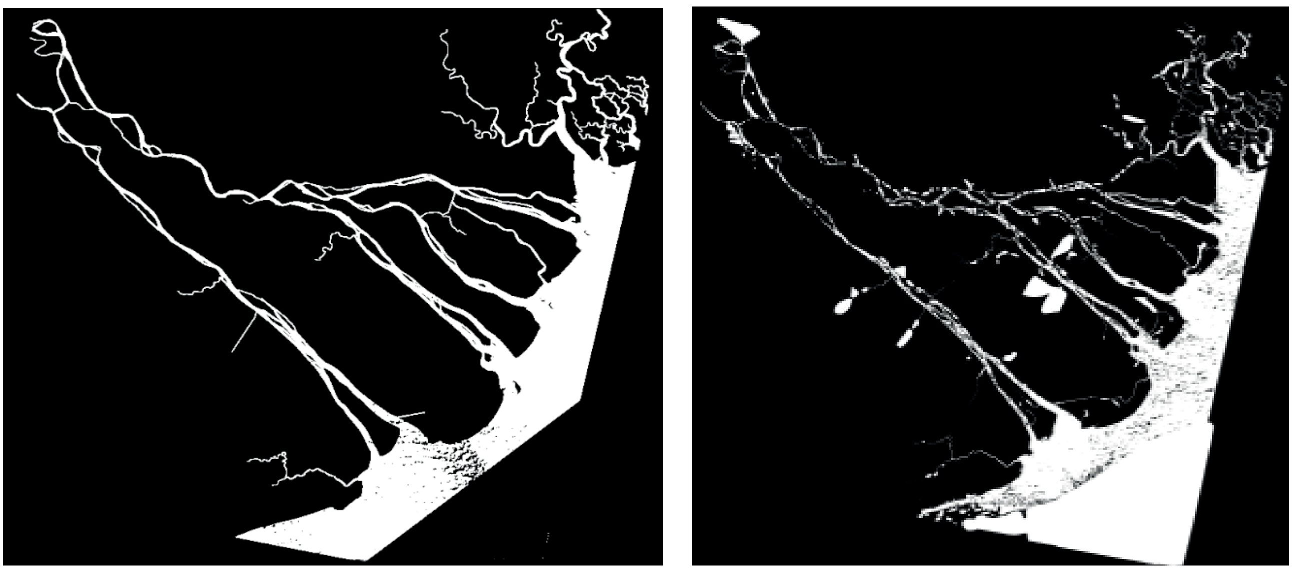

Figure 8. Digital image of turbidity in Tien and Hau rivers for 2015 (left) for 2014 (right)

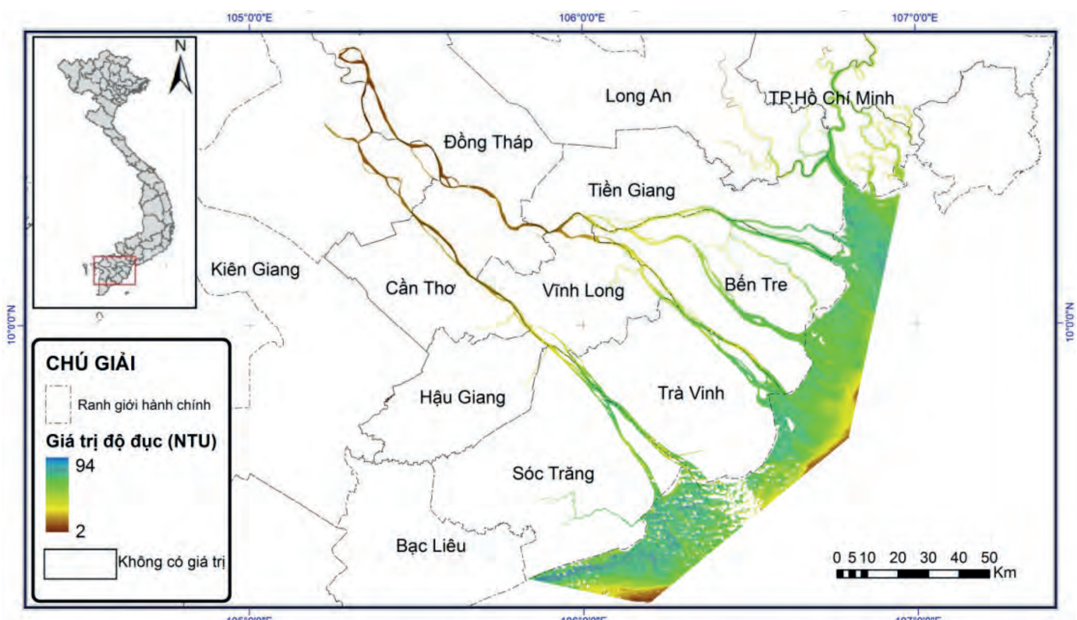

Figure 9. Turbidity distribution map of Tien, Hau river, and coastal estuary (January 24, 2015)

4.3.3. Discussion

Based on the calculation results, some general comments are as follows:

- The mean square error for determining the turbidity is less than 10 *NTU*.
- The accuracy of determination of turbidity reaches 80%.
- The strong correlation coefficient *R*, over 90%. The efficiency coefficient of the *ME* model is approximately 90%.
- Linear regression coefficient α is less than 20% different from the ideal value.
- The linear regression deviation β is all smaller than the field turbidity minimum value (less than 5 *NTU*).
- The above results show that: turbidity model for 2015 and 2014 determined by equations (4) and (5) is reliable, consistent with the objective reality between the results extracted from remote sensing and field sample data.
- The results of the treatment of turbidity classification from the digital image of turbidity (Figure 8) on ArcGIS (Figure 9) showed that: turbidity concentration in Tien and Hau rivers increases when entering the territory of Ben Tre, Tra Vinh, and Soc Trang provinces. Turbidity concentrates in the coastal areas and decreases when offshore from 94 (*NTU*) to 2 (*NTU*) over a distance of 20 km.

5. CONCLUSION

Turbidity is considered an important indicator in assessing the level of silt (sand) in the river, allowing sediment alluvial to build up river banks, monitoring the degree of water corrosion in the bridge structure to build an effective maintenance and conservation program for the bridge in response to climate change.

The use of satellite images to monitor surface water turbidity in particular and the environment, in general, is a great idea in the application of high technology to promote economic development, as well as planning and management resources (water and sand), exploitation, and operation of bridges in the river corridor, minimizing adverse impacts of the water flow on the bridge, is the general trend in the world.

Using satellite remote sensing technology allows monitoring the spatial distribution of water quality, particularly turbidity on the square grid with the resolution equal to the geometrical resolution of the multi-spectral image with low-cost for water metering and sampling at the site. The results using Landsat-8 satellite images allow determining the turbidity in the square grid 30 × 30 m with the accuracy of approximately 80% of Tien River, Hau River, and the coastal area.

With a small number of water sample points (63 points) at the site for both rivers in the Delta Mekong from upstream to near the coastal estuary, a turbidity model was built, and allow to determine turbidity for any point at the time of satellite scanning with a median error less than 10 *NTU*.

For further improved accuracy, requires uniformity between site work (water sampling) at the time the satellite makes the image, and at the same time overcome cloud cover.

The changes of the turbidity in the Tien and Hau river bed, show the erosion situation to identify causes as a scientific basis to propose solutions to stabilize river banks, ensure structural diagrams of bridges (My Thuan Bridge), respond to climate change, and minimizing the impact damage to the bridge is essential.

REFERENCES

[1] Gordon H.R., Brown O.B., Evans R.H., Brown J.W., Smith R.C., Baker K.S., Clark D.K., *A semi-analytic radiance model of ocean color.* J. Geophys. Res., Vol. 93, 1988, pp.10909-10924.

[2] Keiser M., Aboulela H., et. al., *Spectral enhancement of the SPOT imagery data to assess marine pollution near Port Said*, Egypt. PIERS Proceedings, July 2-6, 2008, Cambridge, USA.

[3] Lee Z.P., Carder K.L., Hawes S.K., Steward R.G., Peacock T.G., Davis C.O., *Model for the interpretation of hyperspectral remote sensing reflectance*. Applied Optics, vol. 33, 1994, pp. 5721-5732.

[4] Liew S.C., Saengtuksin B., Kwoh L.K., 2011, *Mapping Water Quality of Coastal and Inland Waters Using High-Resolution Worldview-2 Satellite Imagery*. Proc. 34th. International Symposium on Remote Sensing of Environment, 10-15 April 2011, Sydney, Australia.

[5] Manchino G., Nole A., et al., *Assessing water quality by remote sensing in a small lake: the case study of Monticchio lakes in Southern Italy*. Biosciences and Forestry, 2009, pp. 154-164.

[6] Mobley C.D., *Light and Water: Radiative Transfer in Natural Water*, Academic, New York, 1994.

[7] Mobley C.D., *Estimation of the remote-sensing reflectance from above-surface measurements*. Applied Optics, Volume 38, 1999, pp. 7442-7455.

[8] Morel A., Gentili B., *Diffuse reflectance of oceanic waters: II. The implication of bi-directionality for the remote-sensing problem*, Applied Optics, Vol. 35, 1996, pp. 4850-4861.

[9] Yuan-Fong Su, Jun-Jih Liou, Ju-Chen Hou, Wei-Chun Hung, Shu-Mei Hsu, Yi-Ting Lien, Ming-Daw Su, Ke-Sheng Cheng, Yeng-Fung Wang, 2008. *A multivariate model for coastal water quality mapping using satellite remote sensing images*. Sensors, Vol. 8, 2008, pp. 6321-6339.

[10] Luong Chinh Ke, Ho Thi Van Trang, Vu Huu Liem, Tran Ngoc Tuong, Pham Thi Duyen., *Assessment of surface water pollutant models of estuaries and coastal zone of Quang Ninh – Hai Phong using Spot-5 images*. Polish Academy of Sciences, Geodesy and Cartography. Vol. 64, No 1, 2015, pp. 29-42.

[11] *Dong Thap Department of Agriculture and Rural Development*, Report of the prevention, fighting, and overcoming of riverbank erosion in 2009, 2010, 2011, 2012, 2013, Dong Thap, Vietnam 2013.

[12] Trinh Phi Hoang., *Study of the main weather disturbances causing rain-flooding in the Mekong Delta River*. Science Journal of Pedagogical University Ho Chi Minh City, 43 (81), 2013, pp. 107-116.

[13] *Report of My Thuan cable-stayed bridge – Test results*. Fressinet Vietnam, 2016.

[14] Duong Thi Truc. *The water surface quality of Tien river in the area of Tan Chau district*, An Giang province. Can Tho University Journal of Science, Vol. 55, Issue: Environment and Climate Change (2), 2019, pp. 53-60.

[15] Riki Mukhaiyar. *Digital image and remote sensing image as data for identification of a quality of a non-point source pollutant in Ciliwung river*, Indonesia. International Journal of GEOMATE, Vol. 12, Issue 32, April 2017, pp. 142-151.

Imam Hossain, Jahidul Islam, Al Amin
Structure and Environment 2023, vol. 15, (2), pp. 73-81, Article number: el 007
https://doi.org/10.30540/sae-2023-007

Structure and Environment
ISSN 2081-1500
e-ISSN 2657-6902
https://content.sciendo.com/sae
https://sae.tu.kielce.pl

sciendo

Kielce University of Technology

DOI: 10.30540/sae-2023-007

EVALUATION OF WIND EFFECTS ON BUILDINGS USING DESIGN CODES AND NUMERICAL WIND TUNNEL TESTS

OCENA WPŁYWU WIATRU NA BUDYNKI Z WYKORZYSTANIEM NORM PROJEKTOWYCH I TESTÓW NUMERYCZNYCH W METODZIE TUNELU AERODYNAMICZNEGO

Imam Hossain*
Bangladesh Army International University of Science and Technology (BAIUST)
Md Jahidul Islam
Military Institute of Science and Technology (MIST)
Al Amin
European University of Bangladesh (EUB)

Abstract

The evaluation of wind effect on the regular shape and simple diaphragm buildings and structures due to wind load has been calculated by several international codes and standards where wind gust nature and dynamic effect could not capture. Bangladesh National Building Code (BNBC) provides the tools for engineers to calculate the wind pressures for the design of a regular-shaped structure with a height to width ratio of less than 5.0, a simple diaphragm, and no unusual geometrical irregularity. If these conditions do not satisfy a wind tunnel testing is required. In this study, a comparative study between two codes in Bangladesh (BNBC-2006 and BNBC-2020), and wind tunnel test results are conducted. An investigation is carried out on four typical buildings with variable heights located within Dhaka, Bangladesh. A computational fluid dynamics (CFD) program RWIND is used to calculate the wind loads on buildings and are compared with those obtained by Bangladesh National Building Codes. Storey shear of four different building models is compared. Between BNBC-2006 and BNBC-2020, there is up to a 53% difference in storey shear. Whereas, up to 30% variation in storey shear is observed between the numerical wind tunnel test data and the data calculated using the BNBC-2020 equations. Finally, this study will help in improving BNBC code provisions for wind load calculations.

Keywords: wind load analysis, wind tunnel test, wind simulation, reinforced cement concrete structure, computational fluid dynamics, Bangladesh National Building Code

Streszczenie

Kalkulację wpływu wiatru na budynki i budowle o regularnych kształtach i prostych konstrukcjach pod obciążeniem wiatrem przedstawiono w kilku normach międzynarodowych, w których jednak nie uwzględniono charakteru podmuchów wiatru i efektu dynamicznego. Bangladeska Krajowa Norma Budowlana (BNBC) zapewnia inżynierom narzędzia do obliczania ciśnienia wiatru przy projektowaniu konstrukcji o regularnym kształcie, o stosunku wysokości do szerokości mniejszym niż 5,0, prostej konstrukcji oraz bez nietypowych nieregularności geometrycznych. Jeśli warunki te nie są spełnione, wymagane jest przeprowadzenie testów w tunelu aerodynamicznym. W niniejszym opracowaniu przeprowadzono badanie porównawcze między dwiema normami obowiązującymi w Bangladeszu (BNBC-2006 i BNBC-2020) oraz wyni-

*Bangladesh Army International University of Science and Technology (BAIUST), Bangladesh, e-mail: imam.ce.bd@gmail.com

kami testów w tunelu aerodynamicznym. Badanie przeprowadzono na czterech typowych budynkach o różnej wysokości zlokalizowanych w Dhace w Bangladeszu. Program RWIND do obliczeń i symulacji dynamiki płynów (CFD) został wykorzystany do obliczenia obciążeń wiatrem na budynkach i porównany z wynikami uzyskanymi według bangladeskich norm budowlanych. Porównano ścinanie kondygnacji czterech różnych modeli budynków. W tym względzie różnice pomiędzy BNBC-2006 i BNBC-2020 wynoszą do 53%. Natomiast między danymi z numerycznego testu w tunelu aerodynamicznym a danymi obliczonymi przy użyciu równań BNBC-2020 zaobserwowano do 30% różnic w odniesieniu do ścinania kondygnacji. Badanie to pomoże też ulepszyć przepisy norm BNBC dotyczące obliczeń obciążenia wiatrem.

Słowa kluczowe: analiza obciążenia wiatrem, test w tunelu aerodynamicznym, symulacja oddziaływania wiatru, konstrukcja żelbetowa, obliczeniowa dynamika płynów, bangladeska krajowa norma budowlana

1. INTRODUCTION

World population growth rapidly increasing day by day which leads to more demand for tall buildings, especially in countries where land is not sufficient because of the high population. For designing Civil Engineering structures there have three important design requirements: more service period, serviceability and people's safety. The present wind loads codes are based on constant values of pressure coefficients for the regular size and shape of structures. Irregular shapes of buildings and structures are not enlisted in those codes, for these types of structures wind load calculation and assess by wind tunnel tests (Fouad et al., 2018). However, these tests are not accessible for most designers due to higher cost and time requirements. There have also been some difficulties to imitate the full-scale Reynold's number (Barlow et al., 1999). In particular for tall buildings that are more vulnerable to wind forces, wind pressure coefficients (Cp) are significant numbers for building engineering applications, such as estimating wind loads or wind-induced air infiltration (Costola et al., 2009). Several factors, including building shape, the placement of the façade, exposure, and wind directions, affect wind pressure coefficients (Charisi et al., 2019).

Full-scale wind-tunnel measurements are thought to be the most accurate techniques for generating actual wind pressure coefficients (Irtaza et al., 2013). During full-scale measurements, it is not essential to replicate boundary conditions, apply physical models, or do any downscaling (Flay et al., 2013). On the other side, the user can precisely alter the approach flow for wind-tunnel measurements, including wind speed, direction, and turbulence (Allegrini et al., 2014). Full-scale measurements take a lot of work, money, and time to complete. Similar to this, wind tunnel measurements cost a lot of money and require much knowledge. Full-scale studies for assessing wind-induced pressures have previously been carried out in low-rise structures with simple shape (Blocken, 2014). Wind-tunnel tests are a valuable method for establishing wind pressure coefficients because full-scale data have been used to confirm reduced-scale measures, such as those employed in wind tunnel testing, and they have shown agreement (Blocken, 2014). The air fluxes are more accurately calculated using variable Cp values than they are using the standard approach, which uses mean Cp values (Charisi et al., 2019).

Advanced development of computer technology in the recent year in computational fluid dynamics (CFD) gains more advantages for a scaled model with boundary layer tests and becoming an efficient and reliable tool for wind load calculation (Raman et al., 2018). The CFD technique gives more detailed data for a wide range of boundary conditions within a short time and is more cost-effective in comparison to wind tunnel tests (Bendjebbas et al., 2016). The majority of numerical research refers to the basic cube form exposed to wind perpendicular to its face for testing and confirming the correctness of computational evaluations of wind pressures (Stathopoulos, 2002 and 2003). This is related to the cube's simple design, which includes key intricate parts of a real building flow, and the amount of full-scale and experimental results in the literature. Wright and Easom (2003) evaluated the mean pressure coefficient on the surface of the Silsoe cube using the standard k-ε model. However, very few studies have been reported on pressure coefficient calculations of a multi-storied reinforced concrete building using numerical wind tunnel tests.

1.1. Research Significance

Bangladesh National Building Code (BNBC) provides the tools for engineers to calculate the wind pressures for designing the regular-shaped building. Where regular-shaped building properties are defined as (i) building height to minimum lateral dimension ratio not more than 5.0, (ii) building natural frequency in the first mode is equal or more than 1 Hz, (iii) simple diaphragm, and no unusual geometrical irregularity, etc. (BNBC, 2006). Significant modifications of wind load calculation have been suggested in the new building design code BNBC-2020 compared to the previous code BNBC-2006. However, the code does not consider the uneven effects (turbulence, torsional effect, etc.) on the building due to a cross-wind, vortex shedding, and instability for galloping or flutter. Furthermore, special consideration is required for channeling impacts in the wake of upwind obstructions (BNBC, 2020). Calculation of wind load is critical for tall, unusually shaped buildings or buildings located in hurricane-prone areas. The BNBC-2020 recommends performing a wind tunnel test. Wind tunnel testing provides more accurate design information, but it is expensive and time-consuming (Soligo, 2019). Alternatively, numerical simulation of the wind tunnel is an easy and effective tool for engineers to evaluate the design information of the concerned building (Daemei, 2019). Therefore, the present study will help the engineering community to adopt a numerical wind tunnel approach for the design of irregular and high-rise building structures.

1.2. Model Verification

For verification, wind tunnel test results of the Commonwealth Advisory Aeronautical Council (CAARC) building are compared with numerical wind simulation program. The geometrical modelling for the numerical simulation of the CAARC building model was built in a 1:400 scale rigid model, for wind tunnel testing. The building model is rectangular with dimensions of 100.0 ft parallel to the wind, 150.0 ft perpendicular to the wind, and 600.0 ft in height. For the numerical wind tunnel test, the wind tunnel dimensions are 4950.0 ft in the windward direction and 3000.0 ft in the spanwise direction, and the total height is twitching the model size equal to 1200.0 ft. The velocity profile for numerical wind tunnel test in CFD simulation takes the following power-law as equation 1 is exponent of 0.16 for verification test results (Juretić et al., 2013):

$$V_z = V_g \left(\frac{z}{z_g} \right)^{\alpha} \tag{1}$$

The simulation results show a close comparison with the experimental results according to the wind tunnel test on the windward face shown in Figure 1. However, for the sidewall and leeward faces, up to 15% variation between the measured and the calculated data are observed. The differences mainly depend on the boundary mesh and turbulence model.

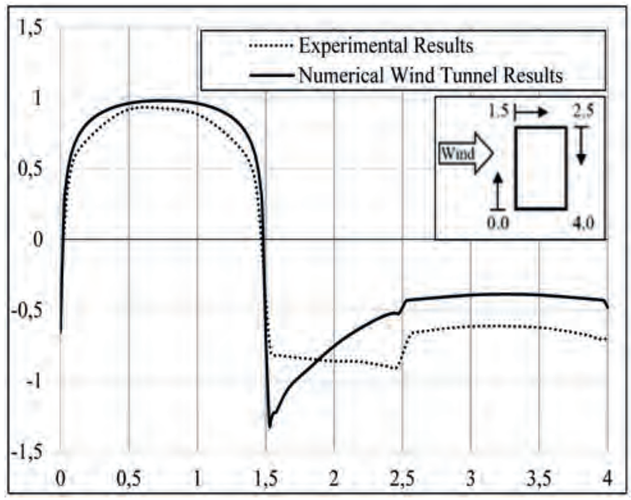

Figure 1. Values of Mean Pressure Coefficients (Cp) over the Perimeter at 2H/3

2. METHODOLOGY

Comparisons are performed with respect to storey shear between the BNBC code values and numerical wind tunnel test data. A numerical wind tunnel test is performed in RWIND shown in Figure 2, which gives the wind pressure coefficients at windward, leeward and side surfaces. The pressure coefficients at 3 and 7 feet of each storey are extracted, and the arithmetic means value for each storey for each vertical panel is calculated.

All the building models are modelled in ETABS, commercial building analysis and design software. Pressure coefficients calculated from the RWIND are assigned to the windward, leeward and two sides surfaces as shown in Figure 3. On each floor, all surface is divided vertically into a number of panels. For each panel pressure coefficient input is given in ETABS. Two sets of pressure coefficients are calculated following the two sets of velocity profiles suggested by BNBC-2006 and BNBC-2020.

On the other hand, constant pressure coefficients are provided on the windward, leeward, and two sides following the BNBC-2006 and BNBC-2020. For analysis purposes, standard dead and live loads are incorporated in ETABS. However, no earthquake load is considered. Concrete compressive strength, reinforcement yield strength, beam and column size are considered as per Table 1. The slab thickness is 150 mm. Analysis of the building structure is performed in ETABS and storey shear is calculated for each storey of the building.

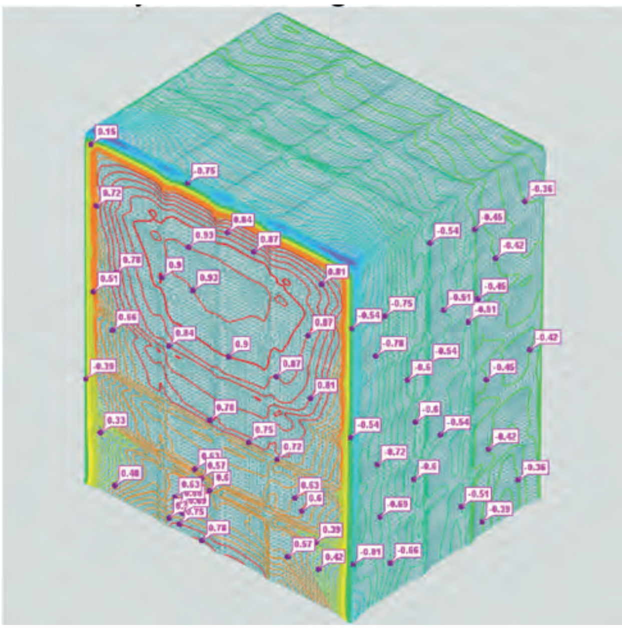

Figure 2. Contours of Cp in the numerical wind tunnel test

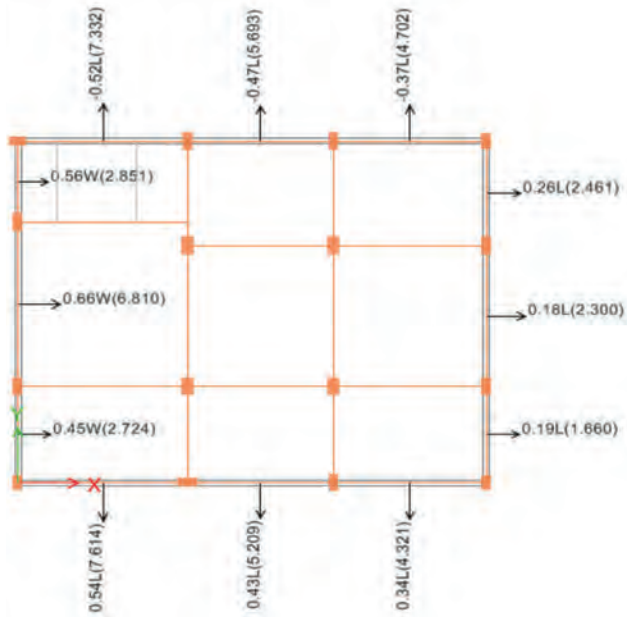

Figure 3. Pressure Coefficient (Cp) is added in ETABS for Analysis

2.1. Building Models

Four reinforced concrete buildings are considered in this study as described in Table 1. Model-01 is a six-storey, Model-02 is a ten-storey, Model-03 is a twenty-storey, and Model-04 is a forty-storey reinforced concrete building and the building geometry considerd as shown in Figure 4. The exposure (terrain) categories applied in this study are A&B according to BNBC-2006 and BNBC-2020 and the buildings are considerd in Dhaka, Bangladesh. For simplicity, the effects of the wind direction, topography, shielding, importance factor, and return period are not considered in the following discussion.

Table 1. Building models

Description	Model-01 (six-storey)	Model-02 (ten-storey)	Model-03 (twenty-storey)	Model-04 (forty-storey)
Plan, B x L [m]	12 x 15	15 x 23	24 x 42	24 x 36
Height, H [m]	18.91	30.05	61.61	122
Storey Height [m]	Ground Floor – 3.66 Typical Floor – 3.05	Ground Floor – 3.05 Typical Floor – 3.05	Ground Floor – 3.66 Typical Floor – 3.05	Ground Floor – 3.05 Typical Floor – 3.05
Materials (ksi)	$f'_c = 3, f_y = 60$	$f'_c = 4, f_y = 60$	$f'_c = 4, f_y = 60$	$f'_c = 4, f_y = 60$
Exposer Category	B	A	A	A
Structure Type	RC Frame Structure	RC Frame Structure	RC Frame Structure	RC Frame Structure
Length-to-width ratio	1.250	1.500	1.795	1.500
Height-to-width ratio	1.550	2.000	2.590	5.000
Corner Columns [mm]	300 x 525	375 x 500	375 x 875	625 x 875
Edge Columns [mm]	300 x 600	375 x 625	375 x 1000	750 x 1000
Central Columns [mm]	375 x 600	500 x 600	500 x 1250	625 x 1250
Beams [mm]	250 x 375	300 x 500	300 x 750	300 x 750

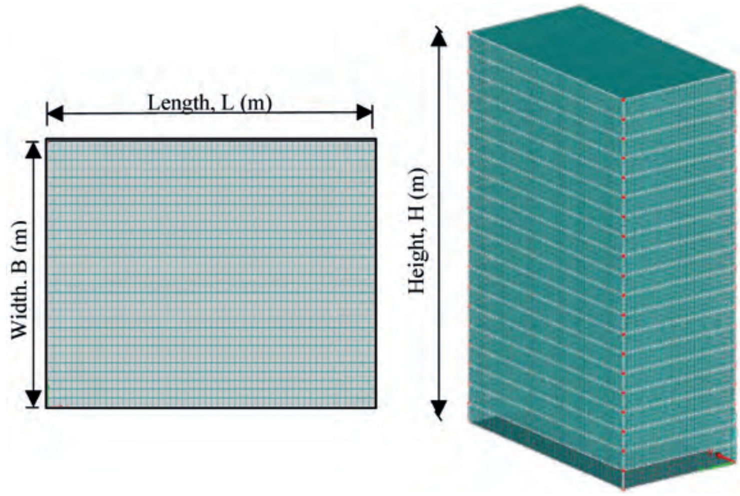

Figure 4. Typical Building Geometry

3. RESULTS AND DISCUSSION

In this study, storey shears for four different reinforced concrete buildings with various numbers of storeys, such as six-storied, ten-storied, twenty-storied and forty-storied, are compared. Building model information is presented in Section 2. Storey shears following BNBC-2006 and BNBC-2020 are calculated using ETABS.

3.1. Model-01 (six-storied structure)

The comparison of the storey shear in the long and short directions for the six-storied building can be seen in Figure 5. For the first storey, the storey shear increased with an increase in height. Above that, the storey shear decreased gradually with an increase in height. Furthermore, BNBC-2020 and BNBC-2006 showed a considerable variation in calculating the storey shear. The storey-wise variation ranged from 50.0% to 53.5% with a mean variation of 51.4% in the long direction, while the variation range was 45.7% to 49.4% with a mean variation of 47.1% in the short direction.

The variation in storey shear for the numerical wind tunnel test (NWTT) using the BNBC-2020 velocity profile and BNBC-2020 manual is smaller compared to the variation in storey shear for the NWTT using the BNBC-2006 velocity profile and BNBC-2006 manual. Storey-wise variation of storey shear between the NWTT of BNBC 2020 with the BNBC-2020 manual calculation ranged from 15.3%

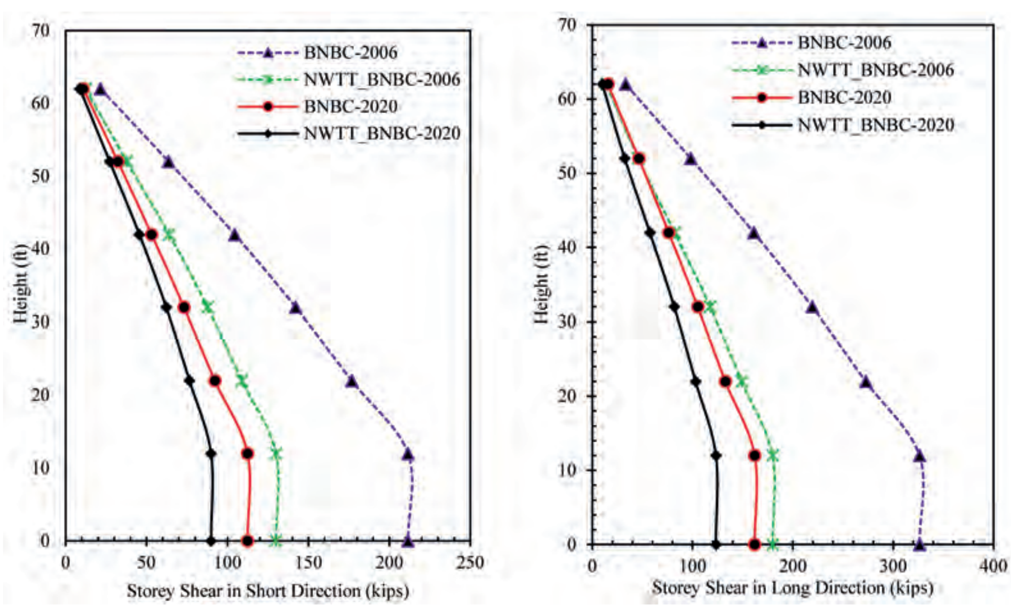

Figure 5. Storey shear along the short and long directions for model-01 (six-storied structure)

to 25.6% in the long direction with a mean of 19.5%, and 12.8% to 22.5% with a mean of 16.7% in the short direction. While the variation between the NWTT of BNBC 2006 with the BNBC-2006 manual calculation ranged from 40.9% to 45.3% in the long direction with a mean of 43.1%, and 33.8% to 38.4% with a mean of 36.2% in the short direction.

3.2. Model-02 (ten-storied structure)

The comparison of the storey shear in both directions of the ten-storied building can be seen in Figure 6. For the first storey, the storey shear increased with an increase in height. Above that, the storey shear decreased gradually with an increase in height. As observed in Figure 8, BNBC-2020 and BNBC-2006 showed significant fluctuations in calculating the storey shear. The storey-wise variation ranged from 43.6% to 51.6% with a mean variation of 47.2% in the long direction, while the variation range was 32.9% to 41.8% with a mean variation of 36.9% in the short direction.

The NWTT using the BNBC-2020 velocity profile showed relatively small fluctuations with the BNBC-2020 manual compared to the fluctuations observed between the storey shear for the NWTT with the BNBC-2006 velocity profile and the BNBC-2006 manual. Storey-wise variation of shear force between the NWTT of BNBC-2020 with the BNBC-2020 manual, ranged from 22.2% to 34.6% in the long direction with a mean of 28.3%, and 26.9% to 37.7% with a mean of 31.6% in the short direction. While the variation between the NWTT of BNBC 2006 with the BNBC-2006 manual, ranged from 49.4% to 58.1% in the long direction with a mean of 52.5% and 44.0% to 49.7% with a mean of 46.55 in the short direction.

3.3. Model-03 (twenty-storied structure)

The storey shear in short and long directions for a twenty-storied typical reinforced concrete building is displayed in Figure 7. Overall, the storey shear decreases with an increase in height. As observed from the figure, BNBC-2020 and BNBC-2006 showed a considerable variation in calculating the storey shear. The storey-wise variation ranged from 45.9% to 60% with a mean variation of 52.3% in the long direction, while the variation ranged from 36.5% to 52.1% with a mean variation of 43.4% in the short direction. The NWTT using the BNBC-2020 velocity profile showed a relatively small variation with the BNBC-2020 manual in comparison to the variation from the NWTT using the BNBC-2006 profile and the BNBC-2006 manual.

Storey-wise variation of wind pressure coefficient between the NWTT with BNBC-2020 with the BNBC-2020 manual, ranged from 23.6% to 40.1% in the long direction with a mean of 30.1%, and 27.5% to 42.9% with a mean of 33.4% in the short direction. On the other hand, the variation between the NWTT with BNBC-2006 with the BNBC-2006 manual, ranged from 51.4% to 64.4% percent in the long direction with a mean of 54.0%, and 48.4% to 60.3% with a mean of 50.7% in the short direction.

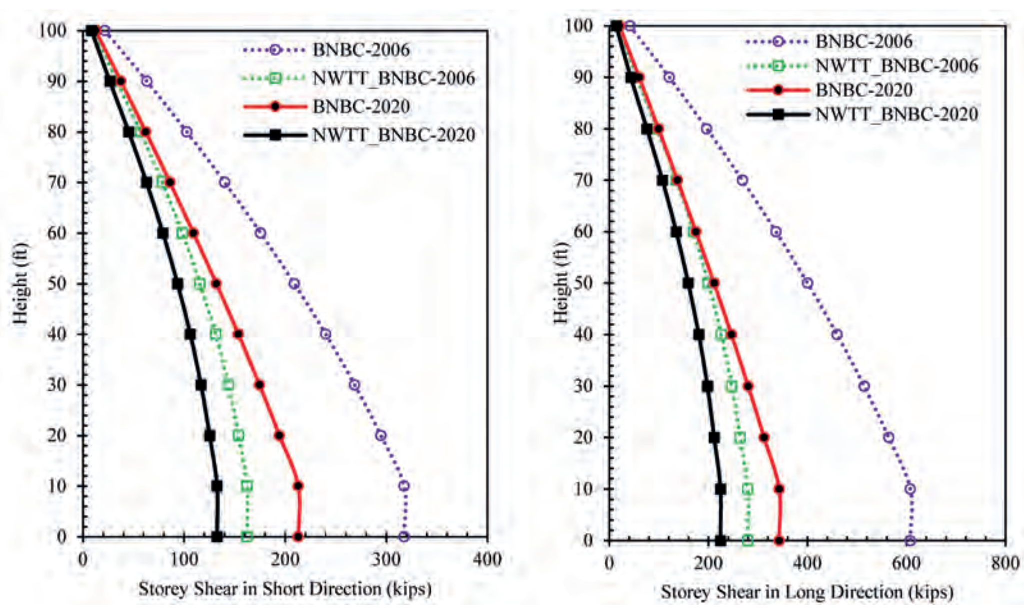

Figure 6. Storey shear variation in the short and long directions for model-02 (ten-storied structure)

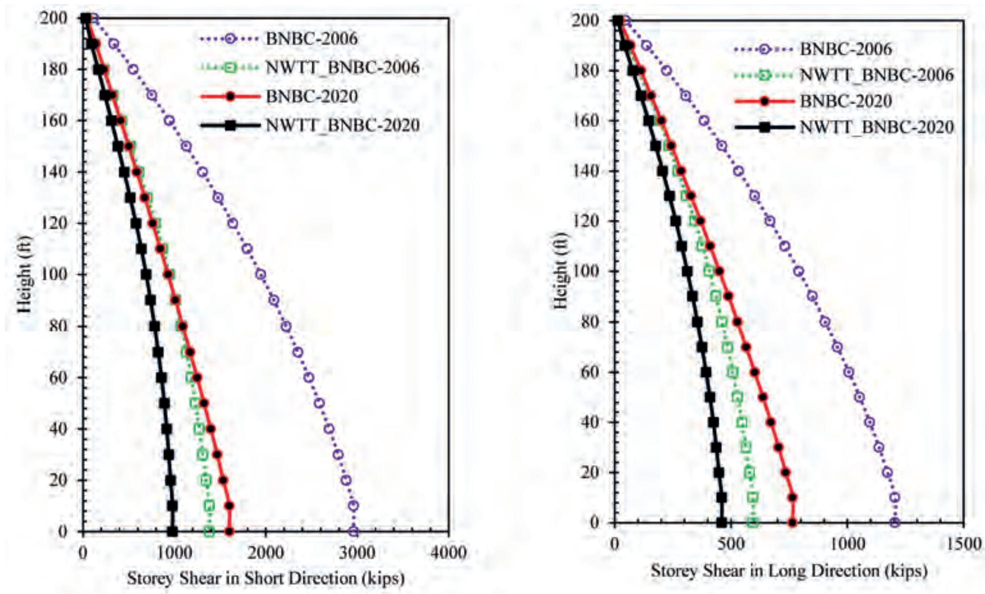

Figure 7. Storey shear along short and long directions for model-03 (twenty-storied structure)

3.4. Model-04 (forty-storied structure)

The storey shear in short and long directions of a typical forty-storied structure is seen in Figure 8. In general, the storey shear decreases with an increase in height. The BNBC-2020 and BNBC-2006 showed a considerable variation in calculating the storey shear. The storey-wise variation ranged from 50.0% to 56.9% with a mean variation of 54.0% in the long direction, while the variation ranged from 35.2% to 43.5% with a mean variation of 40.0% in the short direction.

The NWTT using the BNBC-2020 velocity profile showed a relatively small variation with the BNBC-2020 manual in comparison to the variation from NWTT using the BNBC-2006 velocity profile with the BNBC-2006 manual. Storey-wise variation of storey shear between the NWTT of BNBC-2020 with the BNBC-2020 manual, ranged from 22.4% to 47.5% in the long direction with a mean of 28.9%, and 22.0% to 43.5% with a mean of 40.0% in the short direction. Furthermore, the variation between the NWTT of BNBC-2006 with the BNBC-2006

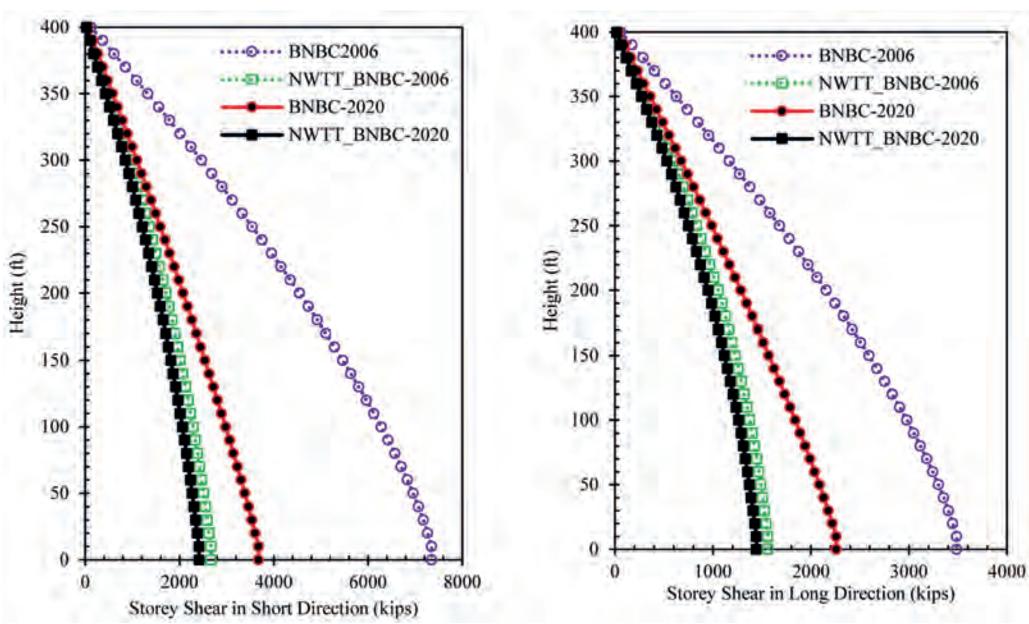

Figure 8. Storey shear along short and long direction for model-04 (forty-storied structure)

manual ranged from 60.9% to 74.2% in the long direction with a mean of 63.5% and 48.9% to 64.8% with a mean of 52.9% in the short direction.

4. CONCLUSIONS

In the present study, storey shear for four different heights of buildings was compared while using wind pressure coefficient from BNBC-2006 and BNBC-2020, and numerical wind tunnel test (NWTT). The summary of the findings is presented here.

1. The NWTT can forecast the results of wind tunnel experiments. Experimental and numerical wind tunnel test data are quite close on the windward face. However, up to 15% variance is recorded on the leeward and side faces.
2. BNBC-2020, NWTT (BNBC-2020), and NWTT (BNBC-2006) showed relatively similar story shear for all the models, however, the BNBC-2006 showed higher than among all. Analysis of the four different storied structures reveals that BNBC-2006 give up to 60% (around) higher storey shear compared to the BNBC-2020. The average variation of story shear among the BNBC-2020, NWTT (BNBC-2020), and NWTT (BNBC-2006) are around 12%.
3. The present study reveals that BNBC-2006 overestimates the storey share by 1.4 times. Therefore, it may be of interest for the designer to adopt a numerical wind tunnel test for the high-rise building wind load analysis or should stict to the BNBC 2020 atleast, rather than using the fixed wind load coefficient proposed by the code BNBC 2006, which is the older version.

REFERENCES

[1] Abdi D.S., Bitsuamlak, G.T., (2016), *Wind flow simulations in idealized and real built environments with models of various level of complexity*. Wind and Structures, 22(4), 503-524. https://doi.org/10.12989/was.2016.22.4.503.

[2] Abdullah F., Islam Z., Asif M.A.T., Ali S., (2021), *A Comparative Study of Lateral Load Analysis Considering Two BNBC Codes Using ETABS Software*, American Journal of Civil Engineering, 9(4), 118-126, https://doi.org/10.11648/j.ajce.20210904.13.

[3] Allegrini J., Dorer V., Carmeliet J., (2014), *Buoyant flows in street canyons: Validation of CFD simulations with wind tunnel measurements*, Building and Environment, 72, 63-74. https://doi.org/10.1016/j.buildenv.2013.10.021.

[4] ASCE/SEI 7-10. (2010), Minimum design loads for buildings and other structures. In American Society of Civil Engineers.

[5] Bangladesh National Building Code, BNBC, 2006, Housing and Building Research Institute and Bangladesh Standard and Testing Institute, Bangladesh.

[6] Bangladesh National Building Code, BNBC, 2020, Housing and Building Research Institute and Bangladesh Standard and Testing Institute, Bangladesh.

[7] Barlow J.B., Rae W.H., Pope A., (1999), *Low-speed wind tunnel testing*. John Wiley & Sons.

[8] Bendjebbas H., Abdellah-ElHadj A., Abbas M., (2016), *Full-scale, wind tunnel and CFD analysis methods of wind loads on heliostats: A review*. Renewable and Sustainable Energy Reviews, 54, 452-472, https://doi.org/10.1016/j.rser.2015.10.031.

[9] Braun A.L., Awruch A.M., (2009), *Aerodynamic and aeroelastic analyses on the CAARC standard tall building model using numerical simulation*, Computers & Structures, 87(9-10), 564-581, https://doi.org/10.1016/j.compstruc.2009.02.002.

[10] Charisi S., Thiis T.K., Aurlien T., (2019), *Full-scale measurements of wind-pressure coefficients in twin medium-rise buildings*, Buildings, 9(3), 63, https://doi.org/10.3390/buildings9030063.

[11] Computers and Structures Inc., (2022). ETABS Integrated Software for Structural Analysis and Design. [Online] Available: https://www.csiamerica.com/products/etabs. [10 January 2022].

[12] Costola D., Blocken B., Hensen J.L.M., (2009), *Overview of pressure coefficient data in building energy simulation and airflow network programs*, Building and Environment, 44(10), 2027-2036, https://doi.org/10.1016/j.buildenv.2009.02.006.

[13] Dlubal Software GmbH, (2022), RWIND Simulation, Wind Simulation (Wind Tunnel), [Online] Available: https://www.dlubal.com/en/products/stand-alone-structural-analysis-software/rwind-simulation. [6 March 2022].

[14] Douvi C.E., Tsavalos I.A., Margaris P.D., (2012), E*valuation of the turbulence models for the simulation of the flow over a National Advisory Committee for Aeronautics (NACA) 0012 airfoil*. Journal of Mechanical Engineering Research, 4(3), 100-111. https://doi.org/10.5897/jmer11.074.

[15] El-Behery S.M., Hamed M.H., (2011), *A comparative study of turbulence models performance for separating flow in a planar asymmetric diffuser*. Computers & Fluids, 44(1), 248-257, https://doi.org/10.1016/j.compfluid.2011.01.009.

[16] Flay R.G., Carpenter P., Revell, M., Cenek, P., Turner, R., King, A., (2013), *Full-scale wind engineering measurements in New Zealand*, In The 8th Asia-Pacific conference on wind engineering, (pp. 10-14), https://doi.org/10.3850/978-981-07-8012-8_key-09.

[17] Fouad N.S., Mahmoud G.H., Nasr N.E., (2018), *Comparative study of international codes wind loads and CFD results for low rise buildings*. Alexandria Engineering Journal, 57(4), 3623-3639, https://doi.org/10.1016/j.aej.2017.11.023

[18] Hasan M., Debnath S., Akther A., (2022), *Comparative Study of Lateral Loads and Its Cost Effect on RC* Moment Frame and Wall-frame Building According to BNBC 2020 in Different Zones of Bangladesh.

[19] Irtaza H., Beale R.G., Godley M.H.R., Jameel A., (2013), *Comparison of wind pressure measurements on Silsoe experimental building from full-scale observation, wind-tunnel experiments and various CFD techniques*. International Journal of Engineering, Science and Technology, 5(1), 28-41, https://doi.org/10.4314/ijest.v5i1.3.

[20] Juretić F., Kozmar H., (2013), *Computational modeling of the neutrally stratified atmospheric boundary layer flow using the standard k–ε turbulence model,* Journal of Wind Engineering and Industrial Aerodynamics, 115, 112-120, https://doi.org/10.1016/j.jweia.2013.01.011.

[21] Liu Z., Chen J., Xia Y., Zheng Y., (2021), *Automatic sizing functions for unstructured mesh generation revisited.* Engineering Computations, https://doi.org/10.1108/ec-12-2020-0700.

[22] Tan H., Pillai K.M., (2009), *Finite element implementation of stress-jump and stress-continuity conditions at porous-medium, clear-fluid interface*. Computers & Fluids, 38(6), 1118-1131, https://doi.org/10.1016/j.compfluid.2008.11.006.

[23] Vino G., Watkins S., Mousley P., Watmuff J., Prasad S., (2005), *Flow structures in the near-wake of the Ahmed model*. Journal of Fluids and Structures, 20(5), 673-695, https://doi.org/10.1016/j.jfluidstructs.2005.03.006.

Acknowledgement

The authors would like to thank the Department of Civil Engineering of the Military Institute of Science and Technology for its support.

Dzukogi, Usman Abubakar, Yusuf Alapata, Ahmed
Structure and Environment 2023, vol. 15, (2), pp. 82-89, Article number: el 008
https://doi.org/10.30540/sae-2023-008

Structure and Environment
ISSN 2081-1500
e-ISSN 2657-6902
https://content.sciendo.com/sae
https://sae.tu.kielce.pl

sciendo

Kielce University of Technology

DOI: 10.30540/sae-2023-008

FACTORS RESPONSIBLE FOR SOCIO-SPATIAL SEGREGATION IN THE HOUSING NEIGHBOURHOODS OF MINNA, NIGERIA

CZYNNIKI ODPOWIEDZIALNE ZA SEGREGACJĘ SPOŁECZNO-PRZESTRZENNĄ W DZIELNICACH MIESZKANIOWYCH MIASTA MINNA W NIGERII

Dzukogi, Usman Abubakar*
The Federal Polytechnic Bida, Nigeria

Yusuf Alapata, Ahmed
University of Ilorin Nigeria

Abstract

Segregation in the housing sector has exposed urban dwellers to series of unfavourable conditions in most cities of developing countries, which are as a result several factors. This paper is aimed at examining the factors influencing segregation in the housing neighbourhoods of Minna, Nigeria. Two-stage cluster sampling methods were adopted in the selection of neighbourhoods and households across the entire sample frame in the administration of 374 questionnaires across the 25 clustered neighbourhoods. Chi-square and Relative Importance Index (RII) as well as mean score to determine neighbourhood geographical segregation indicators pattern across all the 25 neighbourhoods in the study area. The study established that there is a significant difference between low, medium, and high density neighbourhoods in terms segregation factors in the study area. It was therefore suggested that a good urban governance structure should be put in place that will discourage class divisions among spatial entities of the city.

Keywords: segregation, factors, urban space, neighbourhoods, housing

Streszczenie

W większości miast krajów rozwijających się segregacja w sektorze mieszkaniowym postawiła mieszkańców miast w obliczu szeregu niekorzystnych warunków, wynikających z kilku czynników. Niniejszy artykuł ma na celu zbadanie czynników wpływających na segregację w dzielnicach mieszkaniowych miasta Minna w Nigerii. Zastosowano dwuetapowe metody próbkowania klastrowego w doborze dzielnic i gospodarstw domowych w całym operacie losowania w celu rozdania 374 kwestionariuszy w 25 klastrach dzielnic. Wykorzystano wskaźnik chi-kwadrat i wskaźnik względnego znaczenia (RII), a także średni wynik w celu określenia wzorca wskaźników segregacji geograficznej we wszystkich 25 dzielnicach na badanym obszarze. Badanie wykazało, że istnieje znacząca różnica między dzielnicami o niskiej, średniej i wysokiej gęstości zaludnienia pod kątem czynników segregacji na badanym obszarze. W związku z tym zasugerowano, że należy wprowadzić dobrą strukturę zarządzania miastem, która zniechęci do podziałów klasowych między jednostkami przestrzennymi miasta.

Słowa kluczowe: segregacja, czynniki, przestrzeń miejska, dzielnice, mieszkalnictwo

*The Federal Polytechnic Bida, Nigeria, e-mail: usmandzukogi@gmail.com

1. INTRODUCTION

Housing segregation is generally understood to be the concentration of ethnic, national-origin, or socioeconomic groups in given neighbourhoods of a city or metropolitan area (Iceland, 2014). Kemper (1998a, 1998b) cited in Muhammad, Kasim, and Martin (2015a) viewed housing segregation as a spatial separation of population sub-groups within a specific geographical area like a large city. Such sub-groups can be defined formally in terms of age, occupation, income, birthplace, ethnic origin or other measures; or they could equally be specified as social minorities separated from the dominant groups of power differentials (Berkes Gaetani, 2019). Although, segregation is an innately spatial concept, the geographical dimension of social segregation is understood and analysed using quite simple spatial descriptions theories on the relation between spatial and social phenomena (Legeby, 2010).

Segregation in the housing sector has exposed urban dwellers to series of unfavourable conditions in most cities of developing countries, which resulted in series of infringement on their opportunities, prospects and welfare (Seethaler-Wari, 2018; Dzukogi et al., 2022). This enhances physical and social depletion of neighbourhoods, growing poverty, isolations, slum and squatter development, underemployment, and susceptibility to crimes and toxic pollutants (Aliyu et al., 2012; Muhammad, Kasim, Martin, 2015a; Muhammad, Kasim, Martin, et al., 2015). Residential segregation is a situation where population groups are sorted into various neighbouhood context and shapes within an environment living and social space, classifying inhabitants on numbers of unique peculiarities like race/ethnicity, religion and economic/social status of individuals and groups within the population (Muhammad, Kasim, Martin, 2015b).

Contrary to the faster and more complex process of recent urbanization, spatial segregation, inequality and separation is on the rise (Schütz, 2014; Aliyu et al., 2020). The influencing factors of segregation are complex and differ from place to place. The complexity starts with the fact that segregation can be coercive or in other cases, sought by marginalized groups (Schütz, 2014). Deliberate segregation can happen either in order to strengthen their community or because of fear from violence and pandemics. Recently, COVID-19 pandemic has exposed some of the segregations in the global cities (Mohammed et al., 2021).

Recently, it has become lucid that the issue of segregation in the housing neighbourhoods of developing world has become apparent and increasingly is on the rise. In the urban areas of the developing world, different groups are geographically, economically and socially separated (Catney, 2015). In most developing world cities, housing segregations are based on ethnicity, income, occupational structure, nationality, political affiliation, religion and the likes (Muhammad et al., 2018). This is common in South African cities (Rodrigues, 2009). Other contributing factors of segregation are: gaps in income, obsolete legal frameworks, marginalization and stigmatization of an area (UN Habitat, 2001).

In Nigeria, housing segregation existed prior to the arrival of colonialist (Aliyu et al., 2012; Muhammad, Kasim, Martin, 2015a). Housing segregation before the British colonial rule was based on political class not income, ethnicity or race, for example, people of diverse tribes and nationals cohabited in the north. The colonial administrators' form of housing segregation brought about the emergence of the Sabon Gari and Tudun Wada settlements (new towns) which housed the southern Nigerians living in the north and northern Nigerians living in the south respectively.

Several factors influence residential segregation in Nigeria as observed by Mohammed et al. (2015b), separation and differentiation of neighbourhoods surfaced along the line of ethnicity, and religious affiliation in the past and recently enhanced by individual aggregate socioeconomic characteristics, preference, choice and taste of neighbourhood all showing a significant relationship and influencing residential segregation. Minna is not an exception to this phenomenon (Mohammed et al., 2019). It is on this that the paper examines the factors influencing segregation in the housing neighbourhoods of Minna, Nigeria.

2. METHODOLOGY

2.1. Study Area

Minna, the capital city of Niger State and a renowned railway town, is located at approximately latitude 9°71' North and longitude 6°33' East. Over the years, the town has undergone a significant transformation from a small traditional settlement to a bustling urban center, equipped with modern facilities and amenities. The total population of Minna is estimated to be around 201,429 people, out of the total population of Niger State, which stands at 3,950,249, with an annual growth rate of 2.3% (NPC, 2006). The town is composed of 25 neighborhoods, including Bosso Town, Shango, Sauka Kahuta, Barkin Sale, Kpakungu, Minna central, Tudun Fulani, Chanchaga, Bosso

Estate, Tayi Village, Angwan Daji, Tunga, Tudun Wada North, Tudun Wada South, Makera, Sabon Gari, Maitumbi, Nassarawa, F-Layout, Limawa, Fadikpe, GRA, Dutsen Kura Hausa, Dutsen Kura Kwari and Tungan Goro, as presented in Figure 1.

2.2. Data and Analysis

This empirical research employed a survey research method to collect primary data on the factors influencing urban segregation. The data was collected based on the research structure, taking into account the number of segregation indicators. The selection of neighbourhoods and households was carried out using a two-stage cluster sampling method, and a sample of 374 households was selected across 25 clustered neighbourhoods. The primary data was collected through various means, including field survey, physical observations and measurements, and questionnaire administration. The data generated included population, ethnic composition, employment status, household income, occupation, education level, gender, age, religion, housing occupation status, political affiliation, rental value, indigene status, family size, social inclination, infrastructure, general health status, crime rate, and security.

The study measured various factors influencing segregation, including mean score and Relative Importance Index (RII) for individual and aggregate socioeconomic characteristics, neighbourhood choice or preferences, physical characteristics of the urban environment, and political/institutional factors. The study then used Chi-square to test the significant difference between low, medium and high densities based on the outcomes of the RII of the factors influencing urban segregation.

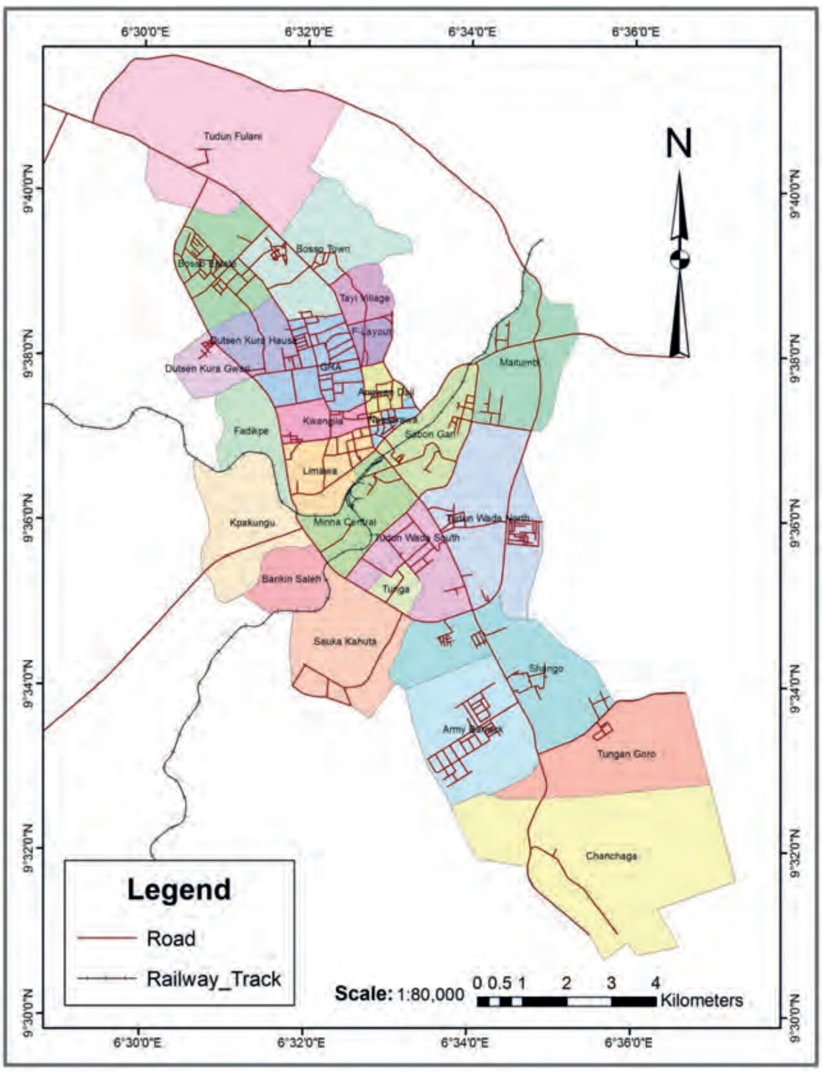

Figure 1. Research sample points

Source: Niger State Ministry of Lands and Housing, 2018.

3. FINDINGS

3.1. Physical characteristics of the urban environment

The result in Table 1 indicates that the factors under the physical characteristics of the urban environment influence urban segregation differently across low, medium and high density neighbourhoods of Minna. RII of these factors (physical characteristics of the urban environment) revealed that they influence residential segregation in low density except for topography which has less influence with RII of 0.473. Similarly, in the medium density all the physical characteristics of the urban environment influence urban segregation except condition of road and topography with RII of 0.472 and 0.376 respectively. The implication of this finding is that topography have less influence on urban segregation, this is because in Minna, topography is not a setback for development as most part of the city is characterised with hills and all densities could be found in such areas. The study also revealed that in high density neighbourhoods, almost all physical characteristics of the urban environment has less influence on urban segregation.

Table 1. Physical characteristics of the urban environment

Density	Variables	N	Mean	RII
Low density	The physical layout	33	4.58	0.915
	Accessibility	33	4.46	0.891
	Condition of roads	33	4.00	0.8
	Drainage condition	33	3.85	0.77
	Density	33	4.49	0.897
	Topography	33	2.36	0.473
	Type of housing	33	4.36	0.873
Medium density	The physical layout	83	3.63	0.725
	Accessibility	83	4.23	0.846
	Condition of roads	83	2.36	0.472
	Drainage condition	83	3.24	0.648
	Density	83	2.65	0.53
	Topography	83	1.88	0.376
	Type of housing	83	3.02	0.605
High density	The physical layout	257	1.86	0.371
	Accessibility	257	1.51	0.302
	Condition of roads	257	1.76	0.351
	Drainage condition	257	2.75	0.55
	Density	257	1.64	0.328
	Topography	257	1.51	0.301
	Type of housing	257	1.77	0.353

Source: Field survey, 2020.

The outcomes of the RII of the physical characteristics of the urban environment as factors influencing urban segregation were tested to ascertain the significant difference between low, medium and high densities in Minna and the result is shown in Table 2. The chi-square calculated value of 42.00 and *p* value of 0.227 were obtained for the difference between low and medium densities, low and high densities and medium and high densities respectively. The chi-sqaure *p* value is greater than the 5 percent (0.05); therefore the result indicates that there is statistically significant difference between low, medium and high densities in terms of physical characteristics of the urban environment as a factor influencing urban segregation.

Table 2. Chi-squared tests for physical characteristics of the urban environment

	Value	df	p
High and Low Densities			
X^2	42.00	36	0.227
N	7		
High and Medium Densities			
X^2	42.00	36	0.227
N	7		
Medium and Low Densities			
X^2	42.00	36	0.227
N	7		

3.2. Individual and aggregate socioeconomic characteristics

The findings of this study revealed in Table 3 that some factors under individual and aggregate socioeconomic characteristics influence housing segregation in the city of Minna. It reveals clearly that family status determines people's choice of where to live in the low density neighbourhoods with an RII value of 0.903. In the low density neighbourhoods, income is the second most influential factor that determines choice of neighbourhoods of residence with RII of 0.806.

In the medium density neighbourhoods, ethnicity accounts for an RII of 0.795 which is the most influential factor under individual and aggregate socioeconomic characteristics. This is followed by income which accounts for an RII of 0.745. In the high density, ethnicity account for highest RII with 0.914, followed by indigene with 0.861 RII, and religion and language spoken with RII of 0.858 each respectively.

It can be deduced from the finding that income clearly influences choice of neighbourhoods of residence in all densities of Minna. It is also clear that ethnicity and language spoken highly influenced choice of neighbourhoods of residence in the medium and high densities. It can also be deduced that religion highly influenced choice of neighbourhoods of residence in the high densities of Minna.

Table 3. Individual and aggregate socioeconomic characteristics

Density	Variables	N	Mean	RII
Low density	Sex	33	1.24	0.248
	Age	33	1.55	0.309
	Religion	33	2.58	0.515
	Income	33	4.03	0.806
	Ethnicity	33	2.76	0.552
	Family status	33	4.52	0.903
	Language spoken	33	3.12	0.624
	Ancestor	33	1.21	0.242
	Indigene	33	3.39	0.679
	Non-indigene	33	2.33	0.467
Medium density	Sex	83	1.33	0.265
	Age	83	1.30	0.26
	Religion	83	2.96	0.593
	Income	83	3.72	0.745
	Ethnicity	83	3.98	0.795
	Family status	83	2.69	0.537
	Language spoken	83	3.27	0.653
	Ancestor	83	2.90	0.581
	Indigene	83	2.55	0.511
	Non-indigene	83	2.71	0.542
High density	Sex	257	1.60	0.321
	Age	257	1.67	0.334
	Religion	257	4.29	0.858
	Income	257	3.60	0.719
	Ethnicity	257	4.57	0.914
	Family status	257	3.94	0.788
	Language spoken	257	4.29	0.858
	Ancestor	257	3.84	0.768
	Indigene	257	4.31	0.861
	Non-indigene	357	2.29	0.458

Source: Field survey, 2020.

The chi-square test in Table 4 shows a calculated value of 80.00 for high and low densities and high and medium densities respectively, and calculated value of 90.00 for medium and low densities. The calculated *p* value of 0.242 were obtained for high and low densities and high and medium densities. For medium and low densities, calculated *p* value of 0.231 was obtained. All the chi-square *p* values were greater than 0.05, which indicates statistically significant difference among the low, medium and high densities in term of individual and aggregate socioeconomic characteristics as factors responsible for the choice of neighbourhood of residence.

Table 4. Chi-squared tests for individual and aggregate socioeconomic characteristics

	Value	df	p
High and Low Densities			
X^2	80.00	72	0.242
N	10		
High and Medium Densities			
X^2	80.00	72	0.242
N	10		
Medium and Low Densities			
X^2	90.00	81	0.231
N	10		

3.3. Individual preferences of neighbourhood

The analysis of factors under individual preferences/choice of neighbourhood shows that in the low density neighbourhoods only three factors in Table 5 highly influence urban segregation which includes adequate security, ease of transportation and adequate electricity with RII value of 0.897, 0.873 and 0.83 respectively.

In the medium density neighbourhoods of Minna, the findings revealed that proximity to markets and shopping malls, availability of health care facility and adequate electricity were strong factors that determines the choice of neighbourhoods by the residence which amount to RII of 0.761 for proximity to markets and shopping malls, 0.728 for availability of health facilities and 0.704 for adequate electricity.

In contrast, the finding revealed in the table that proximity to place of worship is most determinants factor for the choice of neighbourhood of residents with RII of 0.925. Another factor under individual preference of neighbourhood that is high is housing affordability with RII of 0.899. However, for the both medium and high densities, proximity to markets and shopping malls were important factors that influence individual's choice of neighbourhood of residence.

Table 5. Individual preferences of neighbourhood

Density	Variables	N	Mean	RII
Low density	Various ethnic groups living in the neighbourhood	33	2.12	0.424
	Quality and accessibility of schools around	33	2.39	0.479
	Near to place of work	33	1.85	0.37
	Houses are affordable	33	1.70	0.339
	Ease of transportation	33	4.36	0.873
	Proximity to markets and shopping malls	33	2.27	0.455
	Proximity to place of worship	33	1.88	0.376
	Adequate electricity	33	4.15	0.83
	Availability of health care facility	33	2.70	0.539
	Adequate security	33	4.49	0.897
Medium density	Various ethnic groups living in the neighbourhood	83	2.82	0.564
	Quality and accessibility of schools around	83	3.39	0.677
	Near to place of work	83	3.19	0.639
	Houses are affordable	83	2.58	0.516
	Ease of transportation	83	3.41	0.682
	Proximity to markets and shopping malls	83	3.81	0.761
	Proximity to place of worship	83	2.34	0.467
	Adequate electricity	83	3.52	0.704
	Availability of health care facility	83	3.64	0.728
	Adequate security	83	3.24	0.648
High density	Various ethnic groups living in the neighbourhood	257	2.16	0.431
	Quality and accessibility of schools around	257	1.78	0.356
	Near to place of work	257	4.13	0.826
	Houses are affordable	257	4.49	0.899
	Ease of transportation	257	1.57	0.314
	Proximity to markets and shopping malls	257	4.22	0.844
	Proximity to place of worship	257	4.63	0.925
	Adequate electricity	257	1.50	0.3
	Availability of health care facility	257	1.78	0.356
	Adequate security	257	1.81	0.361

Source: Field survey, 2020.

The chi-square test in Table 6 shows a calculated value of 80.00 for high and low densities and high and medium densities respectively, and calculated value of 9.00 for medium and low densities. The calculated *p* value of 0.242 were obtained for high and low densities and high and medium densities. For medium and low densities, calculated *p* value of 0.231 was obtained. All the calculated *p* values were above 5% (i.e. 0.05), therefore, there is statistically significant difference among all densities in terms of individual preferences of neighbourhoods.

Table 6. Chi-squared tests for individual preferences of neighbourhood

	Value	df	p
High and low densities			
X^2	80.00	72	0.242
N	10		
High and medium densities			
X^2	80.00	72	0.242
N	10		
Medium and low densities			
X^2	90.00	81	0.231
N	10		

3.4. Political/institutional factors

The study revealed in Table 7 that most of the political and institutional factors do not influence urban segregation in the medium and high density neighbourhood in the study area. However, rental price influence the choice of neighbourhood of residence in the medium and high densities with RII of 0.872 and 0.932 respectively.

In the low density neighbourhoods, local housing policies, zoning laws and estate agent advise influence the residence choice of their neighbourhoods with RII of 0.836, 0.836 and 0.624 respectively.

Table 7. Political/institutional factors

Density	Variables	N	Mean	RII
Low density	Local housing policies	33	4.18	0.836
	Zoning laws	33	4.18	0.836
	Estate agent advise	33	3.12	0.624
	Rental price	33	1.88	0.376
Medium density	Local housing policies	83	2.31	0.463
	Zoning laws	83	2.48	0.496
	Estate agent advise	83	3.00	0.6
	Rental price	83	4.36	0.872
High density	Local housing policies	257	1.25	0.25
	Zoning laws	257	1.27	0.254
	Estate agent advise	257	1.32	0.263
	Rental price	257	4.66	0.932

Source: Field survey, 2020.

The chi-square analysis revealed in Table 8 that a calculated value of 8.00 for high and low densities and medium and low densities respectively, and calculated value of 12.00 for high and medium densities. The calculated *p* value of 0.238 were obtained for high and low densities and medium and low densities. For high and medium densities, *p* value of 0.213 was obtained. All the *p* value of the chi-square table were above 0.05 and therefore, there is a significant statistical difference between the low, medium and high densities in terms of political/institutional factors responsible for the residence choice of neighbourhoods.

Table 8. Chi-squared tests for political/institutional factors

	Value	df	P
High and low densities			
X^2	8.00	6	0.238
N	4		
High and medium densities			
X^2	12.00	9	0.213
N	4		
Medium and low densities			
X^2	8.00	6	0.238
N	4		

4. DISCUSSIONS

As presented by the result of this study, the physical characteristics of urban environment greatly influence urban segregation in different ways across all residential density of Minna. It was revealed by the RII of the physical factors that all other factors influence segregation in the low density neighbourhoods except topography with 0.473 RII while round condition and topography was found to be influencing factor of segregation in medium density with 0.472 and 0.376 RI respectively. It can therefore be said that topography is a physical characteristics of urban settlement with less effect on segregation owing to the fact that it is not a setback for development in Minna as the city is characterised with hills where all densities could be found. The study also revealed that in high density neighbourhoods, almost all physical characteristics of the urban environment has less influence on urban segregation.

In the low residential neighbourhoods of Manna with a RII of 0.903, it was revealed that the family socioeconomic status determines individual family's choice of where to live with income being the second most influential factor having 0.806 RII. However, ethnicity accounted for an RII of 0.795 under individual and aggregate socioeconomic characteristics in medium density neighbourhoods with income following suit at 0.914 RII. The highest RII of 0.914 was recorded for ethnicity in the high density neighbourhoods followed by indigene with 0.861 and religion as well as spoken language with 0.858 RII respectively. This indicated that income is a common influencing factor for choice of neighbourhoods in all densities of Minna while it was clearly revealed that ethnicity and religion influences choice of neighbourhood residence in medium and high densities while religion greatly influences high densities choice of neighbourhood residence in Minna. This finding is similar to that of Muhammad et al. (2015b) where individual preference and socioeconomic characteristics were the leading factors influencing segregation in Bauchi city of Nigeria.

In relation to individual preference and choice of neighbourhood as an influencing factor of segregation, results shows that adequate security, constant power supply and ease of transportation are the three main factors determining urban segregation while for the medium density neighbourhoods, nearness to market and commercial centres, availability of healthcare facilities and adequate power supply are key determinants of choice of neighbourhoods by the residence. However, proximity to place of worships and housing affordability is the highest influencing factor of neighbourhood choice by residents of high density areas of Minna. However, for the both medium and high densities, proximity to markets and shopping malls were important factors that influence individual's choice of neighbourhood of residence.

Furthermore, it was evident from the findings that political and institutional factors plays no role in enhancing urban segregation in the medium and high density neighbourhood of the area understudied. Contrastingly, rental price shares a strong relationship with choice of neighbourhood of residence in the medium and high densities with RII of 0.872 and 0.932 respectively. More so, findings revealed that in low density neighbourhoods of Minna, local housing policies, zoning laws, and estate agents advice plays a role in residence choice of neighbourhood having 0.836, 0.836 and 0.932 respectively as its RII.

5. CONCLUSION

The findings of this study establish that there are several factors that contribute to spatial segregation in the housing neighbourhoods of the study area. It is concluded that the social divide and inequities in the urban space of the study area were largely due to individual preference and choice of neighbourhood as an influencing factor of segregation. Also, some households choose their neighbourhood of residence according to their earnings. Minna metropolis is characterised by a spatial mismatch in terms of residence by household employment status. Some neighbourhoods in the study area are characterised by the type of ethnic composition and some residents choose neighbourhoods based on the religious composition of the neighbourhoods. The research has established that there is a significant difference between low, medium, and high density neighbourhoods in terms of segregation factors in the study area. It is therefore imperative that a good urban governance structure should be put in place that will discourage class divisions among spatial entities of the city, which will promote the integration of religious, ethnic, economic, and social groups in the city.

REFERENCES

[1] Aliyu A.A., Mohammed J.K., Bello M.Z., Kasim Z., (2020), *Assessment of Inequality in the Distribution of Water Facilities in Lapai, Nigeria*, Structure and Environment, 12(4), 166-176.

[2] Aliyu A.A., Binti Kasim R., Martin D., Mohd Diah M.L., Mohd Ali H., (2012), *Implication of Intangible Location Attributes on Residential Segregation in Jos, Nigeria*, Journal of Sustainable Development, 5(11), https://doi.org/10.5539/jsd.v5n11p65.

[3] Berkes E., Gaetani R., (2019), *Income segregation and rise of the knowledge economy*, Rotman School of Management Working Paper, 3423136.

[4] Catney G., (2016), *The Changing Geographies of Ethnic Diversity in England and Wales, 1991-2011*, Population, Space and Place, 22 (8), pp. 750-765.

[5] Dzukogi U.A., Shafii, Y.M., Mohammed J.K., (2022), *Perspectives of Housing Segregation: A Systematic Review*, Confluence of Research, Theory and Practice in the Built Environment, pp. 943-953.

[6] Iceland J., (2014), *Residential Segregation: A Transatlantic Analysis.* A Project of the Migration Policy Institute, p. 19, Transatlantic Council on Migration.

[7] Kemper F.J., (1998a), *Residential segregation and housing in Berlin: Changes since unification*. GeoJournal, 46(1), pp. 17-28.

[8] Kemper F.J., (1998b), *Restructuring of housing and ethnic segregation: Recent developments in Berlin*. Urban Studies, 35(10), pp. 1765-1789.

[9] Legeby A., (2010), *Urban segregation and urban form: From residential segregation to segregation in public space*. Skolan för arkitektur och samhällsbyggnad, Kungliga Tekniska högskolan.

[10] Mohammed J.K., Aliyu A.A., Dzukogi U.A., Olawale A.A., (2021), *The Impact of COVID-19 on Housing Market: A Review of Emerging Literature*. International Journal of Real Estate Studies, 15(2), pp. 66-74.

[11] Mohammed M., Jiman C., Aliyu K., Mohammed J.K., (2019), *Comparative Environmental Justice Among Dutsen Kura Hausa and Dutsen Kura Gwari Neighbourhoods of Minna, Nigeria*, ATBU Journal of Environmental Technology, 12(1), pp. 1-12.

[12] Muhammad M.S., Kasim R., Martin D., (2015a), *A Review of Residential Segregation and Its Consequences in Nigeria*. Mediterranean Journal of Social Sciences, 6(2), pp. 376-384. https://doi.org/10.5901/mjss.2015.v6n2s1p376.

[13] Muhammad M.S., Kasim R., Martin D., (2015b), *An Evaluation of Factors Influencing Residential Segregation in Selected Areas of Bauchi Metropolis, Northern Nigeria*, Mediterranean Journal of Social Sciences, https://doi.org/10.5901/mjss.2015.v6n2s1p127.

[14] Muhammad M.S., Kasim R., Martin D., Aliyu, A.A., (2018), *Framework of the Existing Patterns of Residential Segregation and Housing Quality in Nigeria*, Research on Humanities and Social Sciences, 8(12), pp. 33-41.

[15] Muhammad M.S., Kasim R., Martin D., Mohammed M.I., Adamu D., (2015), *Housing Quality in Segregated Residential Neighborhoods in Bauchi Metropolis*. 5(11), 9.

[16] Rodrigues C.U., (2009), *Angolan cities: Urban (re)segregation?* In F. Locatelli & P. Nugent (Eds.), African Cities (pp. 37-54), Brill. https://doi.org/10.1163/ej.9789004162648.i-308.17.

[17] Schütz S., (2014), *Urbanization and Segregation: What can bridge inequalities in urban life?,* https://www.metrodemedellin.gov.co/index.php?option=com_content&view=artic le&id=61&Itemid=165&lang=en.

[18] Seethaler-Wari S., (2018), *Urban planning for the integration of refugees: The importance of local factors*. Urban Planning, 3(4), pp. 141-155.

[19] UN-Habitat, (2001), *Spatial segregation*, [Online], Available: http://www.un.org/ga/Istanbul+5/50.pdf [2014-04-02].

Karol Skowera
Structure and Environment 2023, vol. 15, (2), pp. 90-98, Article number: el 009
https://doi.org/10.30540/sae-2023-009

Structure and Environment
ISSN 2081-1500
e-ISSN 2657-6902
https://content.sciendo.com/sae
https://sae.tu.kielce.pl

sciendo

Kielce University of Technology

DOI: 10.30540/sae-2023-009

FUSION OF DIFFERENTIAL ANALYSIS OF VOLUMETRIC STRAIN METHOD (DILATOMETRIC THERMOPOROMETRY) AND MERCURY INTRUSION POROSIMETRY METHOD FOR PORE SPACE CHARACTERIZATION IN CARBONATE ROCKS

POŁĄCZENIE METODY RÓŻNICOWEJ ANALIZY ODKSZTAŁCEŃ ORAZ METODY POROZYMETRII RTĘCIOWEJ DO OKREŚLENIA CHARAKTERYSTYKI PRZESTRZENI POROWEJ W SKAŁACH WĘGLANOWYCH

Karol Skowera*
Kielce University of Technology

Abstract

Many characteristics of capillary-porous materials, including limestones and dolomites, depend on the structure of the pore space of a given material, so the article attempts to accurately determine the geometric characteristics of pores and their ability to transport water. Much information on the pore structure of carbonate rocks can be obtained from literature studies. There is a lack of information on the use of full hysteresis dilatometric thermoporometry methods for this purpose, as well as the fusion of differential analysis of volumetric strain (DAVS) results with mercury intrusion porosimetry (MIP) results.

The subject of the research presented in this article is the analysis of pore structure in carbonate rocks using the method of differential analysis of volumetric strain and mercury intrusion porosimetry. Based on the measurements made, the pore size, pore volume, content of empty pores and pores containing water incapable of phase transformation were analyzed. The geometry of mesopores of rock samples examined by differential analysis of volumetric strain and mercury intrusion porosimetry was compared. A fusion of the distribution of mesopores from the DAVS study with a part of the distribution of meso- and macropores obtained by the MIP study was performer.

Keywords: differential analysis of volumetric strain method, mercury intrusion porosimetry, carbonate rocks, pore space

Streszczenie

Wiele cech materiałów kapilarno-porowatych, w tym wapieni i dolomitów, zależy od struktury przestrzeni porowej danego materiału, dlatego w artykule podjęto próbę dokładnego określenia cech geometrycznych porów i ich zdolności do transportu wody. Wiele informacji na temat struktury porów skał węglanowych można uzyskać ze studiów literaturowych. Brakuje informacji na temat wykorzystania w tym celu metod termoporometrii dylatometrycznej z pełną histerezą, a także połączenia wyników różnicowej analizy odkształceń (DAVS) z wynikami porozymetrii rtęciowej (MIP).

Przedmiotem badań przedstawionych w niniejszym artykule jest analiza struktury porów w skałach węglanowych z wykorzystaniem metody różnicowej analizy odkształceń i porozymetrii rtęciowej. Na podstawie przeprowadzonych pomiarów przeanalizowano wielkość porów, objętość porów, zawartość porów pustych oraz porów zawierających wodę niezdolną do

*Kielce University of Technology, Poland, e-mail: kskowera@tu.kielce.pl

przemiany fazowej. Porównano geometrię mezoporów próbek skalnych badanych metodą różnicowej analizy odkształceń i porozymetrii rtęciowej. Wykonano fuzję rozkładu mezoporów z badania DAVS z częścią rozkładu mezo- i makroporów uzyskanych w badaniu MIP.

Słowa kluczowe: różnicowa analiza odkształceń, porozymetria rtęciowa, skały węglanowe, przestrzeń porowa

1. INTRODUCTION

The structure of the pore space of rocks decisively affects their durability and other performance characteristics. Precise determination of the geometric characteristics of pores and their connections is a difficult task. There is no single consistent method for this purpose. Only the combination of several dedicated testing techniques allows a more realistic depiction of the complete pore structure of a specific material [1-3]. Of particular interest is the imaging of mesopores (2÷50 nm – according to IUPAC [4]), which determine the material's essential properties in the context of the movement of gases and liquids in its interior [1, 5-9].

The paper analyzes the possibility of using tests performed by DAVS analysis and MIP tests for qualitative and quantitative assessment of pores. An important goal was also to develop DAVS testing methodologies, enabling analysis of „bottle" pores and geometric features of their connections to the overall pore system. The study was limited to carbonate rocks that are among the most diverse in terms of pore structure, and are commonly exploited and used in the construction industry.

Pores are responsible for the flow and retention of liquids in rock materials. They are characterized by a wide range of diameters. The largest of them are possible to see even with the eye. The total volume of pores, in the main, depends on the type of rock. In magmatic rocks, they mostly occur as microcracks between individual crystals and their size depends on the formation process of the rock. In sedimentary rocks, pores are formed as undensified free spaces between individual components of the rock. In both cases, the vast majority of these pores are accessible to water [10].

How do we properly define the object that is a „pore" or perhaps more precisely a „pore space"? A completely general definition of pore is probably not possible. However, it can be said that a pore is defined as a part of pore space that is bounded by solid surfaces and planes, in which the hydraulic radius of the pore space is minimal.

Many different definitions of pores and their dimensions have been used over the years. One of the more well-known concept of so-called „air voids", was first used by Rumpf [11]. Pioneering studies of pore and pore space connections, Fatt's research, realized in 1950, and his 1956 publications [12-14], are considered to be the first.

Without familiarity with the subject matter in question, the depiction of pores in the material can give an illusory picture of them. The shape of pores in a material is influenced by many factors. These include, for example, the origin of the rock, the genesis of its formation, as well as its mineral composition. However, given the nature of water freezing processes in the rock material, the shape of the pores is not as important as their smallest dimension. In addition, the smaller the dimensions of the pores, the more important adhesion forces become. They cause at least an increase in resistance to water flow. This phenomenon is caused by the ordering of dipoles near the walls of the micropores [15].

Accurately determining the geometric characteristics of pores is not a simple task. In addition, wishing to analyze also the connections of pores in the material, there is no single method that will allow one hundred percent certainty of the measurement results. According to [16], the physical properties of elements made of rock materials that directly or indirectly affect the durability of such an element do not depend only on the material itself, but also on the conditions in which it is located. By combining research methods sometimes taken from other scientific fields, such as medicine or aerospace, it is possible to better understand the phenomena occurring inside rock materials [17]. Comparative studies were also conducted by Padhy and his team [2]. Evaluating the geometric structure of the pore space with a single method requires in some cases to make sure that the results of studies conducted by other methods are correct and convergent and the conclusions drawn are valid [18-21].

An additional problem in the analysis of porosity and pore space is posed by pores „bottle pores". The name refers to pores that are connected to the rest of the system by narrow constrictions. At the same time, more than one constriction can lead to a larger pore. Their presence in the material can lead to a distortion of the actual picture of the geometrical characteristics of the pores toward smaller pores [22, 23].

Due to the acting pressures inside the material, the tensile strength, mineral composition and (above all) – the geometric characteristics of the pores – have an impact on its durability in addition to the amount of absorbed water. This is particularly important when rock materials are used as exterior cladding. In rock materials, in which the predominant group is large pores in which most of the water freezes as soon as the temperature passes below 0°C, no relationship has been observed between the internal surface of the pores and the material's resistance to cyclic freezing and thawing. The situation is different for pore-containing materials in which water does not freeze immediately after passing below 0°C. In this type of material, a correlation between frost resistance and internal surface area has been observed [24]. In addition, studies have shown that the ratio of the amount of water in the smallest pores to its total content in the material determines how the destruction inside the material will occur [25] – whether it will be caused by the occurrence of hydraulic or osmotic pressures.

There are many papers in the literature on the problem of the hysteresis of the water-ice phase transition during the cooling and heating of a material. However, there is no single clear answer as to how the various factors affect the on the formation of ice in capillary-porous material and also what exactly happens during the cooling process of the material and during its heating [1, 6, 26, 27]. It is also suggested that the course of the ice melting process is influenced not only by the diameter of the pores but also by their shape [28]. However, it is assumed that one of the reasons for the differences in the course of the exo- and endothermic phases may be the mechanism controlling the formation of ice in large pores via smaller pores [1, 6, 27].

2. METHODOLOGY

Rocks and products made from them are widely used in many areas of everyday life and science. It's not just construction and related fields in the broadest sense, but also agriculture or even everyday items. With such extensive use of rock materials, the requirements for their performance characteristics are also increasing. Nevertheless, the porosity of rocks is generally low compared to other building materials such as bricks or concrete.

Using studies of the technical properties of rocks, the aim is to obtain results that are reproducible and comparable, which are necessary to characterize the suitability of the studied rock for practical purposes. Rocks have certain properties that determine their usability. These properties, fluctuate within wide limits and even within a single deposit. The mere determination of the type of rock tells us little about its usable characteristics and technical suitability. Therefore, it seems necessary to determine their variability. In almost every deposit it is possible to distinguish varieties characterized by optimal properties and right next to them varieties with inferior properties [29].

Without a single, proven and scientifically recognized method to accurately determine the distribution of pore sizes, their connections, dimensions – we cannot perform this type of research, without any doubt about the result achieved. Therefore, the author focused on combining two methods – DAVS and MIP to fully determine the pore size distribution in carbonate rocks. The use of two methods also made it possible to cross-check the correctness of the data obtained.

The first method described, which allows indirect determination of pore size distribution in capillary-porous material, is differential analysis of volumetric strain DAVS (dilatometric thermoporometry). The upgraded methodology makes it possible to determine the dimensions of the pore entrances during the cooling process of the sample and the internal dimensions of the pores based on the heating of the sample. The method of differential strain analysis with various modifications has been used in pore space studies for many years [26, 93, 137]. Its main task is to qualitatively and quantitatively evaluate the pores in a material for its ability to absorb water that is or is not capable of freezing under operating conditions [10]. Over the years, the method of differential strain analysis has significantly evolved and been upgraded. Nowadays, differential strain analysis tests are performed using metal measuring dilatometers equipped with conical lids with a spigot for graduated tubes. This method, was widely described in the article [30].

The mercury intrusion porosimetry (MIP) method makes it possible to measure the volume as well as the size of pores in a material. One of the main advantages of this method is the ability to study a wide range of pore sizes. As a result, not only the total porosity value but also the pore size distribution is obtained. The test is based on one of the characteristics of mercury which is the lack of wettability of the surface of most solids. Thus, mercury under reduced pressure does not spontaneously penetrate the interior of the pores. The penetration of mercury into the pores is caused by increasing the pressure during the measurement. As a result of carrying out the measurement, knowing the final amount of injected mercury, it is possible to determine the porosity of the material under study and then using appropriate calculation algorithms – to determine the geometric characteristics of the material taking into account the internal size of the pores. Despite the sophistication of this method, one must be aware that mercury is not able to enter all curves or corners of pores. Mercury porosimetry is a method extensively reported in the literature – for example, Modry et al. [31]; Cameron and Stacey [32]; Leppard and Spencer [33]; Baker [34]. The initial principles of the methodology were presented by Ritter and Drake [35] as early as 1945. Since then, the method has evolved considerably. The basic assumption of this method is that the pores in the material are cylindrical in shape. According to [36], there are actually different types of pores and their connections in capillary-porous materials. The occurrence of pores with narrow entrances, so-called bottle-shaped pores, can cause a shift in the signal obtained from mercury injection toward smaller pores, which may not fully correspond to the actual geometry of the pore space [2, 3, 37, 38].

3. MEASUREMENTS AND RESULTS

More than a dozen samples of carbonate rocks (limestone and dolomite), from domestic deposits, were examined using the differential strain analysis method. Porosimetric tests were also performed on fragments of the same rocks. While more than a dozen samples were used in the study, only selected results are presented in the article. The entire study is presented and described in detail in author doctoral thesis [39].

Cylindrical samples, 50 mm in diameter and 150 mm in length, cut directly from a block of rock taken at the mine, were used for DAVS tests. The rock sample for the DAVS test is shown in Figure 1.

Figure 1. DAVS test specimens with dimensions $\phi 50$ and h = 150 mm [own elaboration]

The porosimetry (MIP) test used small pieces of rock samples that were placed as tightly as possible in a penetrometer. The rock crumbs for the MIP test are shown in Figure 2.

Figure 2. Samples prepared for MIP testing [own elaboration]

The rock samples for testing had a total mass in the range of 5 to 12 grams. The samples were cleaned before testing, then dried at 105°C to constant weight and cooled in a desiccator.

The comparison of the results obtained by the DAVS method and the MIP method began with a general look at the question of the volume of pores occupied by water in vacuum soaking (in DAVS) and mercury (in the MIP method). These data are presented in Table 1.

In addition, it should be noted that the samples selected and presented in this article were from different deposits and geological periods. Sample A2 is a Devonian limestone. Sample C2 is Devonian dolomite. Sample F2 is dolomite from the Jurassic period. Meanwhile, the sample labeled G2 is Jurassic limestone.

Table 1. Total pore volume occupied by mercury in the MIP test in relation to porosity and volumetric absorbability

Sample number	Volumetric absorbability (vacuum met.) [%]	Total porosity [%]	Total pore volume occupied by mercury (MIP) [%]
A2	0.40	4.27	4.10
C2	0.45	6.04	3.55
F2	2.05	5.48	5.35
G2	4.23	9.27	9.03

The porosity of samples A2, C2, F2 and G2 is higher than the total pore volume occupied by mercury. This means, that the destruction of the pore space of the material caused by the high pressures generated during the MIP test did not apply in this case. Such destruction in the structure of the smallest pores can be observed when conducting tests using the MIP method. Particularly large differences in the geometric structure of the pore space are obtained in the part of the pores of small pores (the radius limit of less than 0.02 µm is assumed in the work), where the pressures acting on the pore walls are very large [1-3, 39].

Table 2. Pore volume occupied by ice (DAVS) and mercury (MIP), in radii >0.02

Sample number	Pore volume occupied by ice in the range of radii >0.02 µm (DAVS) [%]	Pore volume occupied by mercury in the range of radii >0.02 µm (MIP) [%]
A2	0.22	0.23
C2	0.20	0.25
F2	0.38	0.44
G2	0.57	0.62

The data presented in Tables 1 and 2 indicate that mercury filled the pores of the sample in the MIP test in a much larger volume than water in the DAVS test. This is true both for the total pore volume in the material and (on a much smaller scale) for the pore volume in the range of radii >0.02 µm. It is clear that one of the reasons for the differences occurring is the failure of all pores in the material to fill with water in soaking by the vacuum method. In the MIP study, very high pressures for mercury injection (up to about 420 MPa) can cause damage in the pore space of the rock, especially in the smaller pores, where the largest differences in water and mercury volumes were observed. The cause is probably local crushing of pore walls, widening of passages, unblocking access to previously separated pores, etc. We don't know this exactly, but results from the world literature indicate that damage in the pore space of the material under study may be created as a result of the application of high pressure during measurement. The effect of this is precisely the differences in the total pore volume determined by the DAVS method compared to MIP.

Based on analysis of the DAVS method results, we are currently unable to define pore sizes with radii greater than 0.02 µm. In this range of pore sizes, the MIP method is very useful because the pressures of mercury forced to move it in the rock sample are not yet very high, and it can be assumed arbitrarily that there is still little or no damage in the pore space of the rock. Determination of geometric pore dimensions is not yet contaminated by possible damage, which is certainly the case at pressures much higher when mercury is forced into pores with small and very small cross sections. These conclusions were supported by the results of DAVS and MIP tests at radii of >0.02 µm. The graphs below clearly show that the total values of the volume occupied by the pores for both methods are similar. The smallest differences were recorded for sample A2. The pore volume occupied by ice in the DAVS study in the range of radii >0.02 µm was 0.22%. In the MIP study, the pore volume occupied by mercury in the same range was 0.23%. On the other hand, we have the F2 sample, for which the difference was 0.06%. This may indicate, for example, the greater „fragility" of the F2 rock. Mercury, even under not much pressure, could damage the pore walls and penetrate those that were not accessible to water during soaking by the vacuum method. The differences could also have resulted directly from the heterogeneity of the material under study. Locally, there may be more numerous voids/pores in the rocks, the effect of which, in comparing the results, are visible differences in the values of, for example, just the volume of pores.

Thus, an opportunity arises to use part of the distribution of pore dimensions and volumes determined by the MIP method to estimate the actual geometric structure of the pore space in rocks. This part of the MIP chart will be used to supplement the quantitative evaluation of pore volumes and dimensions determined by the DAVS method.

Below are selected graphs of the results of pore size distribution determined from the DAVS study (left) based on heating phase analysis, and (on the right) data from MIP analysis. The portion of the pore size distribution that depicts pores with radii >0.02 µm as a single value in the DAVS study was decomposed into smaller subsections based on the MIP study.

Based on the analysis of DAVS results, we are currently unable to define pore sizes with radii above 0.02 µm. In this range of pore sizes, the MIP method is very useful. Thus, this part of the MIP chart was used to supplement the quantitative evaluation of pore volumes and dimensions determined by the DAVS method.

In order to be able to determine the pore space characteristics in more detail, a description of the distribution of pore size and volume occupied by ice was also added to the analysis in individual samples, determined by the exothermic phase in the DAVS study.

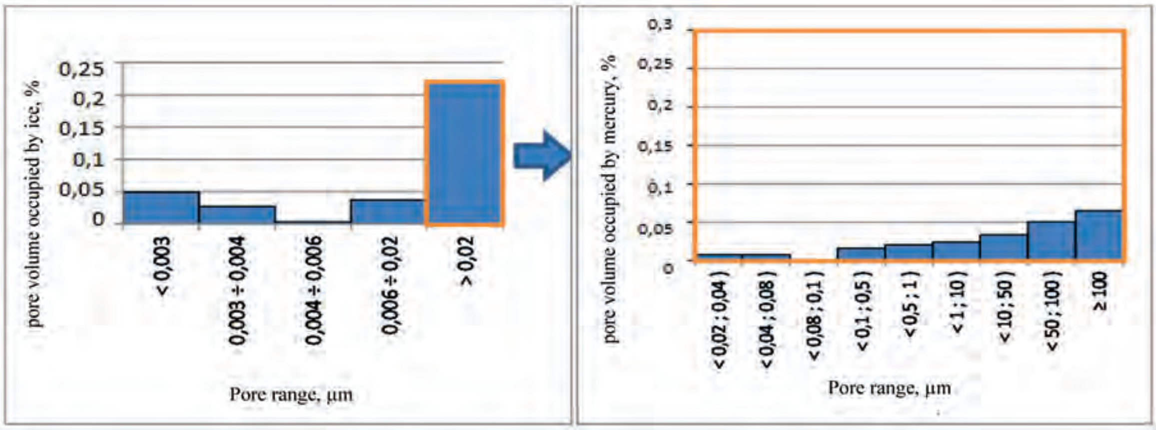

Figure 3. Idea for presentation of pore size distribution according to MIP, referring to pores with radii >0.02 µm in sample A2

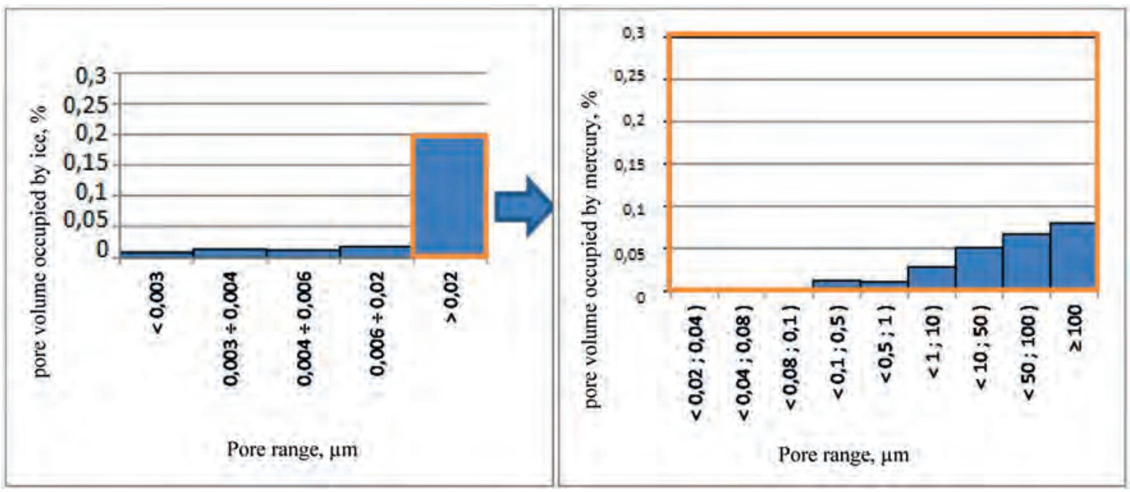

Figure 4. Idea for presentation of pore size distribution according to MIP, referring to pores with radii >0.02 µm in sample C2

The pore size distributions shown in Figure 3 give a wide range of geometric characteristics of the pore space in sample A2. Pores with radii >0.02 µm revealed by the DAVS test are essentially large pores, with radii greater than 0.1 µm. The smaller pores determined by DAVS analysis represent a significant portion of the total porosity. They mainly represent a portion of the volume, which corresponds to connecting pores and small capillaries. The large pores shown on the basis of the MIP study are to some extent connected to other pores by much smaller transitions. The pore size distribution of the A2 sample lacks pores in the 0.08÷0.1 µm range.

The volume of pores with radii >0.02 µm occupied by ice in the DAVS test, represents about 0.22% of the sample volume while in the MIP test it is about 0.23%.

In the case of sample C2, one can notice the complete absence of pores from the range of 0.02÷0.1 µm radius. The distribution characteristics of the remaining pores determined by MIP analysis are similar to those shown in the previous case. Based on the analysis of the results obtained by the MIP method, it can be assumed that the dimensions of the pores with radii above 0.02 µm refer to the internal dimensions of the pores and not their smaller connections. In contrast to sample A2, significantly fewer ice-filled pores were recorded in the range of radius dimension below 0.02 µm. Thus, the pore size distribution illustrates some presence of large pores in the pore space of the material, which are connected by significantly smaller passages. In addition, the pore size distribution of the C2 sample lacks pores in the range of 0.02÷0.1 µm.

The volume of pores with radii >0.02 µm occupied by ice in the DAVS test, represents about 0.20% of the sample volume while in the MIP test it is about 0.25%.

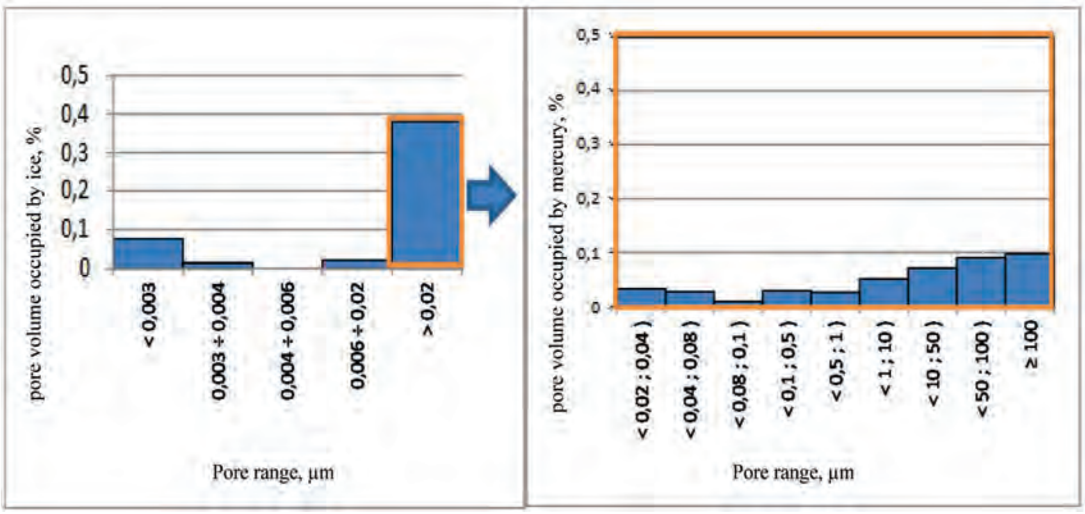

Figure 5. Idea for presentation of pore size distribution according to MIP, referring to pores with radii >0.02 μm in sample F2

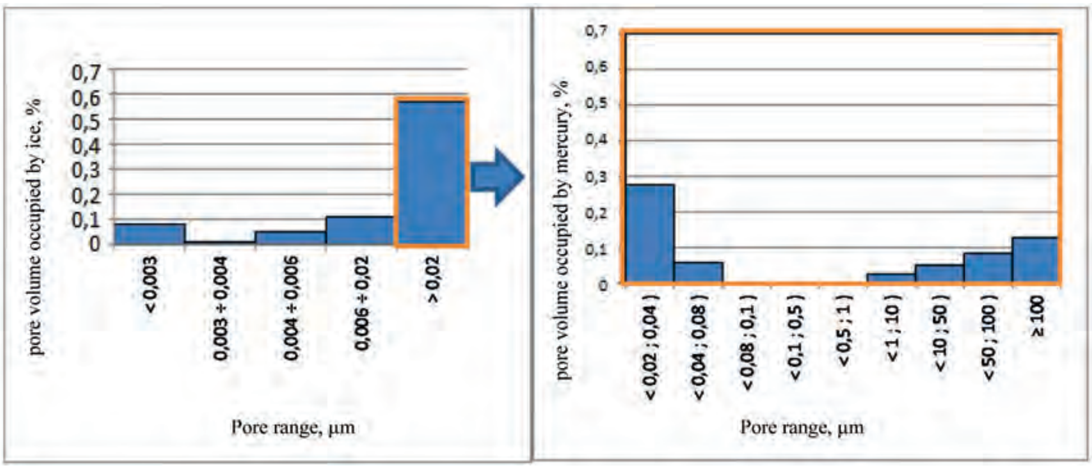

Figure 6. Idea for presentation of pore size distribution according to MIP, referring to pores with radii >0.02 μm in sample G2

The graph from sample F2 shows a relatively numerous group of the smallest pores filled with ice, with radii <0.003 μm, when cooling samples down to –25°C (Figure 5). The second largest pore group in the sample in terms of volume is made up of pores with radii >0.02 μm. Of all the rock samples discussed so far, F2 is characterized by the presence of pores in every defined range of their size. Such a material can fill with water fairly quickly under atmospheric conditions, but there is a sizable volume of pores that will only become active under conditions of water soaking at reduced pressure, or over a longer period of soaking [1, 8, 9, 39]. The volume of pores with radii >0.02 μm occupied by ice in the DAVS test is about 0.39% of the sample volume, and in the MIP test about 0.43% of the sample volume.

The pore size distribution of the G2 sample differs from the previous ones (Figure 6). The pores with radii >0.02 μm, visible on the DAVS graph, are primarily pores with radii in the range of 0.02÷0.04 μm, visible on the MIP chart. This is the range of pores dominant in the studied rock material. Next in terms of total volume are the largest pores with radii >50 μm. The pore size distribution of the G2 sample lacks pores in the 0.08÷1 μm range. Large and small capillary pores predominate. The volume of pores in the G2 sample with radii >0.02 μm occupied by ice in the DAVS test is about 0.59% of the sample volume, and about 0.62% in the MIP test.

4. CONCLUSIONS

The differences in the total volume of pores with radius dimensions above 0.02 μm occupied by freezing water and mercury in the samples tested are small. On the basis of the MIP test alone, we are unable to determine the actual dimensions of pores with radii <0.02 μm. Injection of mercury into such pores is carried out at very high pressures, which can cause damage to the pore walls. It can be assumed that the pressures generated when injecting mercury into pores with radii above 0.02 μm are not large enough to significantly distort the image of the imaged pores, with the result that the pore size distribution in this range is real or close to real. It seems that in order to obtain information about the size and volume of macropores in rocks, the MIP method is appropriate. The DAVS method helps to better visualize the geometric characteristics of pores and their connections in the material at radius dimensions below 0.02 μm. The combination of the two methods makes it possible to present a more complete picture of the size distribution, volume and nature of pore connections in the material.

REFERENCES

[1] Stępień P., *Relationship of water-ice-water phase transformations to pore characteristics of stone materials*. Doctoral Thesis, Kielce Univeristy of Technology, Poland, 2018 – in Polish.
[2] Padhy G.S., Lemaire C., Amirtharaj E.S., Ioannidis M.A., *Pore size distribution in multiscale porous media as revealed by DDIF-NMR, mercury porosimetry and statistical image analysis*. Colloids and Surfaces: A Physiochemical and Engineering Aspects 2007, Volume 300, pp. 222-234.
[3] Wardlaw N.C., McKellar M., *Mercury porosimetry and the interpretation of pore geometry in sedimentary rocks and artificial models*, Power Technology 1981, Volume 29, pp. 127-143.
[4] Compendium of Chemical Terminology Gold Book, 2nd ed.; International Union of Pure and Applied Chemistry, 1997.
[5] Rusin Z., *Technology of Frost-Resistant Concrete*, 1st ed.; Polish Cement: Warsaw, Poland, 2002 – in Polish.
[6] Sun Z., Scherer G.W., *Pore size and shape in mortar by thermoporometry*. Cement and Concrete Research 2010, Volume 40, pp. 740-751.
[7] Mikhail R.S., Copeland L.E., Brunauer S., *Pore Structure and Surface Areas of Hardened Portland Cement Pastes by Nitrogen Adsorption*. Canadian Journal of Chemistry 1964, Volume 42.
[8] Fagerlund G., *Determination of pore-size distribution from freezing-point depression*. Materiaux et Construction 1973, Volume 6, pp. 215-225.
[9] Fagerlund G., *The critical spacing factor. Division of Building Materials*, Lund Institute of Technology, Report TVBM-7058 1993.
[10] Rusin Z., Stelmaszczyk G., *Evaluation of the effect of NaCl on water crystallization in aggregate pores*. In Proceedings of the XLII Scientific Conference of the Committee on Civil Engineering of the Polish Academy of Sciences and the Committee on Science PZiTB, Wisła, Poland, 1996 – in Polish.
[11] Debbas S., Rumpf H., *Chemistry Engineering Science*. 1966.
[12] Fatt I., *The network model of porous media I. Capillary pressure characteristics.* Petroleum Transportation AIME 1956, Volume 207, pp. 144-159.
[13] Fatt I., *The network model of porous media II. Dynamic properties of a single size tube network*. Petroleum Transportation AIME 1956, Volume 207, pp. 160-163.
[14] Fatt I., *The network model of porous media III. Dynamic properties of networks with tube radius distribution*. Petroleum Transportation AIME 1956, Volume 207, pp. 164-181.
[15] Hudec P., *Deterioration of aggregates – the underlying causes*. Katharine and Bryant Mather International Conference – Concrete Durability, ACI 1987.
[16] Torok A., Prikryl R., *Current methods and future trends in testing, durability analyses and provenance studies of natural stones used in historical monuments*. Engineering Geology 2010, Volume 115, pp. 139-142.
[17] Svoboda J., Slovak M., Prikryl R., Siegl P., *Effect of low and high fluence on experimentally laser-cleaned sandstone and marlstone tablets in dry and wet conditions*. Cultural Heritage 2003, Volume 4, pp. 45-49.
[18] Bager D.H., Sellevold E.J., *Ice formation in hardened cement paste, part I – room temperature cured pastes with variable moisture content*. Cement and Concrete Research 1986, Volume 16, pp. 709-720.
[19] Bager D.H., Sellevold E.J., *Ice formation in hardened cement paste, part II – steam-cured pastes with variable moistures content*. Durability of Building Materials and Components 1980, Volume 691, pp. 439-454.
[20] Kozłowski T., *Some factors affecting supercooling and the equilibrium freezing point in soil-water systems.* Cold Regions Science and Technology 2009, Volume 59, pp. 25-33.
[21] Usherov-Mashak A.V., Zlatkowski O.A., *Relationship between the structure of cement stone and the parameters of ice formation during stone freezing*. Colloid Journal 2002, Volume 64, pp. 217-223.
[22] Etris E.L., Brumfield D.S., Ehrlich R., Sterling J., Crabtree Jr., R*elations between pores, throats and permeability: a petrographic/physical analysis of some carbonate grainstones and packstones*. Carbonates and Evaporites 1988, Volume 3, pp. 17-32.

[23] Ishikiriyama K., Sakamoto A., Todoki M., Tayama T., Tanaka K., Kobayashi T., *Pore size distribution measurements of polymer hydrogel membranes for artificial kdneys differential scanning calorimetry*. Thermohimica Acta 1995, Volume 267, pp. 169-180.

[24] Powers T.C., *The air requirement of frost-resistant concreto*. American Concrete Institute 1975, pp. 1-11.

[25] Scanziani A., Singh K., Bultreys T., Bijeljic B., Blunt M.J., *In situ characterization of immiscible three-phase flow at the pore scale for a water-wet carbonate rocks*. Elsevier 2018, Volume 121 pp. 446-455.

[26] Jahnert S., Vaca Chavez F., Schaumann G.E., Schreiber A., Schonhoff M., Findenegg G.H., *Melting and freezing of water in cylindrical silica nanopores*. Physical Chemistry, Chemical Physics 2008, Volume 10, pp. 6039-6051.

[27] Morishige K., Denoyel R., Wernert V., *Pore-blocking-controlled freezing of water in cagelike pores of KIT-5*. The Journal of Chemical Physics 2007, Volume 111, pp. 9488-9495.

[28] Riikonen J., Salonen J., Lehto V.P., *Utilising thermoporometry to obtain new insights into nanostructured materials*. Journal of Thermal Analysis and Calorimetry 2011, Volume 105, pp. 823-830.

[29] Skowera K., Rusin Z., *Physical properties of Devonian limestones from selected deposits in the context of frost resistance*. Mineral Resources Management 2018, Volume 34, pp. 71-84.

[30] Skowera K., Rusin Z., *Differential Analysis of Volumetric Strain Method Characterization in the Context of Phase Change of Water in Carbonate Rocks*. Materials 2022, Volume 15.

[31] Modry S., Svata M., Jindra J., *Bibliography on Mercury Intrusion Porosimetry*. House of Technology 1972.

[32] Cameron A., Stacy W.O., *Chemical Industries,* 1960, Volume 9.

[33] Leppard C.J., Spencer D.H.T., *A low pressure mercury porosimeter for measuring macropores*. Journal of Physics E: Scientific Instruments 1968, Volume 1, pp. 553.

[34] Baker D.J., *A low pressure mercury porosimeter*. Journal of Physics E: Scientific Instruments 1971, Volume 4 pp. 388.

[35] Ritter H.L., Drake L.C., *Pressure porosimeter and determination of complete macropore-size distributions*. Industrial and Engineering Chemistry, Analytical Edition 1945, Volume 17, pp. 782-786.

[36] Diamond S., *Mercury porosimetry an inappropriate method for the measurement of pore size distributions in cement-based materials*. Cement and Concrete Research 2000, Volume 30, pp. 1517-1525.

[37] Villadsen J. *Pore structure in cement based materials*. Technical Report 1992, Volume 227.

[38] Cnudde V., Cwirzen A., Masschaele B., Jacobs P.J.S., *Porosity and microstructure characterization of building stones and concretes*. Engineering Geology 2009, Volume 103, pp. 76-83.

[39] Skowera K., *Analysis of the pore structure in carbonate rocks, using the method of differentia analysis of volumetric strain*. Doctoral Thesis, Kielce University of Technology, 2021.

Małgorzata Doroz-Turek
Structure and Environment 2023, vol. 15, (2), pp. 99-112, Article number: el 010
https://doi.org/10.30540/sae-2023-010

Structure and Environment
ISSN 2081-1500
e-ISSN 2657-6902
https://content.sciendo.com/sae
https://sae.tu.kielce.pl

Kielce University of Technology

DOI: 10.30540/sae-2023-010

LIVING TRACES OF HISTORY – PORTUGUESE APPROACH TO CONSERVATION ON THE EXAMPLE OF RELIGIOUS BUILDINGS IN LISBON

ŻYWE ŚLADY HISTORII – PORTUGALSKIE PODEJŚCIE KONSERWATORSKIE NA PRZYKŁADZIE OBIEKTÓW SAKRALNYCH W LIZBONIE

Małgorzata Doroz-Turek*
Kielce University of Technology

Abstract

The article addresses the issue of the Portuguese conservation approach to religious buildings in Lisbon that have been damaged by cataclysms. The aim is to show approach to both preserving the original substance and changing the function of the sacral building. After the tragic destruction of Lisbon in the mid-18th century was followed by the use of the ruins of the Carmelite monastery church, Convento do Carmo, for adaptation into the Archaeological Museum. Church of the Nossa Senhora da Conceição Velha, also acts as a remnant of historic events. The Church of St Dominic is also an example of atypical conservation and restoration. Another one is the adaptation the São Julião church on the Museum of the Bank of Portugal. That projects are examples of pioneering conservation activities conceived as a result of the conservation practice of Portuguese architects.

Keywords: Portugal, Lisbon, conservation, protection, heritage, adaptation

Streszczenie

Artykuł porusza problem portugalskiego podejścia konserwatorskiego do obiektów sakralnych w Lizbonie, które uległy zniszczeniu w wyniku kataklizmów. Celem jest ukazanie interesującego podejścia zarówno do zachowania oryginalnej substancji, jak i zmiany funkcji obiektów sakralnych. Po tragicznym zniszczeniu Lizbony w połowie XVIII wieku ruiny kościoła klasztoru karmelitów Convento do Carmo wykorzystano do adaptacji na Muzeum Archeologiczne. Znakiem historycznych wydarzeń jest także kościół Nossa Senhora da Conceição Velha. Przykładem nietypowej konserwacji i restauracji jest także kościół Igreja de São Domingos. Kolejnym przykładem jest adaptacja zniszczonego kościoła São Julião na siedzibę Muzeum Banku Portugalii. Projekty te są przykładami pionierskich działań konserwatorskich powstałych w wyniku praktyki konserwatorskiej portugalskich architektów.

Słowa kluczowe: Portugalia, Lizbona, konserwacja, ochrona, dziedzictwo, adaptacja

*Kielce University of Technology, Poland, e-mail: mdoroz@tu.kielce.pl

1. INTRODUCTION

Lisbon is a city situated on the hills at the mouth of the Tagus River[1]. Portugal's largest city also has the largest amount of historic tissue in the country, accumulated here since the Roman times. The current city has absorbed the area of the former port of Belém from where sea expeditions departed as early as in the 15th century. At the beginning of the 16th century, the Hieronymites Monastery – Mosteiro Dos Jeronimos – was founded at the entrance to the harbour; the building represents the best period in the development of Portuguese architecture, known as the Manueline style[2] (Fig. 1). The monastery (1502-1551) was built together with the defensive Tower of Belém – Torre de Belém (1515-1521) [1] [2] ordered by King Manuel I in gratitude for Vasco da Gama's successful expedition to India. Both the monastery and the tower are listed as the UNESCO World Heritage sites since 1983.

Figure 1. View of a section of the façade of the Hieronymites Monastery – Mosteiro Dos Jeronimos and the Santa Maria Church in Belém, Lisbon, 2021, photo: M. Doroz-Turek

In 1755, Lisbon was hit by a huge earthquake that almost completely destroyed the centre of the city, while leaving Belém in better condition. This is why Lisbon represents a peculiar situation where only where there are only a few earlier buildings among in the reconstructed urban tissue. The Lisbon Castle and the cathedral standing on a hill, the ruins of the do Carmo Monastery, or the monuments of Belém are the oldest buildings among the buildings from the late 18th and early 19th centuries. This is a significant difference compared to other Portuguese cities, where we can clearly see the regular development of the urban structure.

2. STATE OF RESEARCH

The issue of Portuguese conservation efforts and adaptations has not been widely commented by the Polish scholars. One of the first to address this topic is conservator Ewa Święcka in her article on the conservation of the Church of St Dominic in Lisbon [3]. Subsequent publications on the Portuguese school of conservation were written by architect Dominika Kuśnierz-Krupa, who discussed the problem mainly using examples of secular buildings [2, 4, 5]. In 2017, an article by Karolina Dudzik-Gyurkovich [6] on the design of public spaces in Lisbon was published.

3. LISBON AND HISTORIC DESTRUCTION

Portugal escaped the wartime devastation of the 20th century, which turned most of Europe's major cities, including some Polish ones, into ruins. Lisbon, however, was affected much earlier by the devastation following natural cataclysms – earthquakes, after which it had to rebuild. On 1 November 1755, the city saw its most severe earthquake, which costed thousands of lives and turned about 85% of the capital's buildings into rubble, including most of Lisbon's temples. Strong shocks were followed by a tsunami, and where the water did not reach, fires broke out destroying what remained. Baixa district turned into rubble, along with the residential buildings of the Ribeira royal palace (standing on the site of today's LisbonPlaza – Praça Comércio), the larger churches, the Carmelite monastery – Do Carmo. The former Moorish fortress, transformed in the 12th century into the castle of St George survived, as did the cathedral – they were both located in the least damaged district of Alfama.

After thewors earthquake, the economically and politically important city had to be rebuilt. The authorities and the residents faced the problem of restoring the buildings, many of which were already then considered as historic. Lisbon was rebuilt according to a project that was modern at the time and followed the principles of Classicist architecture; it was initiated and organised to a large extent by Sebastião José de Carvalho e Melo, Marquis de Pombal –

[1] From 1255, when it was transferred from Coimbra by King Afonso III.

[2] Manueline style – a specifically Portuguese style, a variety of late Gothic architecture in Portugal.

a minister of King Joseph I of Portugal. As many as six reconstruction plans had been created, from which the one drawn up by architects Eugénio dos Santos, Carlos Mardelo and Manuel de Maia [7, 8] was chosen; the plan for the new Lisbon was already drawn up in 1756. The rebuilt area includes the Baixa Pombalina district by the Tagus River with its wide perpendicular streets and the main artery Rua Augusta connecting the main squares of Praça do Comércio and Praça do Figueira. In the 20th century, several great tragedies occurred. First, in 1959, the Dominican church in Lisbon's city centre burnt down, then, another fire broke out in 1988 in the Chiado district.

Alfama is Lisbon's oldest survived district, where buildings are erected on a rocky hillside. On the highest hill, there are the remains of the castle of St George – Castelo de São Jorge. Thanks to the conservation and adaptation works undertaken in the 1930s – which made it possible to make the fortification with its eleven towers available to the public – it is now possible to enjoy this heritage You can also see the ruins of the former royal palace-citadel in the form of the Musealisation of Archaeological site of the Praca de Nova Sao Jorge Castle [9] and the permanent exhibition of the Archaeology Museum designed by João Luís Carrilho da Graça – JLCG Arquitectos[3], a leading contemporary architect from Lisbon. Another interesting conservation project present at the Castle is the display of further layers of a Moorish house built over the remains of a Roman villa. Below the castle, the city's oldest church – the medieval Cathedral of Saint Mary Major called simply Sé de Lisboa – has been preserved (Fig. 2). Its origins date back to 1147; it was transformed, restored and renovated, but has retained its medieval style. Moreover, at the beginning of the 20th century, in order to restore the temple's medieval appearance, most of the Neoclassicist decoration was removed by Augusto Fuschini, following the doctrine of Viollet le Duca, whose influence in Portugal was visible as late as after 1890 [10]. In 1990, an interdisciplinary archaeological and architectural study began in the cloister of the Lisbon Cathedral. An architectural and museum project has been developed to preserve and showcase the exposed artefacts of the ruins to a wider public. The underground exhibition will be accessible to the disabled thanks to the lifts included in the project, while the arranged footbridge will allow free movement over the excavations without damaging them (Fig. 3). An underground crypt was created to display the everyday objects found on the spot. In this way, the sacral building will also become a museum with an interesting exhibition.

Figure 2. Cathedral of Saint Mary Major in Lisbon. Front elevation, 2021, photo: M. Doroz-Turek

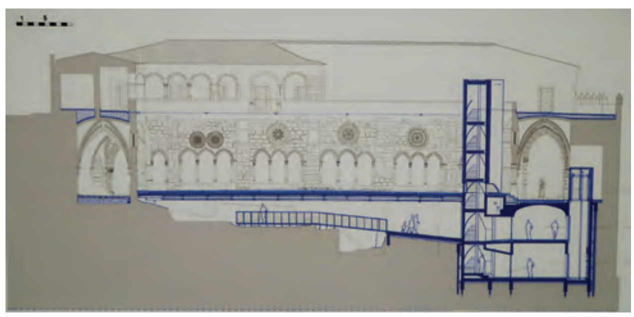

Figure 3. Cathedral of Saint Mary Major in Lisbon. Cathedral cloister, architectural and museum project, cross-section, 2019, photo: M. Barański; designed elements are marked in blue

Despite such massive damage and thanks to the rapid restoration undertaken, as well as early conservation efforts with great respect for heritage, today, in Lisbon,

[3] The Lisbon-based architect was awarded the Piranesi Prix de Rome in 2010 for São Jorge Castle Archaeological Site, which is the result of comprehensive work carried out on the castle since 1996.

we can see historic buildings at every turn, including those accompanied by contemporary interventions. History obliges, which is why Portuguese architectural practice is still closely linked to the country's heritage. In the catalogue of the exhibition "Physics of Portuguese Heritage. Architecture and Memory, a liquid, solid and gaseous equation"[4], organised in December 2018 at the Popular Art Museum in Lisbon, Jorge Figueira recalls: "Adaptive, restorative, memorialist, Portuguese architecture doesn't suffer from a tabula rasa philosophy, nor does it imagine a future that is totally cut off from the past. Ever if only from the long gone years of modern architecture that Portuguese architects so fondly evoke" [11]. Every architect faces a huge responsibility when creating in a place marked with centuries of history. Portuguese architects succeed brilliantly; not only do they enter into dialogue with the context in which they build, but they also express their own era by the means of architecture[5].

The aforementioned exhibition celebrated the past achievements in the area of design in historical heritage that Portuguese architects managed to realise despite the economic crisis in the country and the lack of specialised criticism, which is an obstacle in heritage conservation. It was also a time to reflect on the Portuguese heritage and the history of heritage interventions. For, after the Carnation Revolution of 1974, there was a change and an in-depth analysis of the historical legacy, evidenced for example by the aforementioned reconstruction of the Lisbon's Chiado district by one of Portugal's greatest architects, Álvaro Siza of Carlos Castanheira [13]. Siza saw the 1988 fire that ravaged this part of Lisbon as an opportunity to restore the original Marquis Pombal's design of this place [11].

In recent decades, conservation activity in Lisbon has been very lively. Thanks to contemporary conservation interventions, i.e., adaptation to museum and other functions that are in line with the main idea, historic buildings are being opened to the tourists in a 'new' way. The number of great conservation and adaptation projects in Lisbon is impressive [5]; the city of Porto presents equal achievements in this sphere [4], moreover, every Portuguese region or city has at least one such project. Conservation interventions are carried out not only in the secular buildings, but also in the religious ones. Portuguese conservators and architects are trying not only to improve the condition of the preserved architecture, but also to give it a new purpose. The designs and adaptation works respect the historic tissue, while the new elements not only express their era in a professional manner but also integrate with the old building, entering into a dialogue with the heritage.

4. EXAMPLES OF CONSERVATION AND ADAPTATION INTERVENTIONS IN LISBON

Church Igreja do Carmo, part of the Carmelite Convent – Convento do Carmo, is a unique building located on an elevation in Lisbon's historic Chiado district, by the Largo do Cormo square. The medieval monastery was founded in 1389. The construction of the presbytery part of the monastery church was completed in 1407 and the monastery itself in 1423. The temple has floor plan based on the Latin cross, with a three-nave, four-span body, a transept and a stepped chancel consisting of one main and four side apses closed in a polygonal way. Over time, the buildings have received several additions and alterations: they were adapted to new tastes, emerging architectural and decorative styles. Up to 1755, it was Lisbon's largest Gothic monument. Unfortunately, the earthquake, severely damaged the edifice. The destruction was severe. The church and monastery lost their entire roof and their walls got severely damaged. The décor was lost following the fire.

The reconstruction of the capital, started in 1756, included also the reconstruction of the church, which began with the restoration of the presbytery in the Gothic style. The current pillars and nave arches date from this time. Reconstruction was interrupted in 1834 due to the suppression of religious orders in Portugal. The property of the monastery was taken over by the military authorities and turned into the army's headquarters, which also brought partial reconstruction of the monastery buildings. In the mid-19th century, in the age of Romanticism that praised the love of ruins and medieval buildings, the decision was taken not to rebuild the church in its entirety. The nave body was left without roof and vaults, in the form of a 'permanent ruin'. The façade still shows the ruined internal tripartite structure, which, in the ground floor, features the main portal on the axis and a partially preserved rosette above it. The pointed-arch portal consists of

[4] The exhibition "Físicas do Património Português. Arquitetura e Memória" was organized by the Portuguese Directorate General for Cultural Heritage and it will be held at the museum of Popular Art, in Lisbon, starting december 5th.

[5] It is the architect's task to express architecturally his or her era and simultaneously get involved in a dialogue with the context, in which he or she builds [12].

several archivolts supported by columns with capitals with floral ornamentation and shafts decorated with anthropomorphic figures (Fig. 4). A similar portal survived on the south elevation of the transept: it used to be the side entrance to the church from the city.

In 1864, the church building was handed over to the Association of Portuguese Archaeologists, which set up the Carmo Archaeological Museum in the ruins. The establishment of the museum in 1863 was financed by Joaquim Possidónio Narciso da Silva (1806-1896), founder and president of the Royal Association of Portuguese Civil Architects and Archaeologists (Real Associação dos Arquitectos Civis e Arqueólogos Portugueses), then president of the Carmo Archaeological Museum. Narciso da Silva was the architect of the Portuguese royal family, photographer and archaeologist; he run the museum until his death in 1896. He undertook there several important conservation and restoration works [14]. It was the first art and archaeology museum created to protect the declining national heritage in the form of a church and a monastery following the dissolution of the orders and the innumerable damages caused during the French invasions and the Liberal Wars. By creating the museum, the association is continuing the turbulent history of the site based on the ruins of the Carmo church. It is the site of the manifesto for public awareness of heritage initiated after 1834 and the struggle to preserve and protect heritage transferred from the religious sphere to the secular one as a representative asset belonging to the entire community [15]. In its early years, the museum amassed a substantial collection of artefacts of great historical, artistic and archaeological significance. In the ruins of the nave section, a lapidarium was set up to display numerous architectural and sculptural details from various churches that were liquidated after the earthquake (Fig. 5). The exhibits in the presbytery section, which is the best-preserved part, include a collection of 'azulejos' (tile) ceramic tiles and many other objects, such as the unique pre-Columbian ceramics and mummies donated by the Count of São Lanuáro.

In 1995, the Carmo Archaeological Museum was closed due to the construction of new metro lines in Lisbon running underneath the site and threatening its structure. This time was used to carry out large-scale conservation of the monument, which resulted in the dismantling of the exhibition. The facility reopened in 2001 with a completely redesigned museum space, but an unchanged form of a 'permanent ruin'.

Figure 4. Carmo Archaeological Museum. Front elevation of the church – Igreja do Carmo at the Largo do Cormo square, 2021, photo: M. Doroz-Turek

Figure 5. The corps of the church – Igreja do Carmo, 2021, photo: M. Doroz-Turek

The entire conservation was divided into eight phases with the first five completed in 1996 and the rest as late as in 2000. Firstly, the museum collection was inventoried and moved for the duration of the works to the most secure part of the building: the old sacristy. Prior to the construction work, archaeological and architectural surveys were carried out in all five chapels and part of the main nave. About 150 micropoles were drilled in from the outside to reinforce the structure of the chapels and transepts erected right next to the slope. The arches of the nave were supported and reinforced, a waterproofing layer was also introduced along its entire length. Moreover, the pavement in the entire church was replaced. Prior to the installation of the museum's exhibition in 2000, conservation of the entire collection was carried out by specialists in all techniques proper for the works collected at the museum. New lighting for the building and collections was installed. All that was all linked to the new format of the association's activities, which planned to focus on promoting lectures and meetings, as well as debates and conferences on the current research topics. For this reason, a multimedia room was set up in the old sacristy adjacent to the north side. The revitalisation of the Chiado district by architects Álvaro Siza Álvaro and Carlos Castanheira, after the fire that devastated this part of Lisbon in 1988, is being carried out around this religious complex.

The ruins of Carmo became a living memorial to the tragedy of 1755, and thus a testament to the devastation the city suffered. It is also an early example of the Portuguese school of conservation: honest and not falsifying history [4]. This example proves that a 'permanent ruin' can be combined with contemporary functions.

The Nossa Senhora da Conceição Velha church, known as the Misericórdia Church, was also affected in the Great Lisbon Earthquake. The church was built in the 15th century on the site of a synagogue and was the second largest church representing the Manueline (originally Manuelino) style after the Belém Monastery. Despite its close location to the Praça do Comércio square, it was not qualified for reconstruction in the original plans for the reconstruction of the Lisbon's waterfront. It was not until 1770 that King Joseph ordered the architect Francisco António Ferreira, collaborating with Honorato José Correia, to rebuild the temple structure. The said architects changed the orientation of the church and used details from the first temple on the main façade. The chapel was converted into a presbytery. The southern side entrance became the main entrance, decorated with a magnificent and rich double, semi-circularly closed portal with a tympanum with the figure of Our Lady of Misericordia, as well as figures of nobility and clergy. The portal is largely original, but it also has some reconstructed parts, which, however, did not affect its historic character (Fig. 6). On the sides of the portal designed in the same, Manueline, style, there are two semi-circular windows framed by segmented columns standing out against a plain background. This church is an example of the re-use of the remains of a historic, dilapidated building rebuilt in a simplified form with the use of the structure and valuable elements of architectural details from the ruins of the south side elevation.

Bearing in mind the early restoration repairs in Lisbon, one cannot overlook such example as the aforementioned Hieronymites monastery in Belém (Fig. 1), which survived the cataclysm of the 18th-century earthquake in a relatively good condition. We can notice a stylistic contrast between the decor of the very rich portal of the church in comparison to the southern, previously destroyed wing of the monastery. Stylistic differences are also the aftermath of restoration works undertaken here in the 1860s, when the building, left unattended after the dissolution of the monastery in 1833, was to be adapted by the King's order. Various renovation teams were operating in the large building, trying to remodel and adapt it to the current needs. We can see there traces of various inspirations and decisions to transform the building. The authors are architects: Valentim Jose Correia, Englishman Samuel Barret, and Italian Cinatti. However, in 1878 a large part of the monastery at the entrance to the church collapsed [16] [17]. Fortunately, the renovation and reconstruction of the southern most exposed wing of the monastery was carried out following the ideas of Violet le Duc and Camillo Boito promoted by J. Possidonio Narcison da Silva. When the church and monastery were badly damaged in the 19th century, the Swiss architect Ernesto Korrodi redesigned the bell tower, transforming the pyramidal roof into a dome, the west wing of the monastery and the facade connecting to the church. And he adapted the building to the museum program. The décor was developed with reference to the Manueline style, keeping the style of the sculptural decoration a little less sophisticated. Moreover, most importantly for the Portuguese conservators, the work on this important monument became in 1897 the basis for Ramalho Ortigao's definition of the principles of the conservation approach, which distinguished the value of authenticity of a monument and repair works carried out with the utility of a historic building in mind [10]. Till today, the monastery houses museum exhibitions. This purpose is perfectly served by the spacious interiors adapted for the disabled without interfering with the authentic tissue – which was not only hardly touched, but also further emphasised, to make it an exhibit of its own (Fig. 8, 9).

Another example of original conservation and restoration is the Church of St Dominic – Igreja de São Domingos located in close proximity to Praça Dom Pedro IV square, called Rossio, in the Baixa district. The temple was built on this site in the 13th century and subsequently transformed over the centuries. The church was first damaged in an earthquake in the 16th century, then in the mid-18th century, when, like most of Lisbon's buildings, the structure was turned into rubble. The Church of St Dominic was rebuilt in the Baroque style. The main architect responsible for the reconstruction was Carlos Mardela [8], however the construction itself was eventually supervised by Mauel Caetano de Sousa. The west-oriented façade (Largo de S. Domingos) and the presbytery were designed by the architect Johann Friedrich Ludwig, known in Portugal as João Frederico Ludovice [18]. A model example of a Baroque religious building was then erected in Lisbon [19, 3]. The plan consisted of a single-nave body with shallow chapels on the sides, a transept, a transverse nave, as well as an adjacent presbytery and chapels with altars on the east side. The façade has three-axis and is divided into two levels by an intermediate cornice, with a main portal on the axis and two side portals. The whole is closed by a Baroque gable with an oval window framed by volute edges. Unfortunately, the church was destroyed again in 1959 by fire, which very quickly consumed the wooden roof structure. The vault then collapsed and the flames turned the interior into a charred mess, consuming all the rich furnishings. Despite the extensive damage, the church was cleaned up and secured with a temporary roof, so to allow it to continue functioning as a temple. The monumentality of its architecture, especially of its interior, continued to inspire admiration despite the damage, but unfortunately the makeshift protection measures began to be insufficient. The condition of the dilapidated building began to deteriorate. Finally, after more than 40 years, the decision was made to carry out construction works in the church. As a result, an architectural competition for the concept of rebuilding the temple was announced in 1992. The initial intention was to restore it to its original state, but, within the course of operations, this assumption evolved [19].

Due to the risk of fire and the occurrence of seismic shocks, it was decided to base the roof on a lightweight metal structure instead of flammable wood and heavy concrete. The barrel vault, which was reconstructed on the basis of archive photographs, was made of an innovative lightweight metal structure additionally supporting the roof. On what concerns the interior of the church, it was ultimately decided not to restore it. The crushed stone details of the altars were supposed to show the enormity of the fire damage. This decision provided the interior of the church with a unique character. As for the frescoes, despite many design ideas [3], the walls and vaults were finally painted red with the 'texture' of marble to further enhance the impression evoked by this original interior. The grey stone decorative elements, with numerous cavities and cracks left by the fire, stand out well against this background (Fig. 7). The conservation measures were chosen to preserve not only the authentic tissue, but also traces of events that took place in the temple years ago [3]. The church was reopened in 1997 after the completion of restoration work.

Another very interesting conservation-adaptation project is the current seat of the Bank of Portugal, with contribution of the dilapidated and desacralized São Julião church (Fig. 10), designed by Gonçalo Byrne and João Pedro Falcão de Campos. The bank's seat is located in a gradually integrated complex of eight buildings and a church, acquired by the bank between 1868 and 1933.

The Baroque, hall-like Church of São Julião was built in 1802 within the reconstruction of Lisbon [20]. It had been restored after a fire in 1856, but then became desacralized and ultimately sold to the Bank of Portugal in 1935. Initially, the main nave was used as a garage by the bank, accessed through the main entrance, and the altar area was converted into a safe, which damaged some of the walls. It is interesting to note that in 1970 it was planned to move the church to another location. A detailed inventory with numbering of each stone was even made so that it could be reconstructed in its new location after demolition. Ultimately, due to political changes, this concept was never implemented. Unfortunately, the removal of the inked numbers caused many problems during the restoration works carried out later.

The entire complex was deteriorating and needed renovation combined with restoration. The project to renovate the bank's seat with structural reinforcement was initiated in 2007 by architects Gonçalo Byrne and João Pedro Falcão de Campos. In connection with these works, a desire has also been expressed to install the Banco de Portugal Money Museum in the S. Julião Church. The new century saw enormous potential in this space. This is how one of the most important projects being undertaken in Baixa Pombalina was undertaken.

The general contract for the renovation and restoration works was signed in 2009. The work began with archaeological investigations during which, in 2010, the 13th-century city walls that protected the capital from the river were discovered here. In the basement of the museum, we have a section of King Denis original defensive wall on display, which has become an integral part of the exhibition. The Interpretation Centre's exhibition set up to present the Lisbon's medieval history is located in the former crypt of the São Julião Church. The temple's galleries were used to display historical coins, banknotes and Portuguese securities. Walking through the galleries, we can take a look into the interior of the church.

The restoration of the ensemble has restored the uniqueness of the church and its spatiality. In the new intervention, the deterioration of the altar section combined with the renovated part of its nave is evident. The absence of an altar made it possible to unite the space of the church with the inner patio of the complex. The connection of these parts is symbolically marked by the two 15-metre-long silk gold curtains with inscriptions from Book of Disquiet by Fernando Pessoa – this artistic setting is the work of Francisco Providência (Fig. 11). The stone and frescoes were restored not only outside but also inside; some were also reconstructed, but others left in a form broken at the interface with the new material and form. The nave of the church was adapted into a large hall for holding classes, concerts and conferences. The Money Museum, designed by Francisco Providência, was arranged in the rooms around this nave. The spacious interiors became an attractive environment for visitors. The exhibition used mainly multimedia technology to display the collection and offer a range of interactions.

The glass corner window visible on the outside of the building is a symbolic contemporary cornerstone of the new building adaptation. From inside, we can enjoy a perspective view of the Praça do Municipio square (Fig. 10). From the inside, we have a perspective view of the Praça do Municipio square. This accent of the design integrates the interior through its form, connecting with the geometric floor of the neighboring square (Fig. 12).

A very interesting example of the use of historical sacral space is the Governor's Palace in the in Belém, the historic part of Lisbon. The historic building was renovated, adapted and expanded into a Boutique Hotel and SPA. In the JCP+CM Design Studio JorgeCruzPinto+CristinaMantas Architects, the architects thought about and realized a dialogue between history and the present, using the same existing materials, namely: hard limestone, white plaster and stucco, tiles, pine wood and zinc [21]. Before the construction works, archaeological research was carried out on the investment site, during which the existence of Roman industrial structures (tanks) found, probably from the 1st to the 5th century. The discovery are exposed in the entrance zone to the courtyard in front of the palace, the plan of which is shown on the glazing (Fig. 13).

The renovation of the palace included the restoration of the original Baroque chapel, in which will located the main hall with the hotel reception and SPA. The condition of the chapel at the beginning of the work was good. The walls of the interior of the former chapel were lined with original Portuguese tiles, there was a Baroque altar with a painting of the Annunciation of the Blessed Virgin Mary and a beam of light from the Holy Spirit. The first owner was not interested in restoring the chapel, during the work the painting disappeared, the altar and tiles were dismantled and placed in boxes (Fig. 14). The financial crisis of the owner caused the interruption of works for several years, during which time the owner of the palace changed. The architects convinced the new investor to restore the original beauty of the chapel (Fig. 14).

When adapting it to a different, secular function, the focus was on restoring the splendor of the interior by recreating elements related to the sacred function. The tiles on all walls were restored and the gaps were supplemented with replacements in order to continue the religious figurative narratives (Fig. 15, 16). The wooden ceiling, preserved but in very poor condition, was reconstructed using the same materials and following the historical pattern (fig. 17). The architect replaced the unpreserved baroque altar with a contemporary installation modeled on it, and the organ is also suggested by a contemporary installation, a curved contour made of shiny steel pipes (Fig. 17). However, these elements, despite the secular function of the hotel's representative room, strengthen the baroque, liturgical character of the former interior (Fig. 15, 16). The project approved in 2011 was implemented by 2015 [21].

Figure 6. Facade of the Nossa Senhora da Conceição Velhachurch, 2019, photo: M. Barański

Figure 7. Mosteiro Dos Jeronimos in Belém, Lisbon. The interior of the museum, 2021, photo: M. Doroz-Turek

Figure 8. Mosteiro Dos Jeronimos in Belém, Lisbon. The interior of the museum, 2021, photo: M. Doroz-Turek

Figure 9. Interior of the Church of St Dominic – Igreja de São Domingos, 2021, photo: M. Doroz-Turek

Figure 10. Façade of the São Juliãochurch, 2019, photo: M. Barański

Figure 11. Interior of the São Juliãochurch, 2019, photo: M. Barański

Figure. 12. View from the window of the São Juliãochurch over the Praça do Municipiosquare, 2019, photo: M. Barański

Figure 13. Governor's Palace, Belém. Plan of ancient ruins on the glass fence, 2021, photo: M. Doroz-Turek

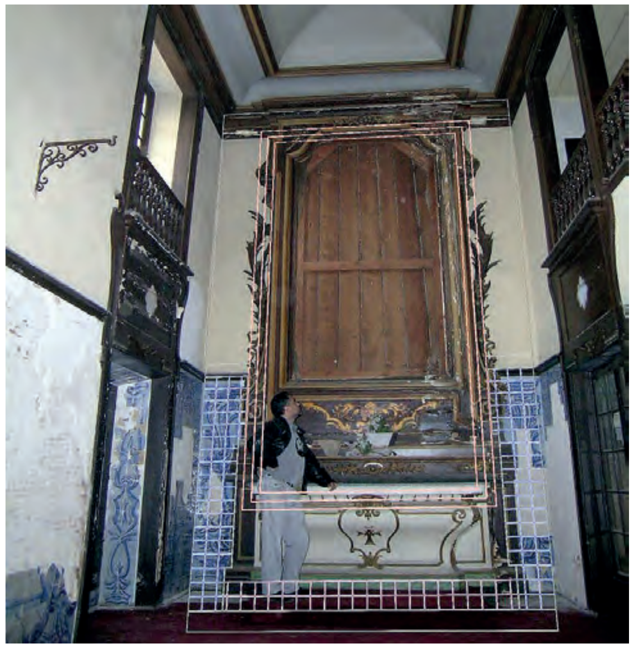

Figure 14. Chapel of Governor's Palace, Belém. Befor work, photo: J. Cruz Pinto

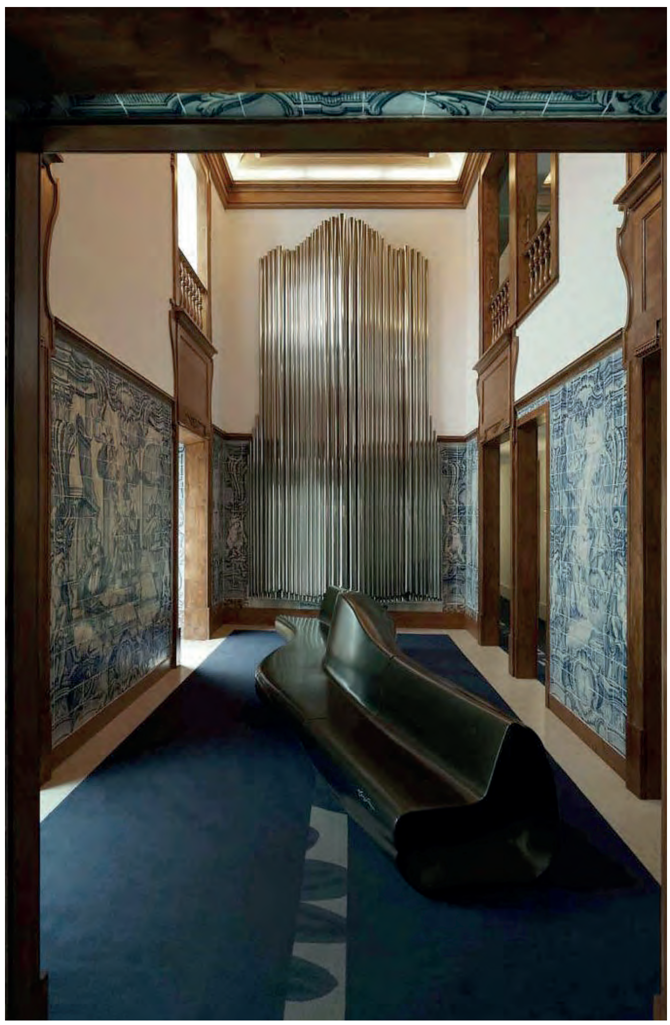

Figure 15. Chapel of Governor's Palace, Belém. After work, photo: J. Cruz Pinto

Figure 16. Chapel of Governor's Palace, Belém. After work, photo: J. Berchez

Figure 17. Chapel of Governor's Palace, Belém. Ceiling after work, photo: J. Berchez

5. CONCLUSIONS

The Lisbon realisations are model conservation and adaptation interventions in historic heritage in religious buildings. Portuguese architects are well-experienced in this area; they continue the dialogue with history that was already undertaken in the 19th century: they recognise the history and abstain from falsifying the past, even though they make use of new architectural and artistic measures. Each project is different, treated individually and refined in every aspect: conservation, utilitarian, technical and artistic. The tragic disasters that had struck these monuments created a kind of challenge awaiting individual answers. This idea was supported not only by *the vitruvian triad*, but, in a sort of a way, also by the fourth aspect of safeguarding and preserving the authenticity of the historic monuments. The examples presented show how to adapt buildings, so that they bear witness to the past and serve future generations, how to maintain their historic character and at the same time create a new history and a new quality of architecture. When their authenticity is preserved and protected, they can continue to act as live traces of history, but, at the same time, gain new life through such measures.

REFERENCES

[1] Moreira R., *A Torre de Belém, in O Livro de Lisbo*a, Lisboa 1994.

[2] Kuśnierz-Krupa D., *Zabytkowe fortyfikacje w krajobrazie miejskim Portugalii (wybrane przykłady) / Historic fortifications in the urban landscape of Portugal (selected examples*), „Landscape Architecture", 4/2013, pp. 56-63.

[3] Święcka E., *Pamięć płomieni; konserwacja kościoła Dominikanów w Lizbonie. Die Erinnerung der Flammen; Konservierung der Dominikanerkirche in Lissabon / Flames Memory; conservation of the Dominican church in Lisbon,* [w:] "Ruins of sacral monuments – protection and adaptation for new functions", International Scientific Conference, Gubin, 6-8 November 2008, pp. 463-476.

[4] Kuśnierz-Krupa D., *Konserwatorski profesjonalizm* w *Lizbonie / Conservator's professionalism* in *Lisbon*, „Karta Krakowska 2000 – 10 lat później, praca zb., A. Kadłuczka (red.), seria architektura: monografia 400, Kraków 2011, pp. 175-181.

[5] Kuśnierz-Krupa D., *„Portugalska szkoła konserwacji" – Muzeum Transportu i Komunikacji Eduarda Souto Moury w Porto / „Portuguese school of conservation" – Museum of Transport and Communication by Eduardo Souto Moura in Porto*, „Jurnal of Heritage Conservation", 31/2012, pp. 31-38.

[6] Dudzik-Gyurkovich K., *Kształtowanie przestrzeni publicznych Lizbony: historia i współczesność / Forming of public spaces of Lisbon: history and the present day*, „Teka Komisji Urbanistyki i Architektury PAN" / „Portfolio of the Urban Planning and Architecture Committee of the Polish Academy of Sciences", oddział w Krakowie, XLV (2017), pp. 387-404.

[7] Franço J.-A., *Une ville des Lumieres: la Lisbonne de Pombal /* A City of the Enlightenment. Pombal's Lisbon, Paris 1965.

[8] Zaharski A., "*Une ville des Lumieres:la Lisbonne de Pombal", José-Augusto França, Paris 1965: [recenzja] / A City of the Enlightenment. Pombal's Lisbon, Paris 1965: [review]*, "*Historical Review*" 57/4, 1966, pp. 670-674.

[9] Naeem A., *Interventions in historical portuguese context & Lisbon's contemporary architects* [w:] Conference: Space International Conference on Architecture, Culture and Society, September 2018, London, UK, pp. 80-89.

[10] Lúcia M. Cardoso R., *The Restoration of Historic Buildings Between 1835 and 1929: the Portuguese Taste, E-Journal of Portuguese History*, January 2005.

[11] *Physics of Portuguese Heritage. Architecture and Memory, a liquid, solid and gaseous equation / Físicas do Património Português.* Arquitetura e Memória, Catalogue / Catálogo, Lisbon 2018. ISBN: 978-972-776-536-2.

[12] Dermini K., *New Architecture as Infill in Historical Context, „Architecture & Urban Planning",* 7/2013, pp. 44-50, doi: 10.7250/aup.2013.005.

[13] Markus E., *Chiado, Lisbon, Portugal* [w:] Winfried Nerdinger (ed.) Geschichte der Rekonstruktion. Konstruktion der Geschichte, München 2010, pp. 384-365.

[14] Cardoso Rosas L. M., *The Restoration of Historic Buildings Between 1835 and 1929: the Portuguese Taste*, E-Journal of Portuguese History, January 2005, pp. 5.

[15] Pereira C.N., *O Carmo: De Igreja A Museu 150 Anos Em Torno Da Salvaguarda Do Património (Carmelita) Português. A Igreja Do Carmo De Lisboa. Notas Sobre O Seu Espólio Disperso*, „Edição especial – atas do Colóquio, *O Património Artístico das Ordens Religiosas: entre o Liberalismo e a Atualidade",* n. 3 (2016): ARTis ON.

[16] Vasconcelos F. de, *Sztuka portugalska / Portuguese Art*, Warszawa 1984.

[17] Guedes M.H., *Dos Mosteiros des Jeronimos*, Lisboa 2019.

[18] Smith R.C.Jr., *João Frederico Ludovice, an Eighteenth Centuary Architect in Portugal,* „The Art. Bulletin" Vol. 18 (No. 3), (Sep.1936), pp. 273-370.

[19] Canas J.F., *A Igreja de S. Domingos de Lsboa O Renascerdos Cinzas*, „Monumentos", No. 6, Março 1997.
[20] Costa M., *The Church of S. Julião and its patron / A Igreja de S. Juliao E O Seu Patrono*, „Revista Municipan magazim", Year XXII, N. 88, 1st quarter 1961, pp. 5-21.
[21] Cruz Pinto J., *A Synchronous Architectural Project Contemporary Renovation in the Governor's Palace in Lisbon,* [w:] World Heritage And Degradation: Smart Design, Planning and Technologies: "Le Vie dei Mercanti", Napoli 2016; 978-88-6542-257-1.

USING SATELLITE IMAGES TO RETRIEVE THE RIVER TURBIDITY AND WATER FLOW VELOCITY FOR MONITORING THEIR INFLUENCES ON BRIDGE SUBSTRUCTURES

WYKORZYSTANIE ZDJĘĆ SATELITARNYCH DO OKREŚLENIA MĘTNOŚCI WODY ORAZ PRĘDKOŚCI PRZEPŁYWU WODY RZEKI W CELU MONITOROWANIA ICH WPŁYWU NA PODPORY MOSTÓW

Luong Minh Chinh*
Thuyloi University Hanoi, Vietnam

Structure and Environment vol. 15, No. 2/2023, p. 63
DOI: 10.30540/sae-2023-006

Abstract

Turbidity is an important indicator of water quality in rivers, lakes, and coastal areas. Research on turbidity issues in these areas is significant not only for the development and utilization of water resources for aquaculture, tourism, and other purposes but also for assessing the level of silt (sand) in the river, allowing sediment alluvial to build up a bank of the river, and monitoring the degree of water corrosion in the bridge substructure. This allows for the building of an effective maintenance and conservation program for the bridge in response to climate change.

Traditional methods have defined the turbidity of water in a local area, on a small scale. Interpolation errors of traditional methods for large areas may exceed over 20%. The use of remote sensing technology as Landsat-8 satellite images with a high geometric resolution of 30-meter multispectral channels allows us to estimate and distribute the water turbidity in a 30 × 30 m grid in detail.

Using multi-temporal Landsat-8 data in 2014 and 2015 for modeling water turbidity of Tien and Hau rivers and coastal areas in South Vietnam, the obtained mean absolute error is approximately 20%, the Root Mean Square Error (RMSE) does not exceed 10 NTU. The models have a high coefficient of efficiency ME, approximately 90% (ME = 0.862), and the correlation coefficient R stronger than 90%. This allows an overall assessment of changes in water flow velocity concerning the amount of sediment in the river.

Streszczenie

Mętność jest ważnym wskaźnikiem jakości wody w rzekach, jeziorach i obszarach przybrzeżnych. Badania nad tą kwestią są istotne nie tylko dla rozwoju i wykorzystania zasobów wodnych na potrzeby akwakultury, turystyki i innych celów, ale także dla oceny poziomu mułu (piasku) w rzece, pozwalającego osadom aluwialnym budowanie brzegu rzeki oraz monitorowanie stopnia korozji w podporach mostu. Umożliwi to opracowanie skutecznego programu konserwacji i utrzymania mostu w odpowiedzi na zmiany klimatyczne.

Tradycyjne metody pozwalają określić mętność wody w obszarze lokalnym, w małej skali. Błędy interpolacji tradycyjnych metod do dużych obszarów mogą przekraczać 20%. Zastosowanie technologii teledetekcji w postaci zdjęć satelitarnych Landsat-8 o wysokiej rozdzielczości geometrycznej 30-metrowych kanałów wielospektralnych pozwala na szczegółowe oszacowanie i rozmieszczenie zmętnienia wody w siatce 30 × 30 m.

Wykorzystując wieloczasowe dane Landsat-8 z lat 2014 i 2015 do modelowania zmętnienia wody rzek Tien i Hau oraz obszarów przybrzeżnych w południowym Wietnamie, uzyskany średni błąd bezwzględny wynosi około 20%, a średni błąd kwadratowy (RMSE) nie przekracza 10 NTU. Modele mają wysoki współczynnik efektywności ME, około 90% (ME = 0,862), a współczynnik korelacji R jest wyższy niż 90%, co stwarza możliwość dokonania ogólnej oceny zmian prędkości przepływu wody w odniesieniu do ilości osadów w rzece.

EVALUATION OF WIND EFFECTS ON BUILDINGS USING DESIGN CODES AND NUMERICAL WIND TUNNEL TESTS

OCENA WPŁYWU WIATRU NA BUDYNKI Z WYKORZYSTANIEM NORM PROJEKTOWYCH I TESTÓW NUMERYCZNYCH W METODZIE TUNELU AERODYNAMICZNEGO

Imam Hossain
Bangladesh Army International University of Science and Technology (BAIUST)
Jahidul Islam
Military Institute of Science and Technology (MIST)
Al Amin
European University of Bangladesh (EUB)

Structure and Environment vol. 15, No. 2/2023, p. 73 DOI: 10.30540/sae-2023-007

Abstract

The evaluation of wind effect on the regular shape and simple diaphragm buildings and structures due to wind load has been calculated by several international codes and standards where wind gust nature and dynamic effect could not capture. Bangladesh National Building Code (BNBC) provides the tools for engineers to calculate the wind pressures for the design of a regular-shaped structure with a height to width ratio of less than 5.0, a simple diaphragm, and no unusual geometrical irregularity. If these conditions do not satisfy a wind tunnel testing is required. In this study, a comparative study between two codes in Bangladesh (BNBC-2006 and BNBC-2020), and wind tunnel test results are conducted. An investigation is carried out on four typical buildings with variable heights located within Dhaka, Bangladesh. A computational fluid dynamics (CFD) program RWIND is used to calculate the wind loads on buildings and are compared with those obtained by Bangladesh National Building Codes. Storey shear of four different building models is compared. Between BNBC-2006 and BNBC-2020, there is up to a 53% difference in storey shear. Whereas, up to 30% variation in storey shear is observed between the numerical wind tunnel test data and the data calculated using the BNBC-2020 equations. Finally, this study will help in improving BNBC code provisions for wind load calculations.

Streszczenie

Kalkulację wpływu wiatru na budynki i budowle o regularnych kształtach i prostych konstrukcjach pod obciążeniem wiatrem przedstawiono w kilku normach międzynarodowych, w których jednak nie uwzględniono charakteru podmuchów wiatru i efektu dynamicznego. Bangladeska Krajowa Norma Budowlana (BNBC) zapewnia inżynierom narzędzia do obliczania ciśnienia wiatru przy projektowaniu konstrukcji o regularnym kształcie, o stosunku wysokości do szerokości mniejszym niż 5,0, prostej konstrukcji oraz bez nietypowych nieregularności geometrycznych. Jeśli warunki te nie są spełnione, wymagane jest przeprowadzenie testów w tunelu aerodynamicznym. W niniejszym opracowaniu przeprowadzono badanie porównawcze między dwiema normami obowiązującymi w Bangladeszu (BNBC-2006 i BNBC-2020) oraz wynikami testów w tunelu aerodynamicznym. Badanie przeprowadzono na czterech typowych budynkach o różnej wysokości zlokalizowanych w Dhace w Bangladeszu. Program RWIND do obliczeń i symulacji dynamiki płynów (CFD) został wykorzystany do obliczenia obciążeń wiatrem na budynkach i porównany z wynikami uzyskanymi według bangladeskich norm budowlanych. Porównano ścinanie kondygnacji czterech różnych modeli budynków. W tym względzie różnice pomiędzy BNBC-2006 i BNBC-2020 wynoszą do 53%. Natomiast między danymi z numerycznego testu w tunelu aerodynamicznym a danymi obliczonymi przy użyciu równań BNBC-2020 zaobserwowano do 30% różnic w odniesieniu do ścinania kondygnacji. Badanie to pomoże też ulepszyć przepisy norm BNBC dotyczące obliczeń obciążenia wiatrem.

FACTORS RESPONSIBLE FOR SOCIO-SPATIAL SEGREGATION IN THE HOUSING NEIGHBOURHOODS OF MINNA, NIGERIA

CZYNNIKI ODPOWIEDZIALNE ZA SEGREGACJĘ SPOŁECZNO-PRZESTRZENNĄ W DZIELNICACH MIESZKANIOWYCH MIASTA MINNA W NIGERII

Dzukogi, Usman Abubakar
The Federal Polytechnic Bida, Nigeria
Yusuf Alapata, Ahmed
University of Ilorin Nigeria

Structure and Environment vol. 15, No. 2/2023, p. 82

DOI: 10.30540/sae-2023-008

Abstract

Segregation in the housing sector has exposed urban dwellers to series of unfavourable conditions in most cities of developing countries, which are as a result several factors. This paper is aimed at examining the factors influencing segregation in the housing neighbourhoods of Minna, Nigeria. Two-stage cluster sampling methods were adopted in the selection of neighbourhoods and households across the entire sample frame in the administration of 374 questionnaires across the 25 clustered neighbourhoods. Chi-square and Relative Importance Index (RII) as well as mean score to determine neighbourhood geographical segregation indicators pattern across all the 25 neighbourhoods in the study area. The study established that there is a significant difference between low, medium, and high density neighbourhoods in terms segregation factors in the study area. It was therefore suggested that a good urban governance structure should be put in place that will discourage class divisions among spatial entities of the city.

Streszczenie

W większości miast krajów rozwijających się segregacja w sektorze mieszkaniowym postawiła mieszkańców miast w obliczu szeregu niekorzystnych warunków, wynikających z kilku czynników. Niniejszy artykuł ma na celu zbadanie czynników wpływających na segregację w dzielnicach mieszkaniowych miasta Minna w Nigerii. Zastosowano dwuetapowe metody próbkowania klastrowego w doborze dzielnic i gospodarstw domowych w całym operacie losowania w celu rozdania 374 kwestionariuszy w 25 klastrach dzielnic. Wykorzystano wskaźnik chi-kwadrat i wskaźnik względnego znaczenia (RII), a także średni wynik w celu określenia wzorca wskaźników segregacji geograficznej we wszystkich 25 dzielnicach na badanym obszarze. Badanie wykazało, że istnieje znacząca różnica między dzielnicami o niskiej, średniej i wysokiej gęstości zaludnienia pod kątem czynników segregacji na badanym obszarze. W związku z tym zasugerowano, że należy wprowadzić dobrą strukturę zarządzania miastem, która zniechęci do podziałów klasowych między jednostkami przestrzennymi miasta.

FUSION OF DIFFERENTIAL ANALYSIS OF VOLUMETRIC STRAIN METHOD (DILATOMETRIC THERMOPOROMETRY) AND MERCURY INTRUSION POROSIMETRY METHOD FOR PORE SPACE CHARACTERIZATION IN CARBONATE ROCKS

POŁĄCZENIE METODY RÓŻNICOWEJ ANALIZY ODKSZTAŁCEŃ ORAZ METODY POROZYMETRII RTĘCIOWEJ DO OKREŚLENIA CHARAKTERYSTYKI PRZESTRZENI POROWEJ W SKAŁACH WĘGLANOWYCH

Karol Skowera
Kielce University of Technology, Poland

Structure and Environment vol. 15, No. 2/2023, p. 90

DOI: 10.30540/sae-2023-009

Abstract

Many characteristics of capillary-porous materials, including limestones and dolomites, depend on the structure of the pore space of a given material, so the article attempts to accurately determine the geometric characteristics of pores and their ability to transport water. Much information on the pore structure of carbonate rocks can be obtained from literature studies. There is a lack of information on the use of full hysteresis dilatometric thermoporometry methods for this purpose, as well as the fusion of differential analysis of volumetric strain (DAVS) results with mercury intrusion porosimetry (MIP) results.

The subject of the research presented in this article is the analysis of pore structure in carbonate rocks using the method of differential analysis of volumetric strain and mercury intrusion porosimetry. Based on the measurements made, the pore size, pore volume, content of empty pores and pores containing water incapable of phase transformation were analyzed. The geometry of mesopores of rock samples examined by differential analysis of volumetric strain and mercury intrusion porosimetry was compared. A fusion of the distribution of mesopores from the DAVS study with a part of the distribution of meso- and macropores obtained by the MIP study was performer

Streszczenie

Wiele cech materiałów kapilarno-porowatych, w tym wapieni i dolomitów, zależy od struktury przestrzeni porowej danego materiału, dlatego w artykule podjęto próbę dokładnego określenia cech geometrycznych porów i ich zdolności do transportu wody. Wiele informacji na temat struktury porów skał węglanowych można uzyskać ze studiów literaturowych. Brakuje informacji na temat wykorzystania w tym celu metod termoporometrii dylatometrycznej z pełną histerezą, a także połączenia wyników różnicowej analizy odkształceń (DAVS) z wynikami porozymetrii rtęciowej (MIP).

Przedmiotem badań przedstawionych w niniejszym artykule jest analiza struktury porów w skałach węglanowych z wykorzystaniem metody różnicowej analizy odkształceń i porozymetrii rtęciowej. Na podstawie przeprowadzonych pomiarów przeanalizowano wielkość porów, objętość porów, zawartość porów pustych oraz porów zawierających wodę niezdolną do przemiany fazowej. Porównano geometrię mezoporów próbek skalnych badanych metodą różnicowej analizy odkształceń i porozymetrii rtęciowej. Wykonano fuzję rozkładu mezoporów z badania DAVS z częścią rozkładu mezo- i makroporów uzyskanych w badaniu MIP.

LIVING TRACES OF HISTORY – PORTUGUESE APPROACH TO CONSERVATION ON THE EXAMPLE OF RELIGIOUS BUILDINGS IN LISBON

ŻYWE ŚLADY HISTORII – PORTUGALSKIE PODEJŚCIE KONSERWATORSKIE NA PRZYKŁADZIE OBIEKTÓW SAKRALNYCH W LIZBONIE

Małgorzata Doroz-Turek
Kielce University of Technology

Structure and Environment vol. 15, No. 2/2023, p. 99

DOI: 10.30540/sae-2023-010

Abstract

The article addresses the issue of the Portuguese conservation approach to religious buildings in Lisbon that have been damaged by cataclysms. The aim is to show approach to both preserving the original substance and changing the function of the sacral building. After the tragic destruction of Lisbon in the mid-18th century was followed by the use of the ruins of the Carmelite monastery church, Convento do Carmo, for adaptation into the Archaeological Museum. Church of the Nossa Senhora da Conceição Velha, also acts as a remnant of historic events. The Church of St Dominic is also an example of atypical conservation and restoration. Another one is the adaptation the São Julião church on the Museum of the Bank of Portugal. That projects are examples of pioneering conservation activities conceived as a result of the conservation practice of Portuguese architects.

Streszczenie

Artykuł porusza problem portugalskiego podejścia konserwatorskiego do obiektów sakralnych w Lizbonie, które uległy zniszczeniu w wyniku kataklizmów. Celem jest ukazanie interesującego podejścia zarówno do zachowania oryginalnej substancji, jak i zmiany funkcji obiektów sakralnych. Po tragicznym zniszczeniu Lizbony w połowie XVIII wieku ruiny kościoła klasztoru karmelitów Convento do Carmo wykorzystano do adaptacji na Muzeum Archeologiczne. Znakiem historycznych wydarzeń jest także kościół Nossa Senhora da Conceição Velha. Przykładem nietypowej konserwacji i restauracji jest także kościół Igreja de São Domingos. Kolejnym przykładem jest adaptacja zniszczonego kościoła São Julião na siedzibę Muzeum Banku Portugalii. Projekty te są przykładami pionierskich działań konserwatorskich powstałych w wyniku praktyki konserwatorskiej portugalskich architektów..

GUIDELINES FOR AUTHORS

Authors of reports of original research should provide a thorough description of their work and its results, followed by the objective discussion of the significance of the work. Underlying data should be represented accurately in the paper. A study should contain sufficient amount of details and references to allow others to replicate the research work. Fraudulent or knowingly inaccurate statements constitute unethical behaviour and are unacceptable. Reviews and professional publications should also be accurate and objective, and editorial opinions should be clearly identified as such.

Authors may be asked to provide the raw data in connection with a paper for editorial review, and should be prepared to provide public access to such data, if practicable, and should in any event be prepared to retain such data for a reasonable time after publication.

Authors should declare that they have created entirely original works. If the authors have used the work and/or words of others, that must be appropriately cited or quoted. Plagiarism takes many forms, from passing off another paper as the author own paper, to copying or paraphrasing substantial parts of another paper (without attribution), or to claiming results from research conducted by others. Plagiarism in all its forms constitutes unethical publishing behaviour and is unacceptable.

Generally, authors should not publish manuscripts describing essentially the same research in more than one journal, or primary publication. Submitting the same manuscript to more than one journal concurrently constitutes unethical publishing behaviour, and is unacceptable. In general, an author should not submit for consideration in another journal a previously published paper. Publication of some kinds of papers (e.g., clinical guidelines, translations) in more than one journal is sometimes justifiable, provided that certain conditions are met. The authors and editors of the journals concerned must agree to the secondary publication, which must reflect the same data and interpretation of the primary document. The primary reference must be cited in the secondary publication.

Proper acknowledgment of the work of others must always be given. Authors should cite publications that have been influential in determining the nature of the reported work. Information obtained privately, as in conversation, correspondence, or discussion with third parties, must not be used or reported without explicit, written permission from the source. Information obtained in the course of confidential services, such as reviewing manuscripts or grant applications, must not be used without the explicit written permission of the author of the work involved in these services.

Authorship should be limited to those who have made a significant contribution to the concept, design, execution, or interpretation of the reported study. All those who have made significant contributions should be listed as co-authors. Where there are others who have participated in certain substantive aspects of the research project, they should be acknowledged, or listed as contributors. The corresponding author should ensure that all appropriate co-authors and no inappropriate co-authors are included in the paper, and that all co-authors have seen and approved the final version of the paper, and have agreed to its submission for publication.

All authors should disclose in their manuscript any financial or other substantive conflict of interest that might be construed to influence the results or interpretation of their manuscript. All sources of financial support for the project should be disclosed. Examples of potential conflicts of interest which should be disclosed include employment, consultancies, stock ownership, honoraria, paid expert testimony, patent applications/registrations, and grants or other funding. Potential conflicts of interest should be disclosed at the earliest stage possible.

When an author discovers a significant error or inaccuracy in his/her own published paper, it is the author's obligation to promptly notify the journal editor or publisher, and cooperate with the editor to retract or correct the paper. If the editor or the publisher learns from a third party that a published paper contains a significant error, it is the obligation of the author to promptly retract or correct the paper, or provide evidence to the editor of the correctness of the original paper.

Paper submission to the Editorial Board is considered equivalent to a declaration that the content of the paper has not been previously published and has not been submitted to another editorial board.

The author's duties

Acceptance of a manuscript for publication in the journal carries with it an understanding that the author, when requested, will fulfil an obligation to contribute their expertise to the review of others' manuscripts. Authors are also requested to name three independent reviewers together with institutional email addresses. The named possible reviewers must not be located within the submitting organisation.

The author's rights

As an author, you (or your employer or institution) have certain rights to reuse your work.

After the paper acceptance

Upon acceptance of a paper, authors will be asked to complete a "***Licence Agreement***" form. The corresponding author will receive an email confirming acceptance of the manuscript, along with a Licence Agreement.

After reading the terms and conditions of the Agreement, the author will be asked to print, sign, and send a scanned copy of the document as an attachment via email to the following address: sae@tu.kielce.pl.

NEW SUBMISSIONS

Submission to this journal proceeds totally online, and you will be guided stepwise through the creation and uploading of your files. The system automatically converts your files to a single PDF file, which is used in the peer-review process.

Formatting requirements

All manuscripts must contain the essential elements needed to convey your manuscript, for example Abstract, Keywords, Introduction, Materials and Methods, Results, Conclusions, Artwork and Tables with Captions.

The text of the paper should be written in Times New Roman font, 12 points with single line spacing and paragraph indent 0.5 cm, the margin on both sides should be 2.5 cm. The paper should be limited to 7,500 words and should include: abstract, keywords, main text, references, tables and figures. The word equivalent for a table is 250 words. The contents of the paper should be appropriately divided into numbered sections and subsections.

Figures and tables in the text

Please ensure the figures and the tables included in the single file are placed next to the relevant text in the manuscript, rather than at the bottom or the top of the file. The corresponding caption should be placed directly below the figure or above the table.

Figures

Figures should be of high quality — resolution of at least 300 dpi, format: TIF (preferred), JPG, EPS or WMF. Do not use frames around figures. Any descriptions found in drawings, photos, and tables should be in English, in Times New Roman font. They should be easily legible when the figure is reduced to a width of 84 mm. The colours on the charts should be contrasting.

Ensure that each illustration has a caption. A caption should comprise a brief title (not on the figure itself) and a description of the illustration. Keep text in the illustrations themselves to a minimum, but explain all symbols and abbreviations used. In addition, a dot should be used as a decimal fraction separator in the drawings.

Tables

Drawings and tables should be numbered consecutively with Arabic numerals, and their titles should be given both in English and Polish. If the drawings or data for the tables have been taken from other papers, the source must be stated in the caption. In addition, a dot should be used as a decimal fraction separator in the tables.

Please submit tables as editable text and not as images. Tables can be placed either next to the relevant text in the article, or at the bottom, or the top of the file. Tables should be numbered consecutively in accordance with their appearance in the text. The table notes should be placed below the table body. Tables should be used sparingly, and it is needed to ensure that the data presented in them do not duplicate results described elsewhere in the paper. Vertical rules and shading in table cells should be avoided.

Mathematical formulas

Please submit maths equations as editable text, and not as images. Present simple formulas in line with normal text where possible, and use the solidus (/) instead of a horizontal line for small fractional terms, e.g., X/Y. In principle, variables are to be presented in italics. Powers of e are often more conveniently denoted by exp. Number consecutively any equations that have to be displayed separately from the text (if referred to explicitly in the text).

Peer Review

This journal operates a single blind review process. All contributions will be initially assessed by the editor with respect to their suitability for the journal. Papers deemed suitable are then typically sent to a minimum of two independent expert reviewers to assess the scientific quality of the paper. The Editor is responsible for the final decision on acceptance or rejection of papers. The Editor's decision is final. If your paper is rejected, please do not resubmit a modified version of this paper, as it will not be considered for publication.

ARTICLE STRUCTURE

Essential title page information

Title

The title of the paper should be concise.

Author names and affiliations

Please clearly indicate the first name(s) and surname(s) of each author, and check that all names are accurately spelled. You can add your name in parentheses in your own script behind the English transliteration. Present the authors' affiliation addresses (where the actual work was done) below the names. Indicate all affiliations with a lower-case superscript letter immediately after the author's name and in front of the appropriate address. Provide the full postal address of each affiliation, including the country name and, if available, the e-mail address of each author.

Corresponding author

Clearly indicate who will handle correspondence at all stages of reviewing and publication, also post-publication. This responsibility includes answering any future queries about Methodology and Materials. **Ensure that the e-mail address is given and that contact details are kept up to date by the corresponding author.**

Abstract

The abstract should consist of 120 to 150 words. It should briefly present the content of the paper, including information about the purpose and scope of the work, results and conclusions. The abstract should not refer to bibliography or equations, nor use unknown abbreviations.

Keywords

Immediately after the abstract, provide 3 to 7 keywords, and avoid general and plural terms and multiple concepts (avoid, for example, "and", "of"). Be sparing with abbreviations: only abbreviations firmly established in the field may be eligible. These keywords will be used for indexing purposes.

Abbreviations

Define abbreviations that are not standard in this field. They should be placed on the first page of the paper. Such abbreviations that are unavoidable in the abstract must be defined at their first mention there, as well as in the footnote. Ensure consistency of abbreviations throughout the article.

Introduction

The main part of the paper should be preceded by a short summary of the state of knowledge in the topics discussed.

State the objectives of the paper and provide an adequate background, avoiding a detailed literature survey, or a summary of the results.

The formulation of the problem should be presented in a clear and concise way.

Materials and methods

Provide sufficient details to allow the procedure to be reproduced by an independent researcher. Methods that are already published should be summarized, and indicated by a reference. If quoting directly from a previously published method, use quotation marks, and also cite the source. Any modifications to existing methods should also be described.

Results

Results should be clear and concise. The results of research should be presented in a synthetic manner, avoiding repetition, e.g., data presented in charts should not be given in a tabular form.

Discussion

This should explore the significance of the results, not repeat them. A combined Results and Discussion section is often appropriate. Avoid extensive citations and discussion of published literature.

Conclusions

The main conclusions of the study may be presented in a short Conclusions section, which may stand alone, or form a subsection of a Discussion or Conclusions. They should be based on the research carried out.

Acknowledgements

Collate acknowledgements in a separate section at the end of the paper before the references and do not, therefore, include them on the title page, as a footnote to the title or otherwise. List here those individuals who provided help during the research (e.g., providing language help, writing assistance or proof reading the article, etc.).

Formatting of funding sources

List funding sources in this standard way to facilitate compliance to funder's requirements:

Funding: This paper was supported by the National Science Centre [grant numbers xxxx, yyyy]; and the Ministry of Education and Science [grant number aaaa].

It is not necessary to include detailed descriptions of the program or type of grants and awards. When funding is from a block grant, or other resources available to a university, college, or other research institution, submit the name of the institute or organization that provided the funding.

If no funding has been provided for the research, it is recommended to include the following sentence:

This research did not receive any specific grant from funding agencies in the public, commercial, or not-for-profit sectors.

References

Citation in text

Please ensure that every reference cited in the text is also present in the reference list (and vice versa). Any references cited in the abstract must be given in full. Unpublished results and personal communications are not recommended in the reference list, but may be mentioned in the text. If these references are included in the reference list, they should follow the standard reference style of the journal and should include a substitution of the publication date with either 'Unpublished results' or 'Personal communication'. Citation of a reference as 'in press' implies that the item has been accepted for publication.

The publications quoted in the paper should be in English. Quoted publications should be numbered in square brackets in the order in which they appear in the text and listed in the references. No reference should be made to unpublished papers, internal reports, etc. The list of publications cited at the end of the article should contain all bibliographic data, that is in the case of:

- book: surname and initials of authors' first names, book title, publishing house, place and year of publication, e.g. Kurdowski W.: *Chemistry of cement and concrete*. PWN, Warsaw 2010;
- paper in a journal: surname and initials of authors' first names, paper title, title of the journal, volume, number, year of publication, number of the beginning and end page of the paper, DOI, e.g., Grzeszczyk S.: *The truth about the geopolymers*, Cement Wapno Beton, 26 (6) (2021), 101-108, DOI: https://doi.org/10.32047/CWB.2021.26.6.1;
- a chapter or article in a collective paper: surname and initials of first names of authors' of a chapter/article, the title of a chapter/article, title of a collective study preceded by the preposition [in:] (volume/number), publishing house, place and year of publication, page number of the beginning and end of the chapter/article, ISBN number, e.g. Kotwica Ł., Małolepszy J.: *The role and effect of chemical admixtures modifying the viscosity of cement slurries*, in: Rheology in concrete technology, Monograph, Publishing house of the Silesian University of Technology, Gliwice 2009, 57-62, ISBN 978-83-7335-609-2;
- papers published in conference materials: surname and initials of the authors' first names, paper title, title of conference materials, publisher, place and date of publication, pages, doi, e.g., Zapała-Sławeta J., Owsiak Z.: *The impact of lithium nitrate on the physical and mechanical properties of Portland cement*. MATBUD"2018th Scientific — Technical Conference on Material Problems in Civil Engineering, Kraków 2018, l-8, DOI 10.1051/matecconf/201816304002;
- electronic publications: surname and initials of authors' names, paper title, (place), year of publication, internet address, date of access.